Heavy Flavor Working Group Report*

Contributing authors: *A. D. Frawley*[1,6], *F. Karsch*[2], *T. Ullrich*[2,3,6] *and R. Vogt*[4,5,6]
[1]Physics Department, Florida State University
[2]Physics Department, Brookhaven National Laboratory
[3]Physics Department, Yale University
[4]Nuclear Science Division, Lawrence Berkeley National Laboratory, Berkeley, CA, USA
[5]Physics Department, University of California at Davis, Davis, CA, USA
[6]Convener

Abstract

In this document we review the physics opportunities provided by an upgrade to the Relativistic Heavy Ion Collider (RHIC) accelerator offering substantially larger luminosities in conjunction with improved capabilities of the two large RHIC detectors, PHENIX and STAR. We focus on heavy flavor probes. This report is a summary of the results of a series of workshops held by the RHIC II heavy flavor working group.

*This work was supported in part by the U. S. Department of Energy under Contract No. DE-AC02-05CH11231 and contract no. DE-AC02-98CH10886, and by National Science Foundation grant PHY-04-56463.

Contents

1. Introduction **3**

1.1 Motivation . . . 3

1.2 Overview of results from the heavy flavor program at RHIC . . . 4

1.3 Overview of the proposed heavy flavor program at RHIC II . . . 5

1.4 Overview of the relationship of RHIC II to the LHC program . . . 6

2. Detector upgrade program at RHIC **8**

2.1 PHENIX upgrades . . . 8

2.2 STAR upgrades . . . 10

3. Projected RHIC II yields **13**

4. Open heavy flavor **17**

4.1 Open Heavy Flavor Theoretical Results . . . 17

4.11 Theoretical Baseline Results . . . 17

4.2 Models of Heavy Quark Energy Loss . . . 19

4.3 Open heavy flavor measurements to date at RHIC . . . 22

4.31 Baseline measurements . . . 23

4.32 Heavy ion measurements . . . 25

4.4 Proposed open heavy flavor experimental program at RHIC II . . . 26

5. Hidden heavy flavor: quarkonium **28**

5.1 Theoretical results . . . 28

5.11 Cross sections in pp collisions . . . 28

5.12 Cold nuclear matter effects on quarkonium production at RHIC . . . 31

5.13 Models of quarkonium production in heavy ion collisions . . . 34

5.2 Status of Quarkonium Physics at the CERN/SPS . . . 39

5.3 Quarkonium measurements to date at RHIC . . . 42

5.31 Baseline quarkonium measurements at RHIC . . . 43

5.32 Quarkonium measurements in heavy ion collisions at RHIC . . . 43

5.4 Proposed RHIC II quarkonia measurements . . . 49

6. Relationship to the LHC program **54**

7. Conclusions **56**

1. Introduction

1.1 Motivation

Because of the large charm and bottom quark masses, they are produced almost exclusively in the initial parton-parton interactions in heavy ion collisions at RHIC energies. In the absence of any nuclear effects, the heavy flavor cross sections in AA collisions at RHIC would simply scale with the number of binary collisions. Thus departures from binary scaling for heavy flavor production in AA collisions provide information about nuclear effects. These can be divided into two categories: effects due to embedding the colliding partons in a nucleus (cold matter effects) and effects due to the large energy density in the final state. The main focus of the heavy flavor program at RHIC is to investigate the properties of the dense matter produced in AA collisions by studying its effects on open heavy flavor and quarkonium production. This in turn requires a detailed understanding of cold matter effects so that they can be unfolded from the dense matter effects.

The program thus requires detailed measurements and calculations of pp and pA heavy flavor cross sections to characterize the cold matter effects if we are to quantify the differences between QGP and non-QGP effects. Up-to-date benchmark calculations of the total open heavy flavor (charm and bottom hadrons) and quarkonium (J/ψ and Υ families) yields and spectra are imperative. Cold matter effects that need to be included are nuclear shadowing, for both open heavy flavor and quarkonium production, and nuclear absorption of quarkonium. Recent calculations of charm and bottom production to FONLL in pp collisions [1] have been published, along with a discussion of the theoretical uncertainties inherent in these calculations and reference calculations of heavy quark, heavy flavor meson and decay lepton spectra. Similar calculations have been done for quarkonium production, including studies of shadowing and absorption effects as a function of rapidity and centrality in d+Au [2] and AA [3] collisions at RHIC.

A number of dense matter effects on heavy flavor production have been predicted. Some of these effects do not change the total cross section but, instead, modify the p_T spectra of heavy flavor hadrons and their decay products. Heavy quark energy loss [4, 5, 6, 7, 8] by collisional and radiative processes, steepens the p_T distribution relative to that in pp collisions. On the other hand, random p_T kicks result in transverse momentum broadening, increasing the average p_T in both cold nuclear matter [9] and in passage through hadron bubbles in the mixed phase of a QGP [10]. If the medium surrounding the heavy quarks after production exhibits collective motion, such as transverse flow [11, 12], the low p_T heavy quarks ($p_T < m$) may be caught in this flow. Some of the effects of energy loss [13, 14] on heavy flavor decays to electrons and charm flow [14] have already been seen in Au+Au collisions at RHIC. Studying heavy flavor energy loss using single electrons requires being able to separate electrons from c and b decays, since the large mass difference suggests that bottom energy loss is weaker than charm [4]. Some QGP studies require an accurate baseline for the total heavy flavor cross sections to interpret other effects. For example, if more than one $c\overline{c}$ pair is produced in an AA event, uncorrelated c and $\overline{c}$ quarks might coalesce to form a J/ψ in a QGP [16, 17, 18, 19]. The total $c\overline{c}$ yield is needed to normalize the J/ψ production rate from this process.

Suppression of J/ψ production was one of the most exciting proposed QGP signatures at the CERN SPS [20]. J/ψ suppression was predicted to occur due to the shielding of the $c\overline{c}$ binding potential by color screening, leading to the break up of the quarkonium states, first the χ_c and ψ', and finally the J/ψ itself as the temperature increases [21, 22]. The QGP suppression may not be so simple, as lattice gauge theory studies of the J/ψ spectral function above the critical temperature for deconfinement, T_c, attest. The J/ψ may exist as a bound state for temperatures considerably larger than T_c [23]. However, the J/ψ may instead be dissociated by hot thermal gluons in medium [24] before it could be suppressed by color screening. Secondary quarkonium production from uncorrelated $Q\overline{Q}$ pairs, either in the plasma phase [17, 19, 26, 27, 28] or in the hadron phase [29, 30], could counter the effects of suppression, ultimately leading to enhanced quarkonium production. Such secondary J/ψ production would lead to different kinematic distributions than the initial production. Because the underlying $c\bar{c}$ distribution falls rapidly with p_T, the p_T distribution produced by coalescence will be softer. If the underlying $c\bar{c}$

distribution peaks at mid rapidity, the J/ψ rapidity distribution from coalescence will be narrower than that produced in the primordial collisions. The coalescence rapidity distribution should be calculated with shadowing effects on the underlying $c\bar{c}$ distribution taken into account since these can cause the $c\bar{c}$ distribution to flatten in more central AA collisions [3]. Elliptic flow effects are also expected on quarkonium production, in addition to open heavy flavors [11, 12].

With higher luminosity at RHIC, the Υ states could also be measured. Since the Υ radius is smaller than that of the J/ψ [22], direct color screening in the QGP would not occur until much higher temperatures. The higher bottomonium states, however, would likely be suppressed at RHIC, as are the χ_c and ψ' in the charmonium family. The feed down structure is more complicated for the Υ since there are three S states (Υ, Υ' and Υ'') and two sets of P states (χ_{b1} and χ_{b2}) below the $B\overline{B}$ threshold. The Υ family suppression should be measurable over a large p_T range, with QGP suppression possible on the Υ' and Υ'' up to $p_T \sim 40$ GeV/c[25]. Because of the small number of $b\bar{b}$ pairs produced at RHIC, bottomonium formation by coalescence of unrelated pairs should be negligible.

1.2 Overview of results from the heavy flavor program at RHIC

Heavy flavor measurements capable of discriminating between theoretical models need large integrated luminosity. In RHIC runs so far we have acquired useful data sets at 200 GeV for pp, d+Au, Cu+Cu and Au+Au collisions. These data sets are not yet fully analyzed for Run 4 (Au+Au) and 5 (Cu+Cu), where the highest luminosities were captured for heavy ions, but preliminary heavy flavor results, at least, are already available for all runs and species.

The data collected to date for pp collisions provide an essential reference for the heavy ion program in the form of the underlying heavy flavor production rates as functions of rapidity and p_T. Equally essential, the data from d+Au collisions provide baseline information about cold nuclear matter effects which must also contribute to heavy flavor production in heavy ion collisions. The existing d+Au data provide useful tests of models that include the effects of shadowing on heavy flavor production and of absorption of J/ψ in cold nuclear matter [2].

Two very striking and unexpected results have already been seen for open heavy flavor in heavy ion collisions at RHIC. The first of these is the observation that the nuclear modification factor for electrons from open heavy flavor, R_{AA}, shows very strong suppression in central Au+Au collisions [31, 32], similar to that seen for pions. The second striking result is that the elliptic flow parameter, v_2, of electrons from open heavy flavor decays appears to favor charm quark flow at low p_T [31]. Until recently, it had been expected that heavy quark energy loss would be considerably smaller than that for light quarks due to interference effects [4]. Generating the necessary energy loss for charm and bottom quarks with realistic gluon densities in the material is a major challenge for models [4, 33]. The relatively large v_2 values at low p_T imply at least some degree of charm quark equilibration with the medium. This also implies very strong interactions of charm quarks with the medium at lower p_T [11, 12].

The first high statistics charmonium results for heavy ion collisions at RHIC were presented at Quark Matter 2005 [34]. Preliminary results were shown for the J/ψ nuclear modification factors, R_{AA}, as a function of the number of participant nucleons for Cu+Cu and Au+Au collisions in the rapidity intervals $|y| < 0.35$ and $1.2 < |y| < 2.2$. Comparison with existing models shows that cold nuclear matter baseline calculations [3] which approximately reproduce the PHENIX d+Au J/ψ rapidity distributions [2] somewhat underpredict the suppression observed in Cu+Cu and Au+Au collisions. On the other hand, several suppression models [19, 35, 36] which were successful in describing J/ψ suppression at the SPS are found to strongly overpredict the suppression at RHIC. Models which incorporate strong suppression combined with J/ψ regeneration from uncorrelated $c\bar{c}$ pairs seem to agree best with the data, although the existing models slightly underpredict the suppression.

In the last few years, theorists have begun exploring the consequences of J/ψ regeneration by coalescence on observables other than the centrality dependence of the nuclear modification factor [16].

This work has led to the prediction that J/ψ formed by coalescence of uncorrelated $c\bar{c}$ pairs will have narrower rapidity and p_T distributions due to the presumed shape of the underlying charm quark distributions. The coalescence contribution to J/ψ production will cause many observables to change with centrality, including the rapidity and p_T dependence of R_{AA}, the shape of the p_T distribution (quantified by the average p_T^2, $\langle p_T^2 \rangle$), and the J/ψ elliptic flow parameter, v_2. Quantitative predictions have been made for $\langle p_T^2 \rangle$ as a function of centrality for Au+Au and Cu+Cu collisions, with and without coalescence [16]. These predictions were compared to the preliminary Au+Au and Cu+Cu data for the first time at Quark Matter 2005. The data favor the calculations that include coalescence. On the other hand, the large coalescence contributions predicted for central Au+Au (and even central Cu+Cu) collisions are qualitatively expected to narrow the J/ψ rapidity distributions if the underlying charm distributions are peaked at mid rapidity. The preliminary data presented at Quark Matter 2005 show no evidence of this narrowing in central collisions. There is still work to do to quantify both the theoretical predictions and the experimental observables. The existing data sets will not provide a useful measurement of the J/ψ v_2 due to insufficient yield.

The running schedule for RHIC over the next five years is not settled. Based on the beam use proposal discussions prior to Run 6, it seems likely that more Au+Au data will be collected, providing up to an order of magnitude increase in integrated luminosity (if there are two more Au+Au runs). There will also be a very large increase in the integrated luminosity for pp collisions due to the requirements of the Spin program. Such luminosity increases will quantitatively improve the measurements of many heavy flavor observables, especially as a function of centrality. The J/ψ R_{AA} and $\langle p_T^2 \rangle$ as well as R_{AA} and v_2 measurements of charm and bottom semileptonic decays to single electrons will all improve significantly, allowing more definitive tests of models. Measurements of other observables will be qualitatively improved. Examples are: definitive v_2 measurements of semileptonic decays at intermediate to high p_T where we might hope to see the transition from charm to bottom dominance and flow to non-flow; a possible first J/ψ v_2 measurement; definitive measurements of J/ψ R_{AA} with rapidity to quantify the coalescence contribution; and measurements of J/ψ R_{AA} to higher p_T, invaluable for understanding coalescence and formation time effects. Finally, it seems likely that a first, low statistics, Υ suppression measurement would be possible.

However, it is clear that the RHIC heavy flavor program will be limited by the capabilities of the accelerator after about 5 more years. The luminosity increase brought by RHIC II, combined with the detector upgrades in place by that time, will be required for the heavy flavor program at RHIC to move to the next level, as described below.

1.3 Overview of the proposed heavy flavor program at RHIC II

The order of magnitude increase in luminosity, combined with the increased capabilities of the upgraded PHENIX and STAR detectors, will make it possible to add many important new probes to the heavy flavor program at RHIC.

One of the most powerful additions from the luminosity upgrade will be the ability to measure yields of the excited states of charmonium - the ψ' and χ_c states. Lattice calculations predict much smaller melting temperatures for the ψ' and χ_c than for the more tightly bound J/ψ so that these excited states should not be able to exist in the QGP at RHIC. Therefore comparison of the ψ' and χ_c yields with the J/ψ yield as a function of centrality is considered to be a direct test of deconfinement.

Testing models in which the observed J/ψ yield in heavy ion collisions is due to competition between gluon dissociation of J/ψ and coalescence formation of J/ψ in the QGP requires very high luminosity. Tests of charm coalescence models include measuring J/ψ v_2 as a function of p_T, J/ψ R_{AA} to much higher p_T to follow the trends of suppression as the J/ψ formation time approaches the QGP crossing time, and J/ψ polarization as a function of collision centrality. The rapidity and p_T dependence of R_{AA} as functions of $\sqrt{s_{NN}}$ and centrality, requiring sufficient luminosity for precision measurements at multiple energies, is not possible on a reasonable time scale at the present RHIC luminosity.

The study of bottomonium states, the Υ family, is only possible at RHIC II luminosities. Like the charmonium states, the dissociation temperatures of the bottomonium states depend on the binding energies. There are, however, two important differences from charmonium. First, the bottomonium binding energies, particularly that of the $\Upsilon(1S)$, are higher so that they should dissociate at higher temperatures. Only the higher-lying bottomonium states are thus likely to break up at RHIC energies. Second, the $b\bar{b}$ production rate in central Au+Au collisions is only $\sim$ 0.05 pairs per collision, making coalescence production of bottomonium much less likely. Thus bottomonium production at RHIC II will provide a very different window on color screening effects than charmonium production. The bottomonium yields at RHIC II should be sufficient for measurements of R_{AA} as a function of centrality in heavy ion collisions for the three Υ S states. The Υ yields at RHIC II and at the LHC will not be sufficient for measurements of v_2 or polarization.

As mentioned earlier, lepton measurements from semileptonic open heavy flavor decays at RHIC have already produced strikingly different results than expected. The strong suppression in R_{AA} coupled with the large v_2 suggest very large heavy quark energy loss in the medium. However, these semileptonic decay spectra contain both charm and bottom contributions, a significant complication. The separation of open charm and bottom can be done in several ways. Charm can be observed via $D^0 \rightarrow K\pi$ and $D \rightarrow K\pi\pi$ hadronic decays, as has been done by STAR. Precise R_{AA} and v_2 measurements are difficult in this channel. Since these events cannot be triggered, they must be extracted from a minimum bias data set that samples only a small fraction of the available luminosity. The combinatorial background is also very large, making statistical precision difficult. The addition of a displaced vertex measurement in STAR will dramatically reduce the combinatorial background but the lack of a trigger for these decays still remains. At RHIC II luminosity, bottom can be observed very cleanly in both PHENIX and STAR via $B \rightarrow J/\psi$ decays using displaced vertices, providing good measurements of the $b\overline{b}$ cross section and R_{AA}. However the yields will likely be too small for v_2 measurements at RHIC II or the LHC. Finally, the combination of RHIC II luminosity with a displaced vertex measurement should allow statistical separation of the charm and bottom contributions to the semileptonic decay spectra, taking advantage of the different c and b quark decay lengths. Such semileptonic decay measurements, while less clean than the direct D and B decay measurements, have the advantage of much larger yields so that separate v_2 measurements for charm and bottom may be possible.

Independent measurements of open charm and bottom R_{AA} and v_2 to high p_T will be very important at RHIC II. At low p_T, these measurements reflect the degree of heavy quark thermalization in the medium. At high p_T, they probe the energy loss of heavy quarks in the medium, providing an independent measurement of the initial energy density relative to the light quark energy loss measurements. The thermalization and energy loss mechanisms at low and high p_T respectively may be quite different due to the possible resonance scattering at low p_T. RHIC II will provide an opportunity to measure the v_2 and R_{AA} of b quark semileptonic decay products separately as well as extend these measurements for c quarks to much higher p_T.

1.4 Overview of the relationship of RHIC II to the LHC program

The heavy flavor production cross sections are significantly higher at the LHC than at RHIC since the Pb+Pb energy at the LHC is a factor of 27.5 higher than the maximum Au+Au energy at RHIC. The $c\overline{c}$ and $b\overline{b}$ cross sections increase by factors of 15 and 100 respectively [9] while the J/ψ and Υ cross sections increase by factors of 13 and 55 respectively [37]. But, because of the higher luminosity and the longer heavy ion runs, the Au+Au integrated luminosity at RHIC II is projected to be 36 times higher than for Pb+Pb at LHC. Therefore the heavy flavor yields per year are expected to be similar at the two facilities.

At $\sqrt{s} = 200$ GeV, bottom decays to leptons begin to dominate the single electron spectrum at $p_T \sim 4$ GeV/c. As the collision energy increases, the lepton spectra from B and D decays move closer together rather than further apart [9]. Thus, the large increase in the $b\overline{b}$ cross section relative to $c\overline{c}$ does

not make single leptons from B and D decays easier to separate. Preliminary calculations show that the $B \rightarrow e$ decay does become larger than that of $D \rightarrow e$, but at $p_T > 10$ GeV/c. The two lepton sources differ by less than a factor of two up to $p_T \sim 50$ GeV/$c$in the range $|y| \leq 1$. Thus interpretation of single lepton results on heavy flavors will be more difficult at the LHC. Other means of separating charm and bottom must be found. ALICE can reconstruct hadronic D^0 decays from $p_T \sim 0$ to $p_T \sim 25$ GeV/c[38] but, like STAR, will have to rely on minimum bias data for these measurements because of the lack of a trigger. While it is not yet clear what CMS and ATLAS will do to reconstruct charm, they should be able to make b jet measurements, similar to the Tevatron. One way that B mesons can be measured at the LHC is through their decays to J/ψ, as discussed further below. It has also been suggested that the $B\overline{B}$ contribution to the dimuon continuum, the dominant contribution above the Υ mass, can be used to measure energy loss [39]. That channel would be fairly clean at the LHC but more difficult at RHIC.

The RHIC II upgrades and the high LHC energies make detailed studies of Υ production and suppression possible. At the LHC, higher initial temperatures make Υ suppression more likely than at RHIC II. But the higher $b\bar{b}$ production rate ($\sim$ 5 per central Pb+Pb collision) means that, unlike RHIC, significant coalescence contributions to Υ production may be expected at the LHC. Thus measurements at the two energies complement each other. At RHIC II, it is likely that PHENIX will be able to measure and resolve the three Υ S states. STAR will see Υ yields similar to those in ALICE but the mass resolution will require fitting to extract yields. At the LHC, all 3 S states will also be measurable. CMS has the mass resolution to separate all three. The Υ states can be measured to $p_T \sim 0$ at all LHC detectors. Only ALICE will be able to measure J/ψ production to $p_T \sim 0$ without a special trigger [37] since CMS and ATLAS require high single muon p_T so that typically only J/ψ with $p_T > 5$ GeV/$c$are accepted. (However, CMS is working on a higher-level trigger to measure lower p_T J/ψ [40].) The larger $b\overline{b}$ cross section at the LHC means that J/ψ production from $B \rightarrow J/\psi X$ cannot be neglected. These decay J/ψ should be separable from the initial production using displaced vertices [37].

2. Detector upgrade program at RHIC

Both PHENIX and STAR have extensive upgrade programs underway that are extremely important for the heavy flavor program. The upgrades that are most relevant to heavy flavor measurements are described here. The impact on the heavy flavor program of these detector upgrades, in combination with the RHIC II luminosity increase, will be discussed in sections 4 and 5.

2.1 PHENIX upgrades

Several PHENIX detector upgrades that greatly enhance the heavy flavor capability of the experiment are expected to be available in the RHIC II time frame. The most important upgrades for the heavy flavor program will be the barrel and endcap Silicon Vertex Detectors, the Nose Cone Calorimeter, and the Muon Trigger Upgrade. The central region of the PHENIX detector, after installation of the silicon trackers and the Nose Cone Calorimeter, is shown in Fig. 1. The pseudorapidity and azimuthal angle coverages of the new detectors are illustrated in Fig. 2.

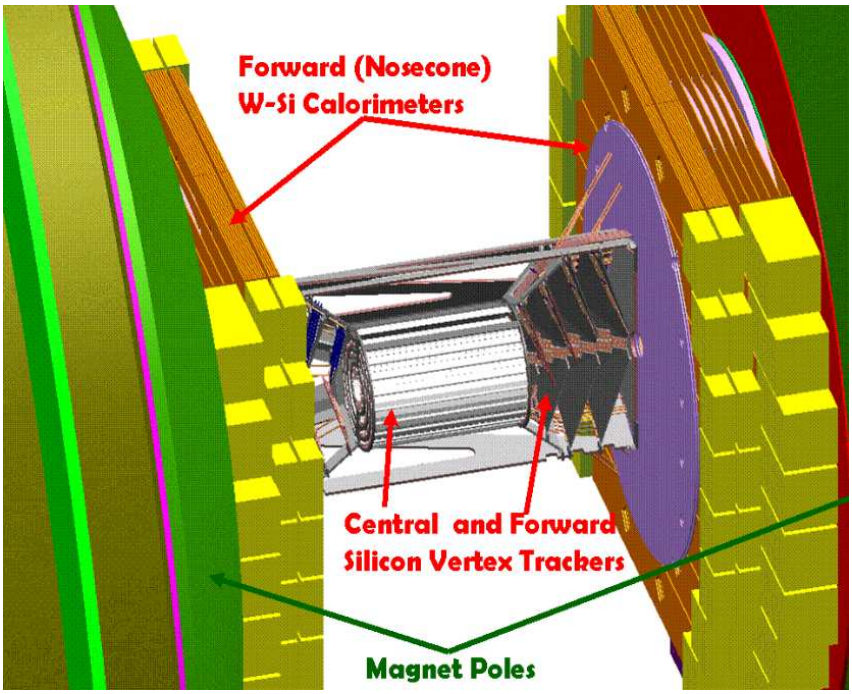

Fig. 1: The central region of the PHENIX detector after the addition of the barrel and endcap silicon vertex detectors and the Nose Cone Calorimeter.

The Silicon Vertex Detector (SVTX) consists of a central arm barrel and two endcap detectors, as shown in Fig. 1. The SVTX barrel will provide a displaced vertex resolution of ~ 50 μm. The SVTX endcaps will provide a displaced vertex resolution of $\sim$ 90 - 115 μm. Together, they will provide inner tracking with full azimuthal coverage for $|\eta| < 2.4$. By connecting to tracks in both the central and muon arms, the SVTX will tag heavy flavor decays by displaced vertices, improve the quarkonium invariant mass resolution and reduce backgrounds for heavy flavor measurements. In the muon arms, a loose displaced vertex cut will eliminate most muon tracks from light hadron decays and a very tight cut, $\sim 2\sigma$ will eliminate punch-through hadrons. The displaced vertex measurement will greatly help $D \rightarrow K\pi$ measurements in the central arms, presently very difficult in PHENIX, by reducing the contribution to the combinatorial background both from prompt tracks (tight vertex cut) and light meson decay tracks (loose cut of $\sim$ 1 cm). It will also reduce high p_T background tracks in the central arms due to misidentified light hadron decays by a loose displaced vertex cut. In addition to identifying semileptonic heavy flavor

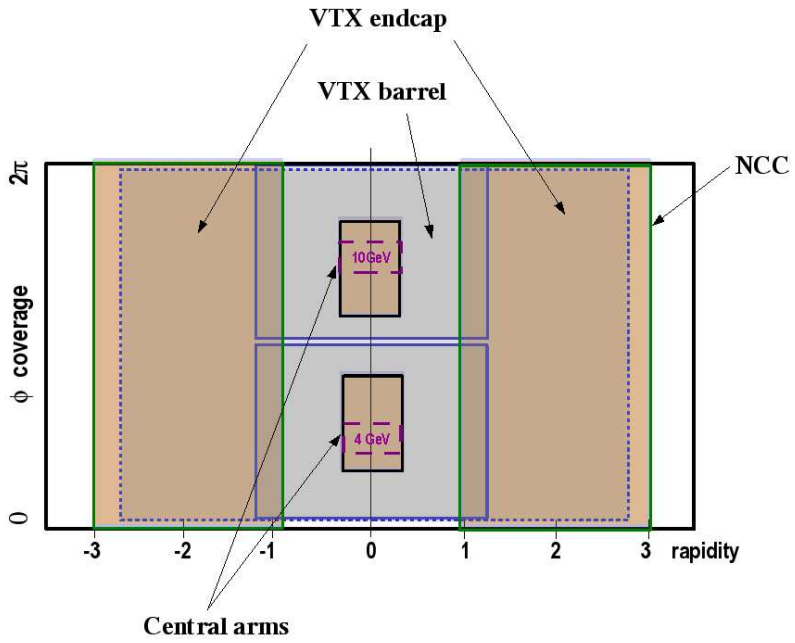

Fig. 2: The pseudorapidity and azimuthal angle coverage of the PHENIX barrel and endcap silicon vertex detectors, and of the Nose Cone Calorimeter.

decays, displaced vertex measurements can help identify J/ψ's from B meson decays since all other J/ψ's are prompt.

The SVTX barrel is presently under construction. It will consist of four concentric silicon layers. The two inner layers, at radii of 2.5 and 5.0 cm, consist of pixel detectors with a segmentation of 50 μm by 425 μm. The outer two layers, with radii of 10 and 14 cm, consist of 80 μm by 3 cm strips. The occupancy of the inner layer will be about 4.5% in central Au+Au collisions. The SVTX barrel produces a dramatic improvement in resolution of high p_T tracks in the central arms. The PHENIX Drift Chamber is outside the magnetic field so that, in the present momentum measurement, there is no information about the initial ϕ angle of the track. The momentum is calculated from the difference between the ϕ angle of the track after passing through the magnetic field and the ϕ angle from the vertex position to the Drift Chamber. This difference is only $\sim$ 40% of the total deflection in the field. By adding a precise measurement of the initial ϕ direction, the SVTX barrel directly measures the full deflection, improving the momentum resolution by a factor of $\sim$ 2.5, greatly improving the Υ invariant mass resolution. Installation of the barrel is expected in 2008.

The forward silicon detector endcaps will consist of four silicon mini-strip planes. The mini-strips have 50 μm pitch in the radial direction and lengths in the ϕ direction varying from 1.9 mm to 13.5 mm, depending on the polar angle. The maximum occupancy per strip is estimated to be less than 1.5% in central Au+Au collisions. The displaced vertex resolution of 90 - 115 μm, depending on the number of layers of silicon traversed by the track, should be compared to a mean vertex displacement of 785 μm for the boosted open charm muons. A prototype covering about 1/4 of one muon arm is presently under construction. Under ideal circumstances, the full SVTX endcaps could be constructed and installed by late FY 2008.

The PHENIX Nose Cone Calorimeters, tungsten-silicon calorimeters that will replace the two central arm magnet nosecones, will provide coverage for $0.9 < |\eta| < 3.5$. The simulated energy resolution for photons is $\sim 27\%/\sqrt{E}$ where E is in GeV. The Nose Cone Calorimeters will contain both electromagnetic and hadronic calorimeter sections. The electromagnetic calorimeter will contain a pre-

shower detector and a shower-max detector designed to discriminate between individual electromagnetic showers and overlapping photons from high momentum π^0 decays. The pre-shower and shower-max detectors are expected to resolve showers with separations down to 2 mm and 4 mm, respectively. The Nose Cone Calorimeters should thus provide good acceptance for $\chi_c \rightarrow J/\psi + \gamma$ decays.

The muon trigger upgrade is required for PHENIX to be able to take complete advantage of the RHIC II luminosity upgrade for muon arm measurements. The existing muon arm level-1 heavy vector meson triggers have enough rejection power to handle Au+Au collision rates of up to $\sim$ 20 KHz and pp collision rates of up to $\sim$ 0.5 MHz. The muon trigger upgrade adds three layers of Resistive Plate Chamber (RPC) detectors, with two dimensional (θ, ϕ) readout, in each muon arm. These layers follow the design of the CMS muon trigger at the LHC with the cathode pad segmentation optimized for the PHENIX environment. The front end electronics and trigger processors will be developed within PHENIX. The muon trigger upgrade will provide an online momentum measurement to improve the level-1 trigger rejection for both single muons (with a p_T cut) and muon pairs (with an invariant mass cut). It will also provide improved high multiplicity background rejection. The muon trigger upgrade is presently under construction.

2.2 STAR upgrades

While work on answering the questions discussed in this document are underway in STAR, to complete many of the challenging measurements, upgrades to the STAR detector are needed. The collaboration has planned a series of upgrades for the near and intermediate term to overcome the current shortcomings and enhance its heavy flavor capabilities. Implementation of these upgrades will also allow optimum utilization of the increased luminosity expected from RHIC II.

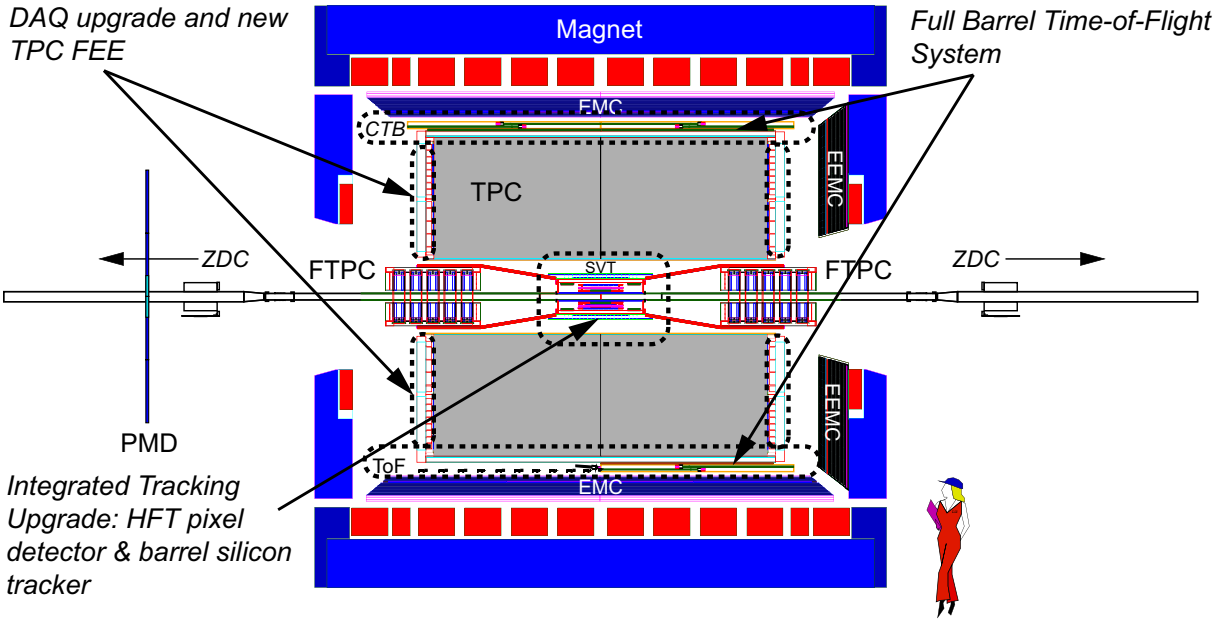

Fig. 3: Layout of the STAR experiment 2005/2006 [41]. The locations of the planned upgrades are enclosed by dashed lines. See text for details.

The current layout of the STAR detector is depicted in Fig. 3. The medium term upgrades to the detector relevant for heavy flavor physics include: a full barrel Time of Flight detector (TOF) replacing the current TOF patch and the Central Trigger Barrel (CTB); new front end electronics for the large Time Projection Chamber (TPC); an upgrade to the data acquisition system (DAQ-1000), and a tracking upgrade including a barrel section with two inner layers of silicon pixel sensors (HFT) and three layers of silicon strip detectors (IST).

The new time of flight system covering the full outer barrel of the TPC is planned for construction and installation in STAR over the next three years. The system uses the Multi-gap Resistive Plate Chamber (MRPC) technology developed at CERN and will consist of 3840 MRPC modules with 23,000 channels of readout. The modules will cover the TPC outer barrel ($-1 < \eta < 1$, $0 < \phi < 2\pi$) and will be mounted in 120 trays which will replace the existing CTB (Central Trigger Barrel scintillation counter) trays.

The TOF doubles the current momentum range over which π, K, and p can be identified and thus considerably improves the reconstruction of charm mesons and baryons. When the TOF measurement is combined with the TPC dE/dx measurement, electrons can be cleanly identified from the lowest momentum measured ($\sim$ 200 MeV/c) up to a few GeV/c. This capability complements the electromagnetic calorimeter which works well for momenta above $\sim$ 2 GeV/c. STAR will then be able to reconstruct soft to medium momentum electrons with high efficiency and purity, providing the capability to make a comprehensive J/ψ measurement. The TOF, in conjunction with the EMC, also allows STAR to implement a level-2 trigger scheme to select $J/\psi \rightarrow e^+e^-$decays in AA collisions.

A series of improvements to the STAR data acquisition system over the past several years has brought the capability from the original design rate of 1 Hz recorded events to 50-100 Hz. To acquire the very large data samples and high data rates needed for heavy flavor measurements, an upgrade has been initiated with the goal of achieving a recorded event rate of at least 1 kHz. This rate could produce data volumes which would significantly exceed the capacity for analysis and storage. The rare-trigger data sets will especially benefit from the upgrade since the pipelined architecture being implemented will virtually eliminate the front end dead time, allowing to make full use of rare event triggers such as the one for the Υ.

Th increase in readout speed can be achieved by replacing the TPC front end electronics, making use of circuits developed for the ALICE experiment at CERN, in conjunction with an upgrade of the STAR DAQ. In addition to the increased physics capabilities from the DAQ upgrade, the replacement of the TPC front end electronics, specifically the RDO boards that collect data from the FEE boards, will make space for a future precision tracking chamber between the TPC end planes and the endcap calorimeter. Replacing the TPC front end electronics also assures that this system will be maintainable for the next decade or more. The readout for the other existing detectors, which will remain in place for the RHIC II era, can be adapted to the new high speed DAQ with minor changes.

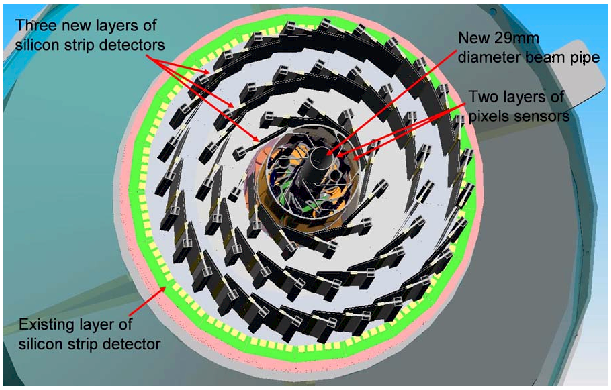

Fig. 4: Layout of the new inner tracker for STAR. End view of small radius beam pipe (1.4 cm radius), two layers of pixel sensor, three new layers of silicon strip sensors, and the existing layer of silicon strip sensor.

In order to address heavy quark energy loss and thermalization, it will be necessary to cleanly identify open charm. The recent results from both STAR and PHENIX on the suppression and flow of non-photonic electrons are intriguing. However, without an identified charm sample, the contributions from semileptonic bottom decays and systematic errors on background subtraction make a clear inter-

pretation of these results difficult. Measurement of the yields of various charm species will also allow a study of the charm hadrochemistry.

Efficient topological reconstruction of open charm decays requires tracking "point-back" resolution to the primary collision vertex of ~ 50 μm or less. Further, the beam pipe and innermost detector layers must be very thin to measure the low p_T particles which comprise the bulk of the cross section and thus minimize the systematic errors in extrapolating the measured yield to the total yield. A thin beam pipe and inner detector layers are also key elements in efficiently vetoing photon conversion electrons which, in combination with the electron identification from the TPC, TOF and electromagnetic calorimeter, will enable measurement of the soft lepton and dilepton spectra. STAR is thus developing a tracking upgrade for the central rapidity region ($-1 < \eta < 1, 0 < \phi < 2\pi$). The essential elements under consideration for this upgrade are a new thin, small-radius beam pipe (0.5 mm thick, 14 mm radius), two layers of thinned (50 μm) CMOS pixel detectors at average radii of 1.5 and 4.5 cm (HFT) and three layers of conventional silicon strip detectors at average radii of 10, 15 and 20 cm (IST), see Fig. 4. The existing layer of double-sided silicon strip sensors at a radius of 25 cm (SSD) will be kept. The three new layers of conventional silicon strip sensors (IST) will connect tracks from the TPC and SSD to hits in the pixel layers. These layers will replace the existing three layers of silicon drift detector (SVT). It will be necessary to replace the SVT since, when RHIC II becomes operational, the SVT will be over 10 years old with a readout too slow to be compatible with the upgraded DAQ. It also has a large amount of infrastructure (cables and cooling) that adds undesirable mass in the region $1 < \eta < 2$.

3. Projected RHIC II yields

In this section we present some estimates of the quality of the heavy flavor measurements that can be achieved at RHIC II luminosities with the upgraded detectors.

Table 1: The anticipated luminosity per week delivered by RHIC. The delivered luminosity has to be reduced by a factor that accounts for detector up time and collision vertex cuts imposed by the detectors. The RHIC I projected luminosities are maximum values achieved by 2008 taken from the RHIC Collider Accelerator Division projections. They represent the performance of a mature RHIC I accelerator. Because the length of the collision diamond is smaller for RHIC II, the gain in usable luminosity is larger than the ratio of delivered luminosities when going to RHIC II. There are no projections available for d+Au and Cu+Cu for RHIC I. The numbers in the "obtained" column are the best weekly luminosities from previous runs.

Species	Energy	Units	RHIC I Obtained/week	RHIC I Projected/week	RHIC II Projected/week
Au+Au	200	μb^{-1}	160	327	2500
Cu+Cu	200	nb^{-1}	2.4	–	25
d+Au	200	nb^{-1}	4.5	–	62
pp	200	pb^{-1}	0.9	26	33
pp	500	pb^{-1}	-	50	166

Table 1 is a summary of the weekly integrated luminosity estimates for RHIC and RHIC II. The weekly luminosity expectations are based on RHIC Collider Accelerator Division guidance. The projected weekly luminosities for RHIC II and for RHIC I in 2008 and beyond (projected RHIC I) are used to estimate the yields shown in later tables.

Table 2 summarizes the projected PHENIX yields for critical heavy flavor signals for the mature RHIC accelerator (in 2008 and beyond) and for a 12 week RHIC II physics run. Table 2 also includes the yields observed in recent RHIC runs. The yields are based on the following:

- The cross sections are taken from Ref. [42].
- The ψ' to J/ψ yield ratio is 0.14.
- The detector acceptances are from PHENIX simulations.
- For charmonia, the cross sections were reduced in Au+Au by a factor of 0.43, approximately accounting for the suppression measured by PHENIX in Au+Au collisions. for the Υ family, no suppression is assumed.
- The minimum bias trigger efficiency for hard processes is assumed to be 0.75 for pp and 0.92 for Au+Au.
- An additional realistic level-1 trigger efficiency of 0.8 is used, where appropriate.
- It is assumed that 80% of the RHIC beam is in the central bucket and thus usable by experiments.
- It is assumed that the root-mean square (RMS) of the collision diamond is 20 cm at RHIC and 10 cm at RHIC II.
- Use of the PHENIX vertex detector is assumed for the projected yields, requiring a collision vertex cut of ± 10 cm.
- A realistic pair-reconstruction efficiency is used (0.8 in pp and 0.4 in Au+Au collisions).
- An efficiency of 0.4 is assumed when using a displaced vertex cut of 1 mm to identify $B \rightarrow J/\psi$ decays.

Table 3 contains a summary of the projected yields from STAR for various critical heavy flavor signals for RHIC and RHIC II. The detector acceptances are from STAR simulations. Otherwise, the assumptions are identical to those used for the PHENIX yields presented in Table 2.

Table 2: The projected yields of several heavy flavor signals in PHENIX for 12 week physics runs at RHIC II and a mature RHIC I. The approximate yields obtained at RHIC to date are also shown. These reflect the fact that RHIC had not yet achieved the full luminosity development for Au+Au by Run 4, or for pp by Run 5. The yields are shown for both pp and Au+Au collisions at $\sqrt{s_{NN}} = 200$ GeV. The projected RHIC I and RHIC II values assume that the PHENIX SVTX detector is in place, limiting the usable collision vertex range to ± 10 cm. The SVTX detector has a much larger impact at RHIC I, where the collision diamond RMS is 20 cm, than at RHIC II where the collision diamond RMS is 10 cm.

Species	signal	$\|\eta\|$	To Date	Projected RHIC I	Projected RHIC II
pp	$J/\psi \to e^+e^-$	< 0.35	$\sim$ 1,000	25,000	55,000
	$J/\psi \to \mu^+\mu^-$	$1.2 - 2.4$	$\sim$ 10,000	208,000	470,000
	$\psi' \to e^+e^-$	< 0.35	–	440	990
	$\psi' \to \mu^+\mu^-$	$1.2 - 2.4$	–	3,700	8,500
	$\chi_c \to e^+e^-\gamma$	< 0.35	–	1,600	3,600
	$\chi_c \to \mu^+\mu^-\gamma$	$1.2 - 2.4$	–	62,000	139,000
	$\Upsilon \to e^+e^-$	< 0.35	–	90	200
	$\Upsilon \to \mu^+\mu^-$	$1.2 - 2.4$	$\sim$ 27	230	500
	$B \to J/\psi \to e^+e^-$	< 0.35	–	130	300
	$B \to J/\psi \to \mu^+\mu^-$	$1.2 - 2.4$	–	1,300	3,000
Au+Au	$J/\psi \to e^+e^-$	< 0.35	$\sim$ 800	3,300	45,00
	$J/\psi \to \mu^+\mu^-$	$1.2 - 2.4$	$\sim$ 7,000	29,000	395,00
	$\psi' \to e^+e^-$	< 0.35	–	60	800
	$\psi' \to \mu^+\mu^-$	$1.2 - 2.4$	–	520	7,100
	$\chi_c \to e^+e^-\gamma$	< 0.35	–	220	2,900
	$\chi_c \to \mu^+\mu^-\gamma$	$1.2 - 2.4$	–	8,600	117,000
	$\Upsilon \to e^+e^-$	< 0.35	–	30	400
	$\Upsilon \to \mu^+\mu^-$	$1.2 - 2.4$	–	80	1,040
	$B \to J/\psi \to e^+e^-$	< 0.35	–	40	570
	$B \to J/\psi \to \mu^+\mu^-$	$1.2 - 2.4$	–	420	5,700

Table 3: The projected yields of several heavy flavor signals in STAR for 12 week physics runs at RHIC II and a mature RHIC I. The approximate yields obtained at RHIC to date are also shown. The projected RHIC I and RHIC II values assume that the STAR Heavy Flavor Tracker is in place, limiting the usable collision vertex range to ± 10 cm. The $D \to K\pi$ yields assume 100 Hz of recorded minimum bias data.

Species	signal	$\|\eta\|$	To Date	Projected RHIC I	Projected RHIC II
pp	$J/\psi \to e^+e^-$	< 1.0	–	1,260,000	1,600,000
	$\psi' \to e^+e^-$		–	23,000	29,000
	$\Upsilon \to e^+e^-$		–	6,600	8,300
	$B \to J/\psi \to e^+e^-$		–	15,000	19,000
Au+Au	$J/\psi \to e^+e^-$	< 1.0	?	16,000	220,000
	$\psi' \to e^+e^-$		–	300	4,000
	$\Upsilon \to e^+e^-$		?	830	11,200
	$B \to J/\psi \to e^+e^-$		–	190	2,500
	$D \to K\pi$		–	30,000	30,000

Table 4: Projected heavy flavor yields in PHENIX and STAR for 12 weeks of $\sqrt{s_{NN}} = 500$ GeV pp running at RHIC II and a mature RHIC I. The projected RHIC I and RHIC II values assume that both the the PHENIX SVTX detector and STAR HF tracker are in place, limiting the usable collision vertex range to ± 10 cm. These detectors have a much larger impact at RHIC I, where the collision diamond RMS is 20 cm, than at RHIC II where the collision diamond RMS is 10 cm.

Experiment	signal	$\|\eta\|$	Projected RHIC I	Projected RHIC II
PHENIX	$J/\psi \to e^+e^-$	< 0.35	183,000	600,000
	$J/\psi \to \mu^+\mu^-$	$1.2 - 2.4$	1,650,000	5,500,000
	$\psi' \to e^+e^-$	< 0.35	3,300	11,000
	$\psi' \to \mu^+\mu^-$	$1.2 - 2.4$	30,000	100,000
	$\chi_c \to e^+e^-\gamma$	< 0.35	31,000	100,000
	$\chi_c \to \mu^+\mu^-\gamma$	$1.2 - 2.4$	1,200,000	4,800,000
	$\Upsilon \to e^+e^-$	< 0.35	900	3000
	$\Upsilon \to \mu^+\mu^-$	$1.2 - 2.4$	2,300	7,700
	$B \to J/\psi \to e^+e^-$	< 0.35	2,300	7,700
	$B \to J/\psi \to \mu^+\mu^-$	$1.2 - 2.4$	23,000	77,000
STAR	$J/\psi \to e^+e^-$	< 1.0	3,700,000	12,000,000
	$\psi' \to e^+e^-$		76,000	220,000
	$\Upsilon \to e^+e^-$		25,000	84,000
	$B \to J/\psi \to e^+e^-$		346,000	1,100,000

Table 5: The estimated heavy flavor yields in the LHC experiments for a 10^6 s Pb+Pb run with 500 μb^{-1} integrated luminosity (the planning numbers for one year). The estimates were all reported by the LHC experiments. As for the RHIC tables, the Υ rates are for all three states. The range of J/ψ values for ATLAS corresponds to different assumptions about trigger thresholds.

Species	signal	ALICE	$\|\eta\|$	CMS	$\|\eta\|$	ATLAS	$\|\eta\|$
Pb+Pb	$J/\psi \to \mu^+\mu^-$	740,000	$2.5 - 4$	24,000	< 2.4	8K-100K	< 2.5
	$J/\psi \to e^+e^-$	9,500	< 0.9				
	$\psi' \to \mu^+\mu^-$	14,000	$2.5 - 4$	440	< 2.4	1,400-1,800	< 2.5
	$\psi' \to e^+e^-$	190	< 0.9				
	$\Upsilon \to \mu^+\mu^-$	8,400	$2.5 - 4$	26,000	< 2.4	15,000	< 2.5
	$\Upsilon \to e^+e^-$	2,600	< 0.9				
	$D \to K\pi$	8,000	< 0.9				

Table 4 contains a summary of expected heavy flavor yields at $\sqrt{s} = 500$ GeV for PHENIX and STAR. Although not directly comparable with heavy ion yields from collisions at $\sqrt{s_{NN}} = 200$ GeV, the order of magnitude larger heavy flavor yields at 500 GeV should help understand the reaction mechanisms in pp collisions.

Table 5 contains a summary of the projected yields from the LHC detector collaborations for various critical heavy flavor signals in a $\sqrt{s_{NN}} = 5.5$ TeV Pb+Pb run of 10^6 s, the standard planning number for a year of running [43, 44, 45]. Note that the estimates by the LHC collaborations generally assume more optimistic reconstruction efficiencies than those used for the RHIC detectors.

Comparison of Tables 2, 3 and 5 reveal that the projected heavy flavor yields for one year of running are similar at the LHC and at RHIC II. The much larger heavy flavor cross sections at the higher LHC energy are largely compensated at RHIC II by the integrated luminosities that result from three times longer runs and an order of magnitude higher luminosity.

4. Open heavy flavor

In this section we present a more detailed discussion of the theoretical motivation for studying open heavy flavor in heavy ion collisions, of the present experimental and theoretical status, and of the proposed experimental program of open heavy flavor measurements at RHIC II.

As described in the Introduction, dense matter effects in nuclear collisions may change the kinematic distributions and the total cross sections of open heavy flavor production. Effects such as energy loss and flow can significantly modify the heavy flavor p_T distributions but do not, in fact, change the total yields. In a finite acceptance detector, however, the measured yields may appear to be enhanced or suppressed, depending on the acceptance. Energy loss steepens the slope of the heavy flavor p_T distribution because the heavy quark p_T is reduced. If the momentum is reduced sufficiently for the quarks to be stopped within the medium, the heavy quarks can take the same velocity as the surrounding medium and 'go with the flow'. The first RHIC results on R_{AA} and v_2 for heavy flavor decays to leptons show that these effects are indeed important for charm quarks. However, higher p_T measurements and reconstructed charm hadrons are needed to solidify and quantify the results. In addition, reconstructed bottom measurements are necessary to cleanly separate leptons from charm and bottom decays to determine the bottom quark's importance in the measured electron R_{AA}.

Effects that may modify the total heavy flavor yields are the initial parton distributions in the nuclei and secondary charm production in the medium. The parton distribution functions needed for perturbative QCD calculations of heavy flavor production are modified in the nucleus, as was observed in nuclear deep-inelastic scattering [46]. At very small momentum fractions, x, the gluon fields may be treated as classical color fields. The modifications of the parton distributions in nuclei relative to free protons would affect the total yields. The effect is expected to be small at mid rapidity and moderate p_T at RHIC but is likely to be more important at large rapidity, where lower x values are probed. Although thermal charm production from the medium is likely to be small at RHIC energies, it could moderately enhance the total yields.

Since the J/ψ yields may be enhanced in nuclear collisions due to coalescence of uncorrelated c and $\overline{c}$ quarks in the medium, it is important for charmonium production in heavy ion collisions to be properly normalized. The ratio of J/ψ to open charm production in pp collisions is not a strong function of energy. Thus the total charm yield sets the scale against which J/ψ suppression relative to enhancement can be quantified. The production of J/ψ through $c\overline{c}$ coalescence is discussed in more detail in the section on quarkonium.

4.1 Open Heavy Flavor Theoretical Results

4.11 Theoretical Baseline Results

We now discuss the most recent theoretical baseline calculations of the transverse momentum distributions of charm and bottom quarks, the charm and bottom hadron distributions resulting from fragmentation and, finally, the electrons produced in semileptonic decays of the hadrons [1].

The theoretical prediction of the electron spectrum includes three main components: the p_T and rapidity distributions of the heavy quark Q in pp collisions at $\sqrt{s} = 200$ GeV, calculated in perturbative QCD; fragmentation of the heavy quarks into heavy hadrons, H_Q, described by phenomenological input extracted from e^+e^- data; and the decay of H_Q into electrons according to spectra available from other measurements. This cross section is schematically written as

$$\frac{Ed^3\sigma(e)}{dp^3} = \frac{E_Q d^3\sigma(Q)}{dp_Q^3} \otimes D(Q \to H_Q) \otimes f(H_Q \to e) \quad (1)$$

where the symbol $\otimes$ denotes a generic convolution. The electron decay spectrum, $f(H_Q \to e)$, accounts for the branching ratios.

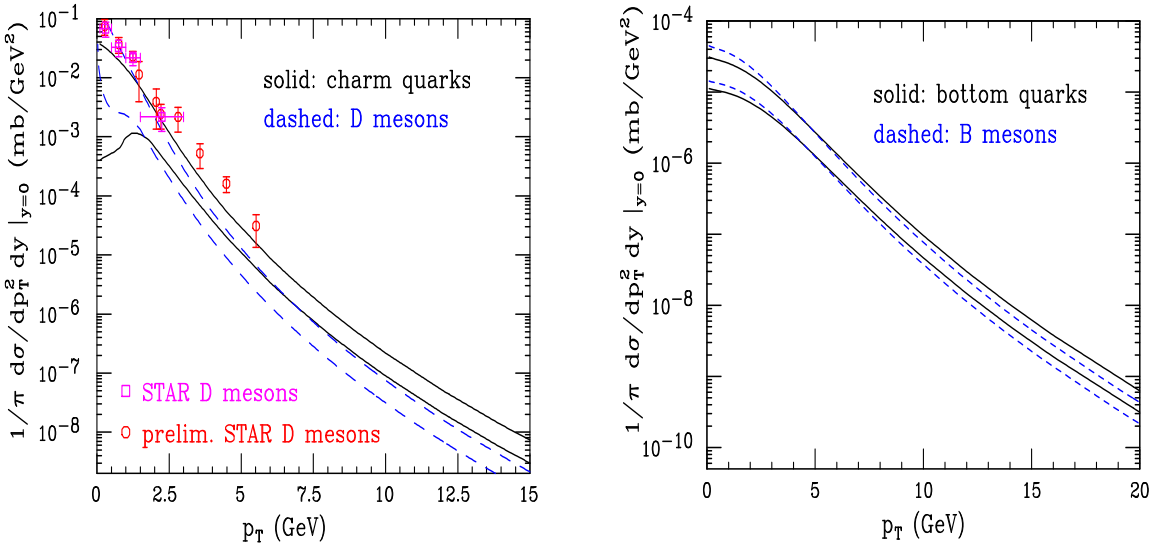

Fig. 5: Left-hand side: The theoretical uncertainty bands for c quark and D meson p_T distributions in pp collisions at $\sqrt{s}$ = 200 GeV, using BR($c \to D$) = 1. The final [47] and preliminary [48] STAR d+Au data (scaled to pp using $N_{\rm coll}$ = 7.5) are also shown. Right-hand side: The same for b quarks and B mesons.

The distribution $Ed^3\sigma(Q)/dp_Q^3$ is evaluated at Fixed-Order plus Next-to-Leading-Log (FONLL) level [49]. In addition to including the full fixed-order NLO result [50, 51], the FONLL calculation also resums [52] large perturbative terms proportional to $\alpha_s^n \log^k(p_T/m)$ to all orders with next-to-leading logarithmic (NLL) accuracy (i.e. $k = n, n-1$) where m is the heavy quark mass. The perturbative parameters are m and the value of the strong coupling, α_s. The central heavy quark masses are m_c = 1.5 GeV/$c^2$and m_b = 4.75 GeV/c^2. The masses are varied in the range $1.3 < m_c < 1.7$ GeV/$c^2$for charm and $4.5 < m_b < 5$ GeV/$c^2$for bottom to estimate the mass uncertainties. The five-flavor QCD scale is the CTEQ6M value, $\Lambda^{(5)}$ = 0.226 GeV. The perturbative calculation also depends on the factorization (μ_F) and renormalization (μ_R) scales. The scale sensitivity, a measure of the perturbative uncertainty, is calculated using $\mu_{R,F}^2 = \mu_0^2 = p_T^2 + m^2$ as the central value while varying μ_F and μ_R independently within a 'fiducial' region defined by $\mu_{R,F} = \xi_{R,F}\mu_0$ with $0.5 \le \xi_{R,F} \le 2$ and $0.5 \le \xi_R/\xi_F \le 2$ so that $\{(\xi_R, \xi_F)\}$ = {(1,1), (2,2), (0.5,0.5), (1,0.5), (2,1), (0.5,1), (1,2)}. The envelope containing the resulting curves defines the uncertainty. The mass and scale uncertainties are added in quadrature.

These inputs lead to a FONLL total $c\bar{c}$ cross section in pp collisions of $\sigma_{c\bar{c}}^{\rm FONLL} = 256^{+400}_{-146}$ μb at $\sqrt{s}$ = 200 GeV. The theoretical uncertainty is evaluated as described above. The corresponding NLO prediction is 244^{+381}_{-134} μb. The predictions in Ref. [9], using m_c = 1.2 GeV/$c^2$and $\mu_R = \mu_F = 2\mu_0$ gives $\sigma_{c\bar{c}}^{\rm NLO} = 427$ μb, within the uncertainties. Since the FONLL and NLO calculations tend to coincide at small p_T, which dominates the total cross section, the two results are very similar. Thus the two calculations are equivalent at the total cross section level, within the large perturbative uncertainties. The total cross section for bottom production is $\sigma_{b\bar{b}}^{\rm FONLL} = 1.87^{+0.99}_{-0.67}$ μb.

The fragmentation functions, $D(c \to D)$ and $D(b \to B)$, where D and B indicate a generic admixture of charm and bottom hadrons, are consistently extracted from e^+e^- data in the FONLL context [53].

The measured spectra for primary $B \to e$ and $D \to e$ decays are assumed to be equal for all bottom and charm hadrons, respectively. The contribution of electrons from secondary B decays, $B \to D \to e$, was obtained by convoluting the $D \to e$ spectrum with a parton-model prediction of $b \to c$ decay. The resulting electron spectrum is very soft, giving a negligible contribution to the total. The decay spectra are normalized using the branching ratios for bottom and charm hadron mixtures [54]:

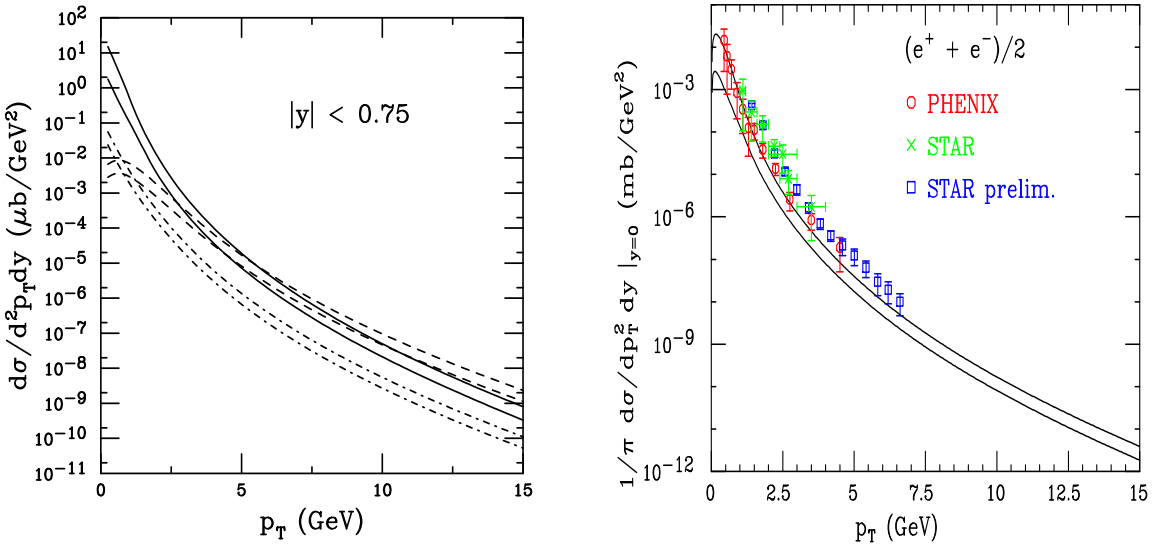

Fig. 6: Left-hand side: The theoretical uncertainty bands for $D \to e$ (solid), $B \to e$ (dashed) and $B \to D \to e$ (dot-dashed) as a function of p_T in $\sqrt{s} = 200$ GeV pp collisions for $|y| < 0.75$. Right-hand side: The final electron uncertainty band in pp collisions is compared to the PHENIX [55] and STAR (final [47] and preliminary [48]) data.

BR$(B \to e) = 10.86 \pm 0.35\%$, BR$(D \to e) = 10.3 \pm 1.2\%$, and BR$(B \to D \to e) = 9.6 \pm 0.6\%$.

The left-hand side of Fig. 5 shows the theoretical uncertainty bands for c quarks and D mesons, obtained by summing the mass and scale uncertainties in quadrature. The band is broader at low p_T due to the large value of α_s and the behavior of the CTEQ6M parton densities at low scales as well as the increased sensitivity of the cross section to the charm quark mass. The rather hard fragmentation function causes the D meson and c quark bands to separate only at $p_T > 9$ GeV/c. The right-hand side of Fig. 5 shows the same results for b quarks and B mesons. The harder $b \to B$ fragmentation function causes the two bands to partially overlap until $p_T \simeq 20$ GeV/c.

Figure 6 shows the individual uncertainty bands for the $D \to e$, $B \to e$ and $B \to D \to e$ decays to electrons on the left-hand side and compares the RHIC data to the total band on the right-hand side. The upper and lower limits of the total band are obtained by summing the upper and lower limits for each component. The secondary $B \to D \to e$ spectrum is extremely soft, only exceeding the primary $B \to e$ decays at $p_T < 1$ GeV/c. It is always negligible with respect to the total yield. While, for the central parameter sets, the $B \to e$ decays begin to dominate the $D \to e$ decays at $p_T \simeq 4$ GeV/c, a comparison of the bands shows that the crossover may occur over a rather broad range of electron p_T, assuming that the two bands are uncorrelated.

4.2 Models of Heavy Quark Energy Loss

While the heavy quarks are in the medium, they can undergo energy loss by two means: elastic collisions with light partons in the system (collisional) and gluon bremsstrahlung (radiative). We will briefly review some of the predicted results for $-dE/dx$ of heavy quarks for both collisional and radiative loss. We then show the predicted effect on the charm and bottom contributions to single electrons at RHIC [4].

The collisional energy loss of heavy quarks through processes such as $Qg \to Qg$ and $Qq \to Qq$ depends logarithmically on the heavy quark momentum, $-dE/dx \propto \ln(q_{\max}/q_{\min})$. Treatments of the collisional loss vary with the values assumed or calculated for the cutoffs. These cutoffs are sensitive to the energy of the heavy quark and the temperature and strong coupling constant in the medium. Thus the quoted value of the energy loss is usually for a certain energy and temperature. The calculation was first done by Bjorken [56] who found $-dE/dx \approx 0.2$ GeV/fm for a 20 GeV quark at $T = 250$ MeV.

Further work refined the calculations of the cutoffs [57, 58, 59], with similar results. Braaten and Thoma calculated the collisional loss in the limits $E \ll m_Q^2/T$ and $E \gg m_Q^2/T$ in the hard thermal loop approximation, removing the cutoff ambiguities. They obtained $-dE/dx \approx 0.3$ GeV/fm for a 20 GeV charm quark and 0.15 GeV/fm for a 20 GeV bottom quark at $T = 250$ MeV [61].

Other models of heavy quark energy loss were presented in the context of J/ψ suppression: Could a produced $c\overline{c}$ pair stay together in the medium long enough to form a J/ψ? Svetitsky [62] calculated the effects of diffusion and drag on the $c\overline{c}$ pair in the Boltzmann approach and found a strong effect. The drag stopped the $c\overline{c}$ pair after traveling about 1 fm but Brownian diffusion drove them apart quickly. The diffusion effect increased at later times. Svetitsky essentially predicted that the heavy quarks would be stopped and then go with the flow. His later calculations of D meson breakup and rehadronization [10] while moving through plasma droplets reached a similar conclusion. Koike and Matsui calculated energy loss of a color dipole moving through a plasma using kinetic theory and found $-dE/dx \sim 0.4 - 1.0$ GeV/fm for a 10 GeV $Q\overline{Q}$ [63]. The collisional loss was thus predicted to be small, less than 1 GeV/fm for reasonable assumptions of the temperature. The loss increases with energy and temperature. Using the hard thermal loop approach, Mustafa *et al.* found $-dE/dx \approx 1 - 2$ GeV/fm for a 20 GeV quark at $T = 500$ MeV [64].

The first application of radiative loss to heavy quarks was perhaps by Mustafa *et al.* [64]. They included the effects of only a single scattering/gluon emission, $Qq \to Qqg$ or $Qg \to Qgg$. In this case, the loss grows as the square of the momentum logarithm, $\ln^2(q_{\max}/q_{\min})$, one power more than the collisional loss, but is of the same order in the strong coupling constant [61]. Thus the radiative loss is guaranteed to be larger than the collisional in this approximation. The heavy quark mass enters their expressions only in the definition of $q_{\max}$ so that the mass dependence of the energy loss is rather weak. They found, for a 20 GeV quark at $T = 500$ MeV, $-dE/dx \approx 12$ GeV/fm for charm and 10 GeV/fm for bottom.

These large values suggested that energy loss could be quite important for heavy quarks. If true, there would be a strong effect on the $Q\overline{Q}$ contribution to the dilepton continuum. Shuryak [65] was the first to consider this possibility for AA collisions. He assumed that low mass $Q\overline{Q}$ pairs would be stopped in the medium, substantially suppressing the dilepton contribution from these decays. However, the stopped heavy quarks should at least expand with the medium rather than coming to rest, as discussed by Svetitsky [62]. Lin *et al.* then calculated the effects of energy loss at RHIC, including thermal fluctuations, for constant $-dE/dx = 0.5 - 2$ GeV/fm [8]. These results showed that the heavy quark contributions to the dilepton continuum would be reduced albeit not completely suppressed. In any case, the energy loss does not affect the total cross section. The heavy quarks are thus piled up at low p_T and midrapidity if stopped completely.

Dokshitzer and Kharzeev pointed out that soft gluon radiation from heavy quarks is suppressed at angles smaller than $\theta_0 = m_Q/E$ [7]. Thus bremsstrahlung is suppressed for heavy quarks relative to light quarks by the factor $(1 + \theta_0^2/\theta^2)^{-2}$, the 'dead cone' phenomenon. The radiative energy loss of heavy quarks could then be quite small. However, Armesto *et al.* [6] later showed that medium-induced gluon radiation could 'fill the dead cone', leading to non-negligible energy loss for heavy flavors. They also found that the energy loss would be larger for charm than bottom quarks.

So far the RHIC heavy ion measurements are not for heavy flavored hadrons but for the electrons from their semileptonic decays. If the effects of energy loss are substantially different for charm and bottom quarks, then the results in Fig. 6 which show that, at high p_T, the single electron spectrum is dominated by b decays, would suggest that, if charm quarks lose more energy than bottom quarks, b-quark dominance of the electron spectra would begin at smaller values of electron p_T in AA collisions. This would, in turn, limit the electron suppression factor, R_{AA}, at moderate p_T since the large bottom contribution would make R_{AA} larger than expected if the spectrum arose primarily from charm quark

[0]His drag coefficient $A(p^2)$ is related to the energy loss per unit length through $A(p^2) = (-dE/dx)/p^2$.

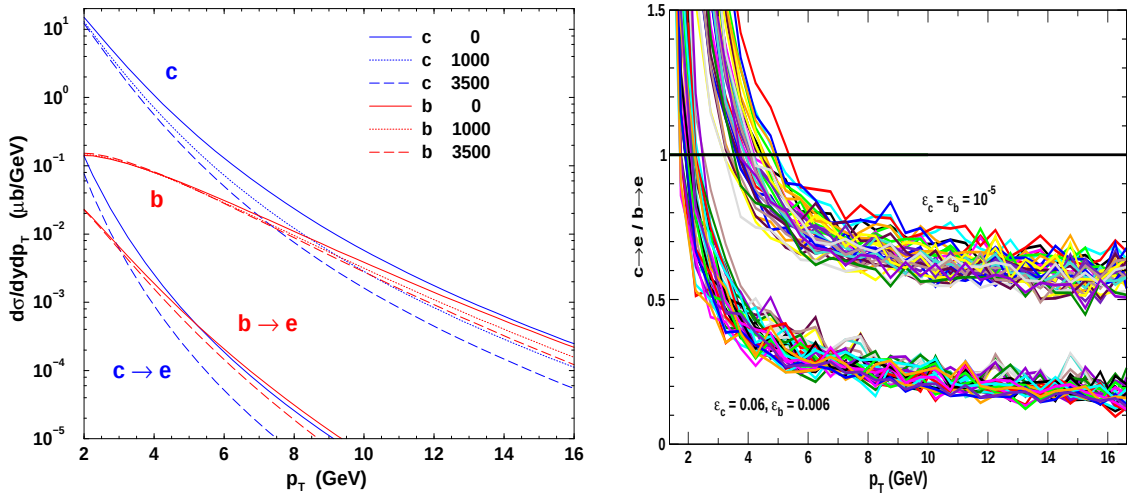

Fig. 7: Left-hand side: The differential cross section (per nucleon pair) of charm and bottom quarks calculated to NLO in QCD [1] compared to single electron distributions calculated with the fragmentation and decay scheme of Ref. [1]. The solid, dotted and long dashed curves show the effects of heavy quark energy loss with initial gluon rapidity densities of $dN_g/dy = 0, 1000,$ and 3500, respectively. Right-hand side: The ratio of charm to bottom decays to electrons obtained by varying the quark masses and scale factors. The effect of changing the Peterson function parameters from $\epsilon_c = 0.06$, $\epsilon_b = 0.006$ (lower band) to $\epsilon_c = \epsilon_b = 10^{-5}$ (upper band) is also illustrated for correlated b and c scales. From Ref. [4].

decays. Recent calculations [60] have revisited the importance of elastic energy loss and have shown that this component may make a larger contribution to the suppression factor than previously expected.

The left-hand side of Fig. 7 compares the c and b distributions at mid rapidity, as well as their contributions to single electrons. Single electrons from bottom dominate the single electron spectra at $p_T \sim 5$ GeV/$c$for all gluon rapidity densities. This conclusion is further supported by the right-hand side of Fig. 7, where the ratio of charm relative to bottom decays to electrons is shown. The crossover region here is rather narrow because μ_F and μ_R are correlated for c and b. In all cases, the bottom contribution to single electrons is large and cannot be neglected in the computation of single electron suppression, shown in Fig. 8. Since bottom energy loss is greatly reduced relative to charm [4], the possible effect on the electron spectrum is reduced, leading to $R_{AA}(p_T < 6 \text{ GeV}/c;\ e) > 0.5 \pm 0.1$. A calculation by Armesto *et al.*, with a somewhat different model of energy loss, showed similar results to those in Fig. 8.

Recently two groups, Moore and Teaney [66] and Rapp *et al.* [67, 68] have calculated R_{AA} and the non-photonic electron elliptic flow, v_2, in a Langevin model of the time evolution of heavy quarks in the medium. Both these groups emphasize that elastic (collisional) energy loss should be important at low p_T relative to radiative loss since the boost for heavy flavor hadrons in the medium should not be large. Both also find a strong correlation between R_{AA} and v_2. The approaches differ somewhat but the trends are similar in the two calculations.

Moore and Teaney [66] calculate the diffusion and drag coefficients for charm quarks in perturbative QCD. The diffusion coefficient is proportional to the inverse square of the strong coupling constant, α_s, *e.g.* $D(2\pi T) \propto \alpha_s^{-2}$. They present the effects of a range of values for $D(2\pi T)$ on R_{AA} and v_2, finding the largest effects at high p_T for small $D(2\pi T)$, corresponding to large α_s or strong coupling in the plasma.

Rapp *et al.* [67, 68] calculated the diffusion and drag coefficients assuming that resonant D and B states in the QGP elastically scatter in the medium. Resonance scattering reduces the thermalization times for heavy flavors relative to those calculated with perturbative QCD matrix elements for fixed $\alpha_s = 0.4$. The effect is larger for charm than for the more massive bottom quarks. Including these states thus reduces the electron R_{AA} at high p_T relative to the results in Ref. [4] while increasing the electron v_2 to $\sim 10\%$ at $p_T \sim 2$ GeV/c, in relative agreement with the data.

Thus, given sufficiently strong coupling and/or resonant states, both R_{AA} and v_2 can be described

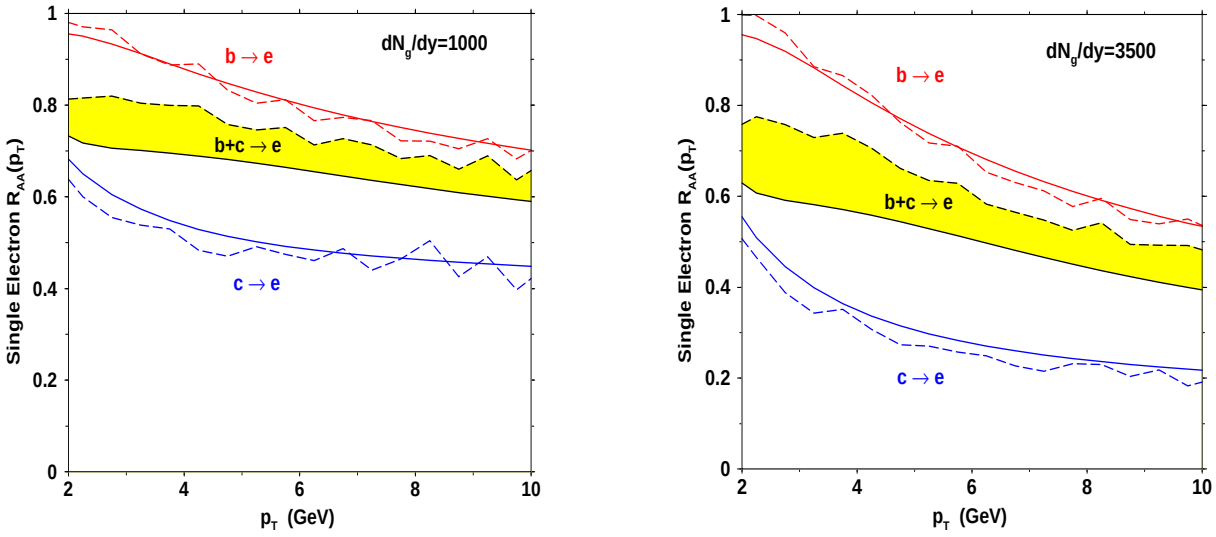

Fig. 8: Single electron attenuation pattern for $dN_g/dy = 1000$, left, and $dN_g/dy = 3500$, right. The solid curves employ the fragmentation scheme and lepton decay parameterizations of Ref. [1] while the dashed curves use the Peterson function with $\epsilon_c = 0.06$ and $\epsilon_b = 0.006$ and the decay to leptons employed by the PYTHIA Monte Carlo. Even for the extreme case on the right, the less quenched b quarks dilute R_{AA} so much that the modification of the combined electron yield from both c and b decays does not fall below $\sim 0.5 - 0.6$ near $p_T \sim 5$ GeV/c. From Ref. [4].

within transport approaches using elastic scattering. More and better data is necessary to distinguish the two approaches.

4.3 Open heavy flavor measurements to date at RHIC

Open heavy flavor production cross sections can be measured by reconstructing the invariant mass of the heavy quark hadron from its hadronic decay products or by detecting leptons from semileptonic decays of those hadrons. While both PHENIX and STAR can measure heavy flavor cross sections by either technique, PHENIX has some advantages for semileptonic decay measurements and STAR has advantages for the hadronic decay measurements.

In both cases, the signal to background rate can be greatly improved if a precise measurement of the decay vertex position is available since hadrons containing c or b quarks typically travel several hundred microns from the collision point before decaying. Both PHENIX and STAR have plans to add secondary vertex detectors capable of the necessary precision but they will not be implemented for several years. In addition to reducing the background rates for open heavy flavor decays to leptons and hadrons, the secondary vertex detectors open up the possibility of a clean bottom cross section measurement using displaced vertex J/ψ decays.

Open heavy flavor cross section measurements based on semileptonic decays of charm and bottom mesons are feasible because a small lepton signal can be identified in a very large hadron background. In addition, background lepton sources are both small and well enough understood that they can be subtracted to get the open heavy flavor signal. However a disadvantage of semileptonic decay measurements is the loss of information about the decaying heavy meson due to the recoil kinematics. As a consequence, charm and bottom decays cannot easily be distinguished. Open charm measurements using hadronic decay products have two advantages: the D meson kinematic properties are reconstructed and separation of charm from bottom is far easier because only a small fraction of D mesons arise from bottom decays [1]. A disadvantage of hadronic decay measurements is the huge combinatorial background in heavy ion collisions.

PHENIX has measured open heavy flavor yields via semileptonic decays to electrons at mid rapid-

ity ($|\eta| < 0.35$) using the Ring Imaging Cerenkov detector and electromagnetic calorimeter for electron identification. At forward and backward rapidity ($1.2 < |\eta| < 2.2$) the two muon spectrometers are used. PHENIX results are available for pp at mid rapidity [69] and forward rapidity [70] as well as for d+Au [71] and Au+Au at mid rapidity [31]. No open charm results from hadronic decays have yet been reported by PHENIX since the small central arm acceptance is a disadvantage for such measurements.

STAR has measured open heavy flavor yields at mid rapidity ($|\eta| < 1.0$) via semileptonic decays using either a combination of the time projection chamber (TPC) and time of flight (TOF) for electron identification or a combination of the TPC and the electromagnetic calorimeter. The backgrounds that must be subtracted are much larger than they are for PHENIX because of the larger photon conversion rates in STAR and the lack of of a hadron blind electron identifier, but this is compensated somewhat by the larger acceptance. STAR electron results are available for pp [47], d+Au [47] and Au+Au collisions [32]. STAR has also measured open charm yields in the range $|\eta| < 1.0$ through hadronic D meson decays [47] for d+Au collisions.

Because the charm cross section is much larger than the bottom cross section at RHIC and dominates the semileptonic decay spectrum for $p_T < 2.5\ \mathrm{GeV}/c$, the integrated non-photonic lepton spectrum is usually assumed to be equal to the charm cross section.

4.31 Baseline measurements

Before any conclusions can be drawn about the hot, dense final state from the results for heavy ion collisions, some baseline information is needed. Data from pp collisions are needed to establish the underlying cross sections and kinematic distributions for open heavy flavor. Also, pA data are needed to isolate effects due to gluon saturation and the intrinsic k_T distributions in the colliding nuclei.

Both PHENIX and STAR have measured the charm production cross section at mid rapidity. These measurements have been extrapolated to all rapidities to yield total cross sections. These total cross sections are compared to each other, to results at other energies, and to pQCD calculations in Fig. 9. Results for d+Au and Au+Au collisions are scaled by the number of binary collisions (N_{coll}) for direct comparison to the pp results. The STAR data points are from combined fits to hadronic decay and semileptonic decay data. The PHENIX points are from semileptonic decay measurements only.

Although the STAR values are somewhat higher than those for PHENIX, the total charm cross sections are in acceptable agreement within the fairly large systematic uncertainties, as can be seen more clearly in Fig. 10, discussed later. The p_T-dependent slopes at mid rapidity are in good agreement for pp collisions [72].

Since charm and bottom quarks are expected to be produced only in the initial nucleon-nucleon interactions, their yield should scale as the number of binary collisions, N_{coll}. Figure 10 shows the PHENIX measurement of the charm invariant yield in Au+Au collisions, scaled by N_{coll}, at mid rapidity as a function of N_{coll} [31]. The pp invariant yields from PHENIX [69] and the STAR invariant d+Au [47] and minimum bias Au+Au yields [32] are also shown. The PHENIX data are consistent with no N_{coll} dependence, as expected. As mentioned previously, the STAR yields are somewhat higher but, within the systematic uncertainties, the two experiments are in acceptable agreement. The linear fits shown in the figure are attempts to quantify deviations from a result independent of N_{coll}. The slope fit to the PHENIX data is not significant within errors.

Note that because these yields are integrated over all p_T, no modification of the charm p_T distributions in the final state medium can be determined from these data. The p_T-dependent effects are discussed in the following section.

A NLO pQCD theoretical uncertainty band [1] is also shown in Fig. 10. While the data tend to lie above the calculation, they agree within the limits of their systematic uncertainties.

Unlike J/ψ measurements, the current d+Au and pp open heavy flavor results are not precise enough for any conclusions to be drawn about either shadowing or k_T broadening. Obtaining meaningful

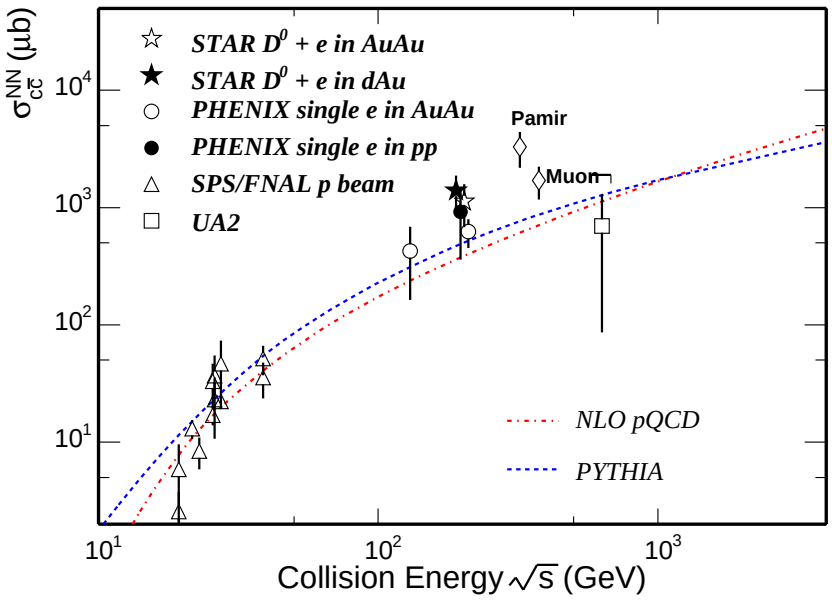

Fig. 9: Comparison of total cross section measurements. The STAR and PHENIX results are given as cross section per binary collisions [72]. The theory curves are from Ref. [47]. The NLO pQCD calculation uses parameters optimized using the low energy data [9].

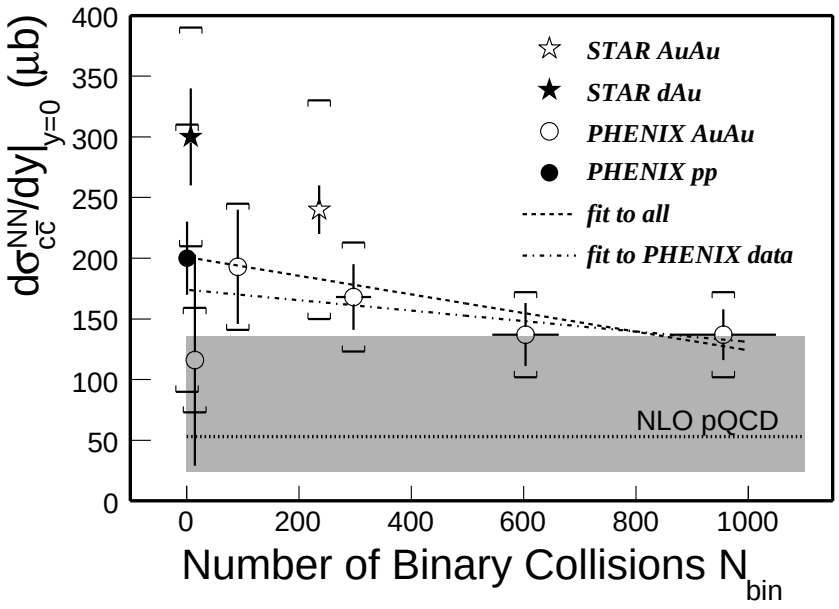

Fig. 10: Comparison of STAR and PHENIX measurements of the mid rapidity invariant charm yields scaled by $N_{\rm coll}$ as a function of $N_{\rm coll}$ [72].

open heavy flavor baseline results is an important priority for the RHIC program over the next few years.

4.32 Heavy ion measurements

Both PHENIX and STAR presented striking preliminary results on suppression of single electrons from open heavy flavor decays in central Au+Au collisions at Quark Matter 2005. PHENIX also showed preliminary results for the electron v_2 (elliptic flow parameter) from open heavy flavor decays

Nuclear modification factors for electrons from semileptonic decays of open heavy flavor in Au+Au central collisions from PHENIX [14] and STAR [32] are compared to theory calculations in Fig. 11 [72]. The data from the two experiments are in reasonable agreement. Both show strong suppression in central collisions at high p_T. The suppression factor, R_{AA}, is 0.2-0.3, similar to that seen for light quark hadrons [73].

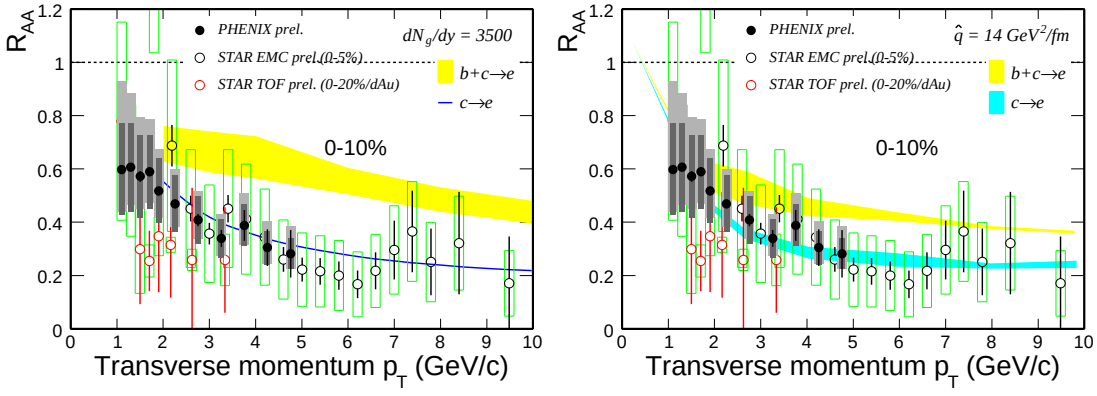

Fig. 11: Comparison of non-photonic electron R_{AA} measurements in central Au+Au collisions by PHENIX and STAR [72]. The data are identical on the two sides. Theory predictions from Ref. [4] (left-hand side) and [33] (right-hand side) are shown.

When comparing the non-photonic electron R_{AA} data to theory, recall that while the electron data contain contributions from both charm and bottom decays, the bottom contribution is expected to dominate for $p_T \sim 4$ GeV/c[1]. Figure 11 shows pQCD calculations of radiative energy loss (discussed earlier) from Djordjevic *et al.* [4] (left) and Armesto *et al.* [33] (right). In the two cases, the calculations are shown for both charm alone and for combined charm and bottom decays. A range of parameters (gluon multiplicity, dN_g/dy, [4] and transport coefficient, $\hat{q}$, [33]) were determined from comparisons with central PHENIX π^0 data. Since the upper limits were used here, these calculations represent the maximum suppression consistent with the π^0 data. The predicted suppression for charm decay electrons is similar to the suppression seen in the data. However, when bottom quark decays are included, as they must be, the calculations predict much less suppression than observed, unless the *c*/*b* ratio is much larger than predicted by pQCD. Thus the non-photonic electron R_{AA} data suggest the need for other energy loss mechanisms. Since light hadron suppression appears to be well described by radiative energy loss, this is a considerable challenge for theorists. If elstic energy loss is added for heavy quarks it must also be included for light hadrons, which may modify some of the parameters such as dN_g/dy and $\hat{g}$.

The elliptic flow parameter, v_2, has been measured for non-photonic electrons in minimum bias Au+Au collisions by PHENIX [15]. The preliminary results are shown in Fig. 12.

While there is no model independent way to extract the charm quark v_2 from the semileptonic decay electron v_2, there are some theoretical calculations available for the expected behavior of the electron v_2 [11, 75]. So far, the main interest has been for $p_T < 2$ GeV/c, where the primary contribution to the lepton spectrum is expected to be from charm quark decays and where the light hadron v_2 results are in good agreement with hydrodynamic models [73].

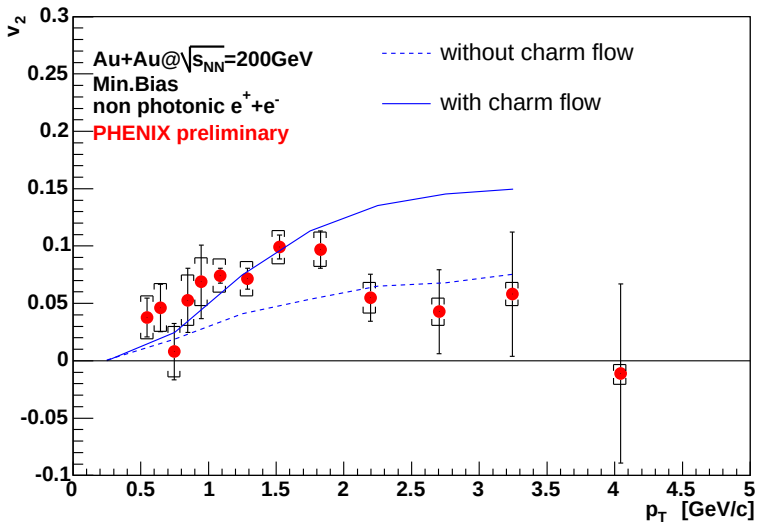

Fig. 12: Comparison of measurement of non-photonic electron v_2 in minimum bias Au+Au collisions from PHENIX [15]. The theory results are from Ref. [11].

Figure 12 shows calculations of the electron v_2 from D meson decays in minimum bias Au+Au collisions by Greco *et al.*, [11] in a quark coalescence model. The dotted curve shows the semileptonic decay electron v_2 if the charm quark v_2 is zero and the D thus acquires all its v_2 from the light quark at coalescence. This represents the extreme case of no reinteraction of the charm quark in the medium. The solid curve shows the electron v_2 if the charm quark is assumed to be completely thermalized in the medium, the opposite extreme. At or below $p_T \sim 1.5$ GeV/$c$the data favor the assumption of complete charm thermalization. This result has been widely interpreted as providing evidence of at least partial charm thermalization.

There is considerable interest in the behavior of the non-photonic electron v_2 for $p_T > 2$ GeV/$c$where the bottom contribution is expected to become important [1]. The PHENIX v_2 results fall toward zero here, consistent with both a larger bottom contribution and a smaller degree of thermalization for higher p_T charm quarks. But, while the PHENIX data have small systematic errors at high p_T, their statistical precision is poor, keeping them from being definitive.

4.4 Proposed open heavy flavor experimental program at RHIC II

Here we focus on the new open heavy flavor physics that becomes available with the combination of the detector upgrades and the RHIC II luminosity upgrade.

With a displaced vertex measurement and RHIC II luminosity, the $B \rightarrow J/\psi$ decay channel can provide a very clean measurement of open bottom production by both PHENIX and STAR (see Tables 2 and 3). The displaced vertex distributions for prompt J/ψ and for $B \rightarrow J/\psi$ decays into the PHENIX muon arms are compared in the left panel of Fig. 13. The yields in Tables 2 and 3 assume a displaced vertex cut of 1 mm. A good measurement of the cross section and R_{AA} vs p_T and y for open bottom production will be possible using $B \rightarrow J/\psi$. Even at RHIC II luminosity, however, the yields are not expected to be large enough to permit a v_2 measurement.

With a displaced vertex measurement and the RHIC II luminosity, separation of the charm and bottom contributions to the semileptonic decay spectra can be done statistically using the different decay

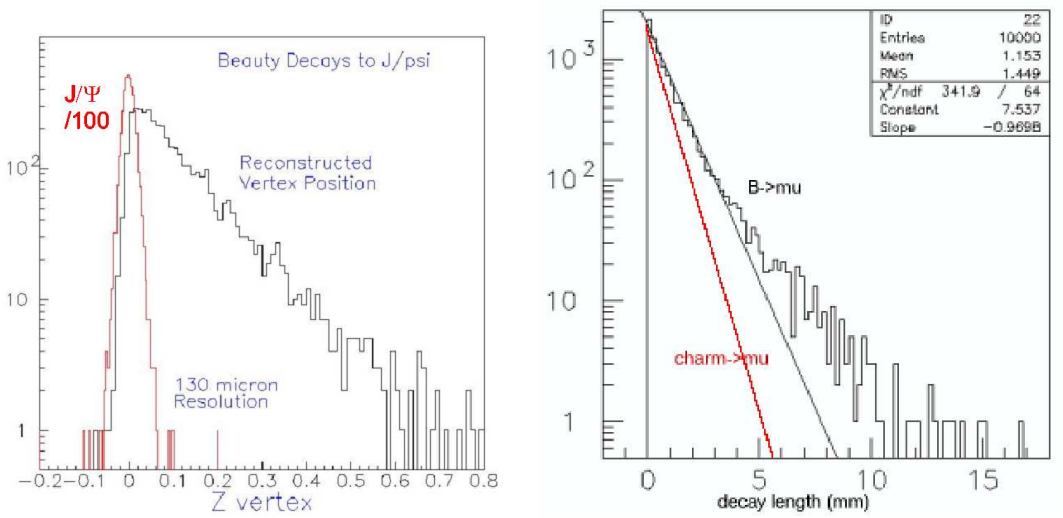

Fig. 13: Left: Comparison of prompt J/ψ displaced vertex distribution (in cm) with that from $B \rightarrow J/\psi$ decays. Note that the prompt J/ψ distribution is scaled down by a factor of 100. Right: Decay length distributions (in mm) from simulations for open charm and bottom.

lengths for charm and bottom mesons (see the right-hand side of Fig. 13). By analyzing data samples with different decay length cuts, the fraction of the signal due to b quarks can be varied. The addition of a displaced vertex measurement will also reduce the single muon background in the heavy flavor measurement since a 1 cm displaced vertex cut reduces the muon yields from light hadron decays by about one order of magnitude. As a result, separate R_{AA} and v_2 measurements as a function of p_T and y should be possible for both open charm and bottom at RHIC II.

Tight displaced vertex cuts will also greatly reduce the background for the $D \rightarrow K\pi$ measurement of open charm yields by eliminating most of the prompt hadron tracks from the combinatorial background. The background reduction will result in much improved cross sections and $R_{AA}(p_T)$. Without a trigger for $D \rightarrow K\pi$ decays, however, this measurement will not greatly benefit from the increased luminosity at RHIC II. Therefore it is not clear if a useful v_2 measurement can be expected. The situation will be similar at the LHC.

5. Hidden heavy flavor: quarkonium

In this section we present a more detailed discussion of the theoretical motivation for studying heavy quarkonia in heavy ion collisions. We also summarize the present experimental and theoretical status and describe the proposed RHIC II experimental quarkonia program.

5.1 Theoretical results

5.11 Cross sections in pp collisions

We discuss quarkonium production in the color evaporation model (CEM) which can be used to calculate the total quarkonium cross sections. The CEM was first discussed some time ago [76, 77] and has enjoyed considerable phenomenological success. In the CEM, the quarkonium production cross section is some fraction F_C of all $Q\overline{Q}$ pairs below the $H\overline{H}$ threshold where H is the lowest mass heavy flavor hadron. Thus the CEM cross section is simply the $Q\overline{Q}$ production cross section with a cut on the pair mass but without any constraints on the color or spin of the final state. The produced $Q\overline{Q}$ pair then neutralizes its color by interaction with the collision-induced color field—"color evaporation". The Q and the $\overline{Q}$ either combine with light quarks to produce heavy-flavored hadrons or bind with each other to form quarkonium. The additional energy needed to produce heavy-flavored hadrons when the partonic center of mass energy, $\sqrt{\hat{s}}$, is less than $2m_H$, the heavy hadron threshold, is obtained nonperturbatively from the color field in the interaction region. Thus the yield of all quarkonium states may be only a small fraction of the total $Q\overline{Q}$ cross section below $2m_H$. At leading order, the production cross section of quarkonium state C in an AB collision is

$$\sigma_C^{\rm CEM} = F_C \sum_{i,j} \int_{4m^2}^{4m_H^2} d\hat{s} \int dx_1 dx_2 \; f_i^A(x_1,\mu^2) \; f_j^B(x_2,\mu^2) \; \hat{\sigma}_{ij}(\hat{s}) \; \delta(\hat{s} - x_1 x_2 s) \; , \tag{2}$$

where $\hat{s}$ is the square of the parton-parton center of mass energy, $ij = q\overline{q}$ or gg and $\hat{\sigma}_{ij}(\hat{s})$ is the $ij \to Q\overline{Q}$ subprocess cross section. The total $Q\overline{Q}$ cross section takes $\hat{s} \to s$ in the upper limit of the integral over $\hat{s}$ in Eq. (2).

The fraction F_C must be universal so that, once it is fixed by data, the quarkonium production ratios should be constant as a function of $\sqrt{s}$, y and p_T. The actual value of F_C depends on the heavy quark mass, m, the scale, μ^2, the parton densities, $f_i^A(x,\mu^2)$ and the order of the calculation. It was shown in Ref. [42] that the quarkonium production ratios were indeed constant, as expected by the model.

Of course the leading order calculation in Eq. (2) is insufficient to describe high p_T quarkonium production since the $Q\overline{Q}$ pair p_T is zero at LO. Therefore, the CEM was taken to NLO [42, 78] using the exclusive $Q\overline{Q}$ hadroproduction code of Ref. [79]. At NLO in the CEM, the process $gg \to gQ\overline{Q}$ is included, providing a good description of the quarkonium p_T distributions at the Tevatron [78]. In the exclusive NLO calculation [79], both the Q and $\overline{Q}$ variables are integrated to obtain the pair distributions. Thus, although $\mu \propto m$ in analytic LO calculations, at NLO, $\mu^2 \propto m_T^2 = m_Q^2 + p_T^2$ where p_T is that of the $Q\overline{Q}$ pair, $p_T^2 = 0.5(p_{T_Q}^2 + p_{T_{\overline{Q}}}^2)$.

We use the same parton densities and parameters that agree with the $Q\overline{Q}$ total cross section data, given in Table 6, to determine F_C for J/ψ and Υ production. The fit parameters [80, 81] for the parton densities [82, 83, 84], quark masses and scales are given in Table 6 while the $Q\overline{Q}$ cross sections calculated with these parameters are compared to $pp \to Q\overline{Q}$ and $\pi^- p \to Q\overline{Q}$ data in Fig. 14.

We now describe the extraction of F_C for the individual quarkonium states. The J/ψ has been measured in pp and pA interactions up to $\sqrt{s} = 63$ GeV. The data are of two types: the forward cross section, $\sigma(x_F > 0)$, and the cross section at zero rapidity, $d\sigma/dy|_{y=0}$. All the cross sections are inclusive with feed down from χ_c and ψ' decays. To obtain $F_{J/\psi}$ for inclusive J/ψ production, the normalization of Eq. (2) is obtained from a fit using the $c\overline{c}$ parameters in Table 6. The comparison of $\sigma_{J/\psi}^{\rm CEM}$ to the

Table 6: Parameters used to obtain the 'best' agreement to the $Q\overline{Q}$ cross sections. The quark mass is given in GeV/c^2. The inclusive J/ψ production fraction, $F_{J/\psi}$, and the inclusive Υ production fraction, F_Υ, obtained from the data are also given.

$c\overline{c}$					$b\overline{b}$				
Label	PDF	m	μ/m_T	$F_{J/\psi}$	Label	PDF	m	μ/m_T	F_Υ
$\psi 1$	MRST HO	1.2	2	0.0144	$\Upsilon 1$	MRST HO	4.75	1	0.0276
$\psi 2$	MRST HO	1.4	1	0.0248	$\Upsilon 2$	MRST HO	4.5	2	0.0201
$\psi 3$	CTEQ 5M	1.2	2	0.0155	$\Upsilon 3$	MRST HO	5.0	0.5	0.0508
$\psi 4$	GRV 98 HO	1.3	1	0.0229	$\Upsilon 4$	GRV 98 HO	4.75	1	0.0225

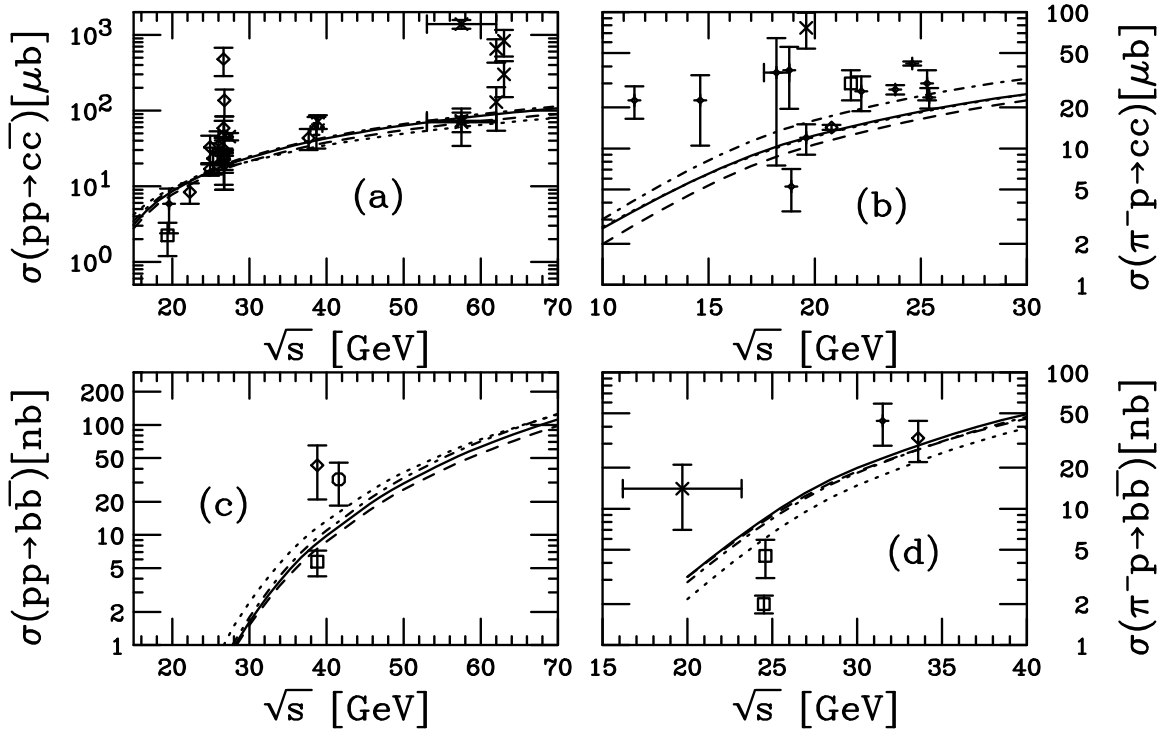

Fig. 14: The $c\overline{c}$, (a) and (b), and $b\overline{b}$, (c) and (d), total cross section data in *pp* and $\pi^- p$ interactions compared to NLO calculations. In (a) and (b), we show $\psi 1$ (solid), $\psi 2$ (dashed), $\psi 3$ (dot-dashed) and $\psi 4$ (dotted). In (c) and (d), we show $\Upsilon 1$ (solid), $\Upsilon 2$ (dashed), $\Upsilon 3$ (dot-dashed) and $\Upsilon 4$ (dotted).

$x_F > 0$ data for all four fits is shown on the left-hand side of Fig. 15. The ratios of the direct production cross sections to the inclusive J/ψ cross section can be determined from data on inclusive cross section ratios and branching fractions. These direct ratios, R_C, given in Table 7, are multiplied by the inclusive fitted $F_{J/\psi}$, also shown in Table 6 to obtain the direct production fractions, $F_C^{\rm dir} = F_{J/\psi} R_C$.

Table 7: Direct quarkonium production ratios, $R_C = \sigma_C^{\rm dir}/\sigma_{C'}^{\rm inc}$ where $C' = J/\psi$ and Υ. From Ref. [85].

	J/ψ	ψ'	χ_{c1}	χ_{c2}	Υ	Υ'	Υ''	$\chi_b(1P)$	$\chi_b(2P)$
R_C	0.62	0.14	0.60	0.99	0.52	0.33	0.20	1.08	0.84

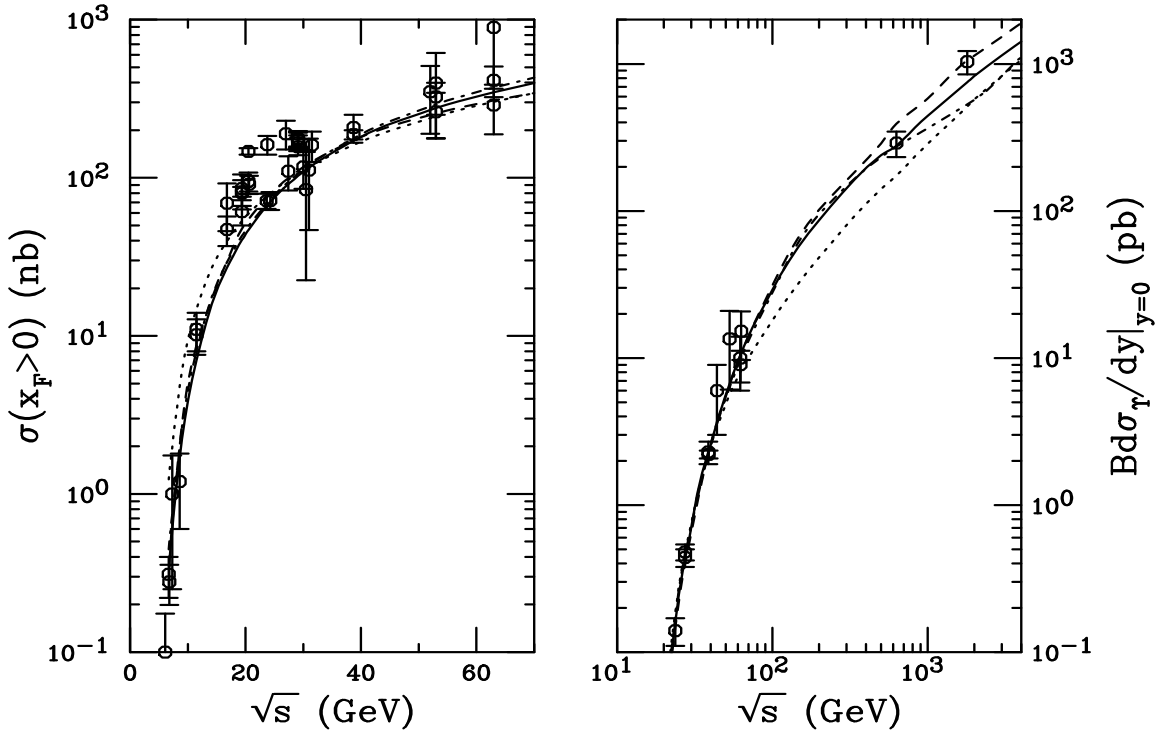

Fig. 15: Forward J/ψ (left) and combined $\Upsilon + \Upsilon' + \Upsilon''$ inclusive (right) cross sections calculated to NLO in the CEM. On the left-hand side, we show $\psi 1$ (solid), $\psi 2$ (dashed), $\psi 3$ (dot-dashed) and $\psi 4$ (dotted). On the right-hand side, we show $\Upsilon 1$ (solid), $\Upsilon 2$ (dashed), $\Upsilon 3$ (dot-dashed) and $\Upsilon 4$ (dotted).

The same procedure, albeit somewhat more complicated due to the larger number of bottomonium states below the $B\overline{B}$ threshold, is followed for bottomonium. For most data below $\sqrt{s} = 100$ GeV, the three bottomonium S states were either not separated or their sum was reported. No x_F-integrated cross sections were available so that the CEM Υ cross section were fittted to the effective lepton pair cross section at $y = 0$ for the three $\Upsilon(nS)$ states. The extracted fit fraction, $F_{\sum\Upsilon}$, combined with $\sigma_\Upsilon^{\rm CEM}$ and compared to the data for all parameter sets in Table 6, is shown on the right-hand side of Fig. 15. Using the individual branching ratios of the Υ, Υ' and Υ'' to lepton pairs and the total cross sections reported by CDF [86], it is possible to extract the inclusive Υ fit fraction, F_Υ, given in Table 6. The direct production ratios obtained in Ref. [25] have been updated in Ref. [85] using recent CDF χ_b data. The resulting direct to inclusive Υ ratios, R_C, are also given in Table 7. The sub-threshold $b\overline{b}$ cross section is then multiplied by $F_C^{\rm dir} = F_\Upsilon R_C$ to obtain the direct bottomonium cross sections.

The total cross sections for the charmonium and bottomonium states in pp collisions at $\sqrt{s} = 200$ GeV are shown in Tables 8 and 9 respectively.

Case	$\sigma^{\rm inc}_{J/\psi}$	$\sigma^{\rm dir}_{J/\psi}$	$\sigma_{\chi_{c1}}$	$\sigma_{\chi_{c2}}$	$\sigma_{\psi'}$
$\psi 1$	2.35	1.46	1.41	2.33	0.33
$\psi 2$	1.76	1.09	1.06	1.74	0.25
$\psi 3$	2.84	1.76	1.70	2.81	0.40
$\psi 4$	2.10	1.31	1.26	2.08	0.29

Table 8: The charmonium cross sections (in μb) for 200 GeV pp collisions. The inclusive and direct J/ψ cross sections are both given.

Case	$\sigma^{\rm inc}_{\Upsilon}$	$\sigma^{\rm dir}_{\Upsilon}$	$\sigma_{\Upsilon'}$	$\sigma_{\Upsilon''}$	$\sigma_{\chi_b(1P)}$	$\sigma_{\chi_b(2P)}$
$\Upsilon 1$	6.60	3.43	2.18	1.32	7.13	5.54
$\Upsilon 2$	7.54	3.92	2.49	1.51	8.15	6.34
$\Upsilon 3$	5.75	2.99	1.90	1.15	6.21	4.83
$\Upsilon 4$	4.31	2.24	1.42	0.86	4.66	3.62

Table 9: The direct bottomonium cross sections (in nb) for pp collisions at 200 GeV. The production fractions for the total Υ are multiplied by the appropriate ratios determined from data.

The energy dependence shown in Fig. 15 for both states is well reproduced by the NLO CEM. All the fits are equivalent for $\sqrt{s} = 100$ GeV but differ by up to a factor of two at 2 TeV. The high energy Υ data seem to agree best with the energy dependence of $\Upsilon 1$ and $\Upsilon 2$ although $\Upsilon 1$ underestimates the Tevatron result by a factor of ≈ 1.4. A similar check cannot be made for the J/ψ because the high lepton p_T cut excludes J/ψ acceptance for $p_T = 0$ at the Tevatron in Run I.

5.12 Cold nuclear matter effects on quarkonium production at RHIC

It is essential that the A dependence be understood in cold nuclear matter to set a proper baseline for quarkonium suppression in AA collisions. The NA50 collaboration has studied the J/ψ A dependence and attributed its behavior to J/ψ break up by nucleons in the final state, referred to as nuclear absorption. However, the parton distributions are modified in the nucleus relative to free protons. This modification, referred to here as shadowing, is increasingly important at higher energies, as emphasized in Ref. [87]. In this section, we discuss the interplay of shadowing and absorption in d+Au and AA collisions at RHIC.

Shadowing, the modification of the parton densities in the nucleus with respect to the free nucleon, is taken into account by replacing f_j^p in Eq. (2) by $F_j^A(x,\mu^2,\vec{b},z) = \rho_A(\vec{b},z)S^j(A,x,\mu^2,\vec{b},z)f_j^p(x,\mu^2)$ and adding integrals over the spatial coordinates. Here S^j is the shadowing parameterization. The density distribution of the deuteron is also included in these calculations but the small effects of shadowing in deuterium are ignored. The PHENIX J/ψ d+Au data as a function of rapidity show a dependence consistent with nuclear shadowing plus a small absorption cross section of 1-3 mb. The J/ψ production cross section is calculated in the CEM using Eq. (2) with the same mass and scale as in $c\overline{c}$ production. The calculations of the d+Au/pp and AA/pp ratios are done at LO to simplify the calculations since the LO and NLO ratios are equivalent [2].

To implement nuclear absorption of the J/ψ in d+Au collisions, the dN production cross section is weighted by the survival probability, $S^{\rm abs}$ [88]:

$$S^{\rm abs}(\vec{b},z) = \exp\left\{-\int_z^\infty dz' \rho_A(\vec{b},z')\sigma_{\rm abs}(z'-z)\right\} \tag{3}$$

, where z is the longitudinal production point and z' is the point at which the state is absorbed. The nucleon absorption cross section, $\sigma_{\rm abs}$, typically depends on where the state is produced in the medium and how far it travels through nuclear matter. If absorption alone is active, *i.e.* no shadowing so that $S^j \equiv 1$,

then an effective minimum bias A dependence is obtained after integrating $S^{\rm abs}$ over the spatial coordinates. If $S^{\rm abs} = 1$ also, $\sigma_{{\rm d}A} = 2A\sigma_{pN}$. When $S^{\rm abs} \neq 1$, $\sigma_{{\rm d}A} = 2A^{\alpha}\sigma_{pN}$ where, if $\sigma_{\rm abs}$ is a constant, independent of the production mechanism for a nucleus of $\rho_A = \rho_0\theta(R_A - b)$, $\alpha = 1 - 9\sigma_{\rm abs}/(16\pi r_0^2)$, where $r_0 = 1.2$ fm. The contribution to the full A dependence of α from absorption alone is only constant if $\sigma_{\rm abs}$ is constant and independent of the production mechanism [88]. The observed J/ψ yield includes feed down from χ_c and ψ' decays, giving

$$S^{\rm abs}_{J/\psi}(b,z) = 0.58 S^{\rm abs}_{J/\psi,\,{\rm dir}}(b,z) + 0.3 S^{\rm abs}_{\chi_c}(b,z) + 0.12 S^{\rm abs}_{\psi'}(b,z)\ . \tag{4}$$

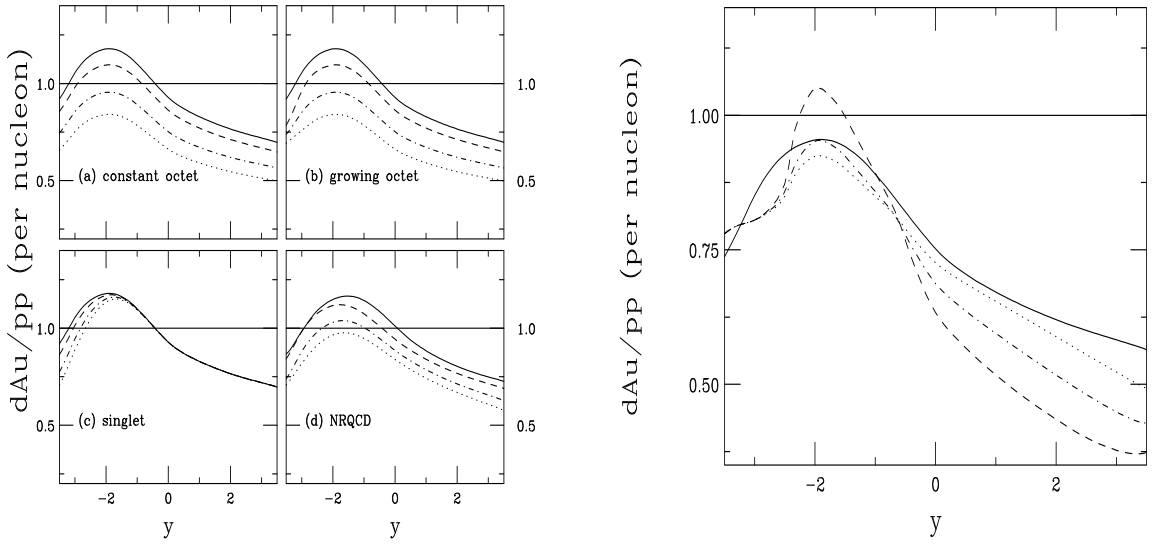

Fig. 16: Left-hand side: The J/ψ d+Au/pp ratio with EKS98 at 200 GeV as a function of rapidity for (a) constant octet, (b) growing octet, (c) singlet, all calculated in the CEM and (d) NRQCD. For (a)-(c), the curves are no absorption (solid), $\sigma_{\rm abs} = 1$ (dashed), 3 (dot-dashed) and 5 mb (dotted). For (d), we show no absorption (solid), 1 mb octet/1 mb singlet (dashed), 3 mb octet/3 mb singlet (dot-dashed), and 5 mb octet/3 mb singlet (dotted). Right-hand side: The J/ψ d+Au/pp ratio at 200 GeV for a growing octet with $\sigma_{\rm abs} = 3$ mb is compared for four shadowing parameterizations. We show the EKS98 (solid), FGSo (dashed), FGSh (dot-dashed) and FGSl (dotted) results as a function of rapidity.

The J/ψ may be produced as a color singlet, a color octet or in a combination of the two. In color singlet production, the final state absorption cross section depends on the size of the $c\overline{c}$ pair as it traverses the nucleus, allowing absorption to be effective only while the cross section is growing toward its asymptotic size inside the target. On the other hand, if the $c\overline{c}$ is only produced as a color octet, hadronization will occur only after the pair has traversed the target except at very backward rapidity. We have considered a constant octet cross section, as well as one that reverts to a color singlet at backward rapidities. For singlets, $S^{\rm abs}_{J/\psi,\,{\rm dir}} \neq S^{\rm abs}_{\chi_c} \neq S^{\rm abs}_{\psi'}$ but, with octets, one assumes that $S^{\rm abs}_{J/\psi,\,{\rm dir}} = S^{\rm abs}_{\chi_c} = S^{\rm abs}_{\psi'}$. As can be seen in Fig. 16, the difference between the constant and growing octet assumptions is quite small at large $\sqrt{s_{NN}}$ with only a small singlet effect at $y < -2$. Singlet absorption is also important only at similar rapidities and is otherwise not different from shadowing alone. Finally, we have also considered a combination of octet and singlet absorption in the context of the NRQCD approach, see Ref. [88] for more details. The combination of nonperturbative singlet and octet parameters changes the shape of the shadowing ratio slightly. Including the singlet contribution weakens the effective absorption. The results are shown integrated over impact parameter. The calculations use the EKS98 shadowing parameterization [89] since it gives good agreement with the trend of the PHENIX data. For results with other shadowing parameterizations, see Refs. [2, 3].

Several values of the asymptotic absorption cross section, $\sigma_{\rm abs} = 1$, 3 and 5 mb, corresponding to $\alpha = 0.98$, 0.95 and 0.92 respectively using Eqs. (3) and (4), are shown in Figs. 16 and 17 for d+Au

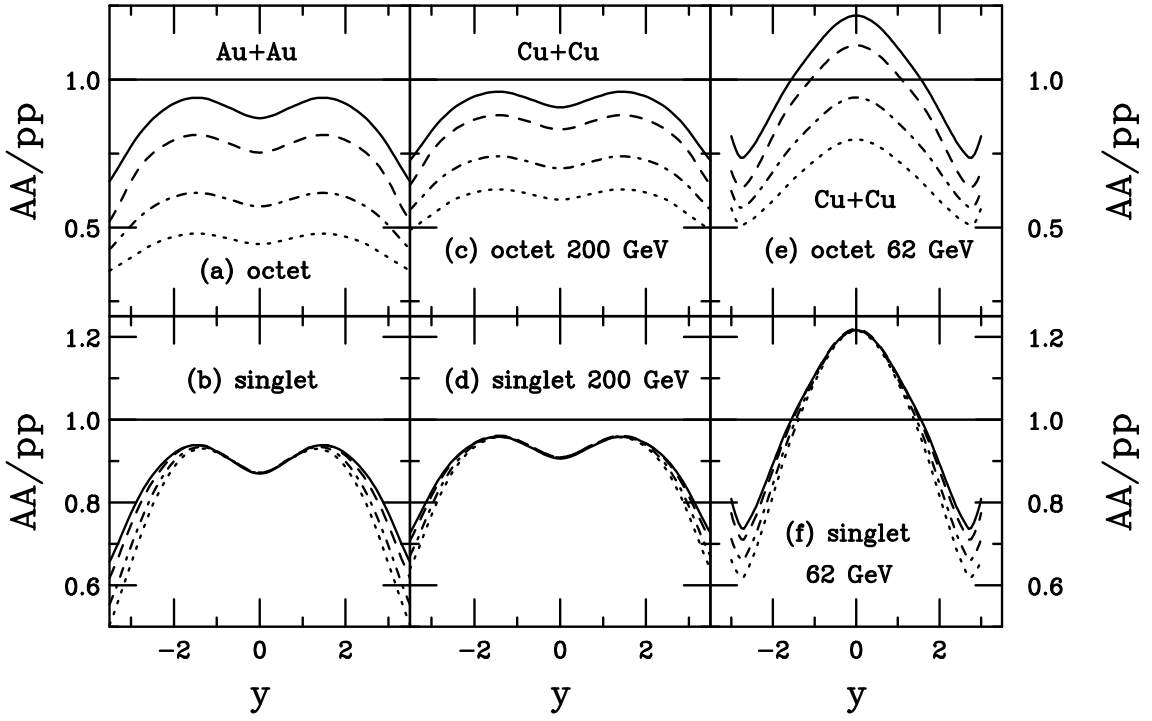

Fig. 17: The AA/pp ratio with the EKS98 parameterization as a function of y for octet (upper) and singlet (lower) absorption. In (a) and (b) we show the Au+Au results at 200 GeV while the Cu+Cu results are shown at 200 GeV (c) and (d) as well as at 62 GeV (e) and (f). The curves are $\sigma_{\rm abs} = 0$ (solid), 1 (dashed), 3 (dot-dashed) and 5 mb (dotted).

and AA collisions respectively. These values of $\sigma_{\rm abs}$ are somewhat smaller than those obtained for the sharp sphere approximation. The diffuse surface of a real nucleus and the longer range of the density distribution result in a smaller value of $\sigma_{\rm abs}$ than a spherical nucleus. As will be seen later, there is good agreement with the trend of the preliminary PHENIX data [90] for $\sigma_{\rm abs} = 0 - 3$ mb. Work is in progress to quantify the shadowing parameterization and absorption cross section more precisely [91].

The current RHIC data are not sufficiently precise to distinguish between J/ψ production and absorption in the CEM relative to that in the NRQCD approach. However, a measurement of the χ_c A dependence may be able to clarify the situation [88]. In the CEM, the J/ψ and χ_c distributions differ only in the value of F_C. In the NRQCD approach, the J/ψ is produced primarily in a color octet state while the χ_c is produced as a color singlet state. Thus while the production of both states would exhibit the same shadowing effect, a difference in the J/ψ and χ_c d+Au/pp ratios due to octet relative to singlet absorption may be measurable.

We now turn to the centrality dependence of J/ψ production in d+Au and AA collisions. In central collisions, inhomogeneous (spatially dependent) shadowing is stronger than the homogeneous (minimum bias) result. The stronger the homogeneous shadowing, the larger the inhomogeneity. In peripheral collisions, inhomogeneous effects are weaker than the homogeneous results but some shadowing is still present. Shadowing persists in peripheral collisions in part because the density in a heavy nucleus is large and approximately constant except close to the surface and because the deuteron wave function has a long tail. Absorption is also expected to be stronger in central collisions.

To study the centrality dependence of shadowing and absorption, the d+Au/pp and AA/pp ratios are presented as a function of $N_{\rm coll}$,

$$N_{\rm coll}(b) = \sigma_{NN}^{\rm in} \int d^2s T_A(s) T_B(|\vec{b} - \vec{s}|) \ ,$$

where T_A and T_B are the nuclear thickness functions and the inelastic nucleon-nucleon cross section,

$\sigma_{NN}^{\rm in}$, is 42 mb at 200 GeV. In Figs. 18 and 19, the $N_{\rm coll}$ dependence is shown for several representative rapidities, $y = -2$, 0 and 2 for RHIC. The inhomogeneous shadowing parameterization is chosen to be proportional to the path length of the parton through the nucleus [87]. For more results, see Refs. [2, 3].

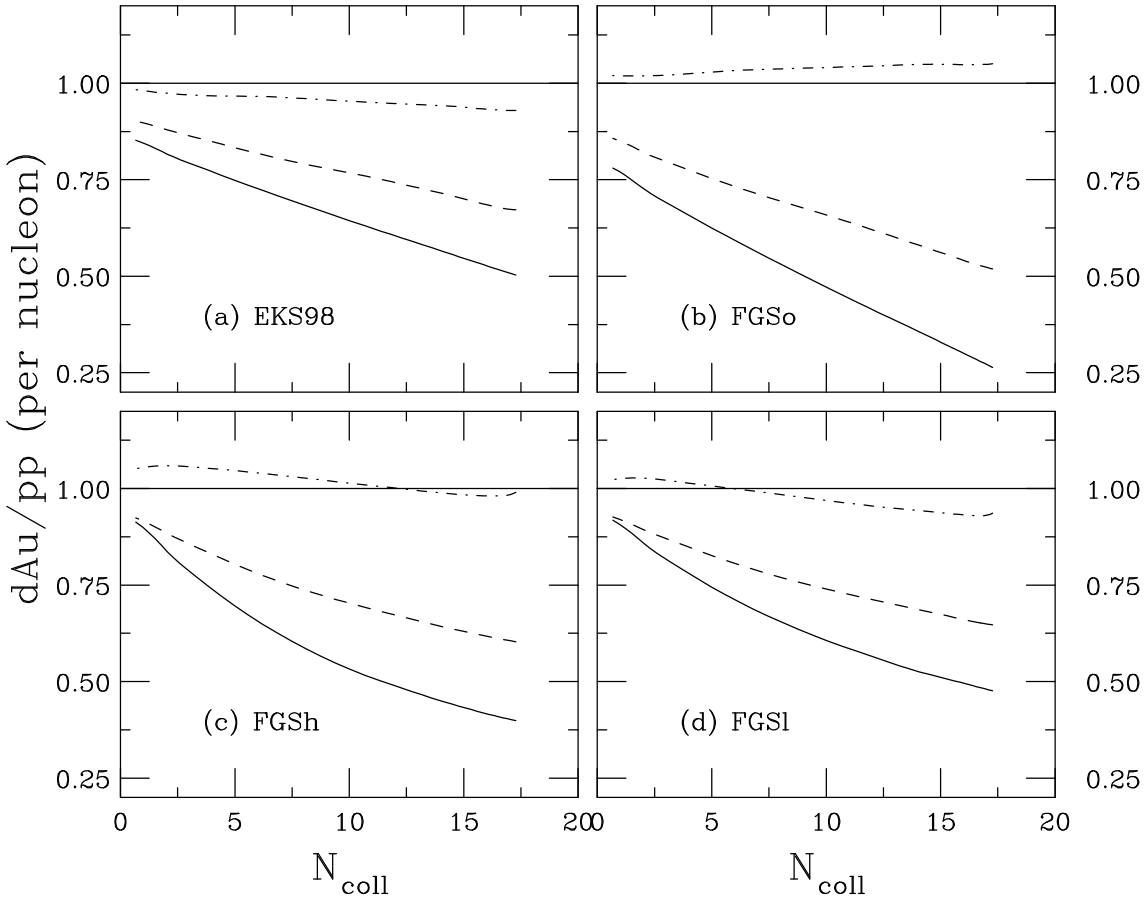

Fig. 18: The ratio d+Au/pp as a function of $N_{\rm coll}$ for the EKS98 (a), FGSo (b), FGSh (c) and FGSl (d) shadowing parameterizations. The calculations with EKS98 and FGSo use the inhomogeneous path length parameterization while that obtained by FGS is used with FGSh and FGSl. Results are given for $y = -2$ (dot-dashed), $y = 0$ (dashed) and $y = 2$ (solid) at 200 GeV for a growing octet with $\sigma_{\rm abs} = 3$ mb.

The dependence of the RHIC ratios on $N_{\rm coll}$ is almost linear, as seen in Figs. 18 and 19. The results are not shown for $N_{\rm coll} < 1$. The weakest $N_{\rm coll}$ dependence occurs in the antishadowing region, illustrated by the $y = -2$ result (dot-dashed curve). The overall dependence on $N_{\rm coll}$ is stronger than that obtained from shadowing alone, described in Ref. [87], where inhomogeneous shadowing effects depend strongly on the amount of homogeneous shadowing. Relatively large effects at low x are accompanied by the strongest impact parameter, b, dependence. In the transition region around mid rapidity at RHIC, the b dependence of the ratio d+Au/pp due to shadowing is nearly negligible and almost all of the $N_{\rm coll}$ dependence at $y \sim 0$ can be attributed to absorption. The $y = -2$ results for color singlet production and absorption, in the antishadowing region, are fairly independent of $N_{\rm coll}$.

5.13 Models of quarkonium production in heavy ion collisions

In-medium properties of quarkonium from lattice QCD:

Properties of heavy quarks have been used to characterize "thermal properties of the QCD vacuum" ever since the first lattice calculations at non-zero temperature [92]. Modifications of the interactions between heavy, static quarks in a thermal heat bath are clearly reflected by changes of the free

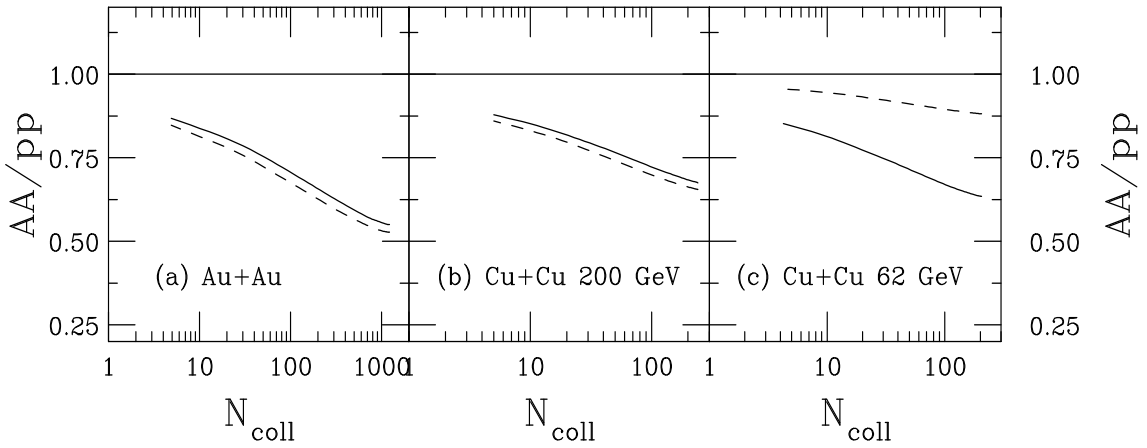

Fig. 19: The ratio AA/pp as a function of $N_{\rm coll}$ for a 3 mb octet absorption cross section and the EKS98 parameterization at $y = 0$ (dashed) and $y = 2$ (solid) for Au+Au at 200 GeV (a) and Cu+Cu at 200 GeV (b) and 62 GeV (c).

energy which, in the zero temperature limit, reduces to the heavy quark potential [93]. To use this information to analyze thermal modifications of quarkonia requires an intermediate, phenomenological step: the construction of a temperature dependent effective potential which then can be used in a nonrelativistic Schrödinger equation [94, 95, 96] or a more refined coupled-channel analysis [97, 98]. Quite generically, the potential model analyses suggest a sequential suppression pattern where heavy quark bound states dissociate at temperatures at which their bound state radii become comparable to the Debye screening radius, illustrated in Fig. 20. Table 10 shows quarkonium dissociation temperatures from Ref. [99].

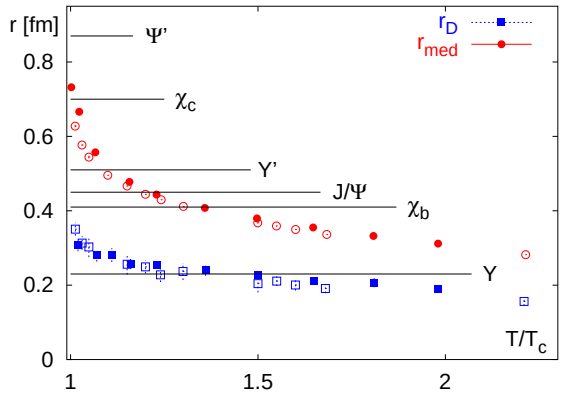

Fig. 20: Mean squared charge radii of some charmonium and bottomonium states compared to the Debye screening radius, $r_D \equiv 1/m_D$ and a related scale, $r_{\rm med}$, an estimate of the distance beyond which the force between a static $Q\overline{Q}$ pair is strongly modified by temperature effects [100]. Open (closed) symbols correspond to SU(3) (2-flavor QCD) calculations [93].

More recently, the calculation of thermal hadron correlation functions and their spectral analysis [101] eliminated some of the ambiguities inherent in the potential model approach. The spectral analysis, at least in principle, provides an ab-initio approach to the calculation of in-medium properties of heavy quark bound states. Its predictive power is reduced only by the application of statistical tools like the Maximum Entropy Method (MEM) which, however, can be steadily improved with further improvement of the available computing resources and numerical techniques. Predictions based on potential model calculations as well as the spectral analysis have been reviewed in recent studies that have been performed to analyze prospects for quarkonium studies at the LHC [37, 102]. In the following, the analysis of

State	$J/\psi(1S)$	$\chi_c(1P)$	$\psi'(2S)$	$\Upsilon(1S)$	$\chi_b(1P)$	$\Upsilon(2S)$	$\chi_b(2P)$	$\Upsilon(3S)$
T_d/T_c	2.10	1.16	1.12	> 4.10	< 1.76	1.60	1.19	1.17

Table 10: Quarkonium dissociation temperatures [99], illustrating the effects of binding energy on the dissociation temperature.

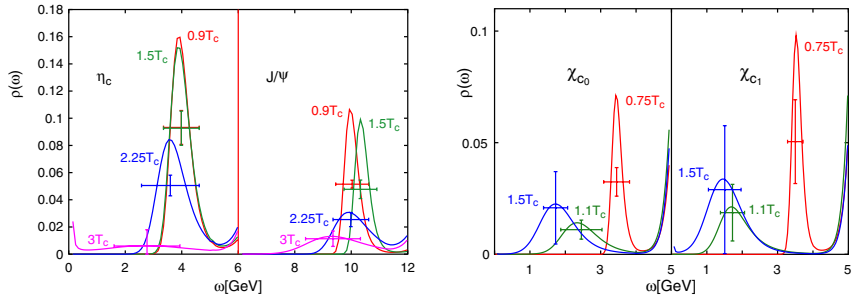

Fig. 21: Spectral functions of η_c, J/ψ (left) and and χ_{c0}, χ_{c1} (right) at various temperatures below and above T_c. The vertical bars give the error on the average value of the spectral function in the bin indicated by the horizontal bars.

thermal hadron correlation functions and the spectral functions extracted from them are discussed.

The finite temperature, Euclidean time correlation functions

$$G_H(\tau, \vec{r}, T) = \langle J_H(\tau, \vec{r}) J_H^\dagger(0, \vec{0}) \rangle \tag{5}$$

of hadronic currents, $J_H = \bar{q}(\tau, \vec{r}) \Gamma_H q(\tau, \vec{r})$, where Γ_H denotes a suitable product of gamma matrices that projects onto the appropriate quantum numbers H, are directly related to spectral functions, $\sigma_H(\omega, T)$. These spectral functions encompass all the information about thermal modifications of the hadron spectrum in channel H, so that

$$G_H(\tau, \vec{r}, T) = \int_0^\infty d\omega \, \frac{d^3\vec{p}}{(2\pi)^3} \sigma_H(\omega, \vec{p}, T) \, \mathrm{e}^{i\vec{p}\cdot\vec{r}} \frac{\cosh(\omega(\tau - 1/2T))}{\sinh(\omega/2T)} \quad , \tag{6}$$

are directly related to experimental observables. In particular, the spectral function in the vector channel, $\sigma_V(\omega, \vec{p}, T)$, is directly related to the differential cross section for thermal dilepton production,

$$\frac{dW}{d\omega d^3p} = \frac{5\alpha^2}{27\pi^2} \frac{\sigma_V(\omega, \vec{p}, T)}{\omega^2(\mathrm{e}^{\omega/T} - 1)} \quad . \tag{7}$$

Note that the rates obtained using this method do not include any contributions arising from the feed down of other channels into the vector channel [85, 103].

Some generic aspects of the influence of a thermal medium on states with different quantum numbers can already be deduced from the temperature dependence of the thermal correlation functions themselves and does not require the additional step of applying the MEM analysis which, after all, is based on probabilistic assumptions. Such comparisons show that zero-momentum, thermal hadron correlation functions in the ground state channels, *i.e.* the vector (J/ψ, Υ) and pseudoscalar (η_c, η_b) channels show only little modification in a thermal medium up to temperatures $T \gtrsim 1.5\ T_c$. Correlation functions corresponding to radially excited charmonium states (χ_c), however, are modified strongly already close to or at T_c.

These generic features are reflected by the spectral functions. Although results from different groups currently still differ in details, the current understanding of charmonium at high temperature may be summarized as follows:

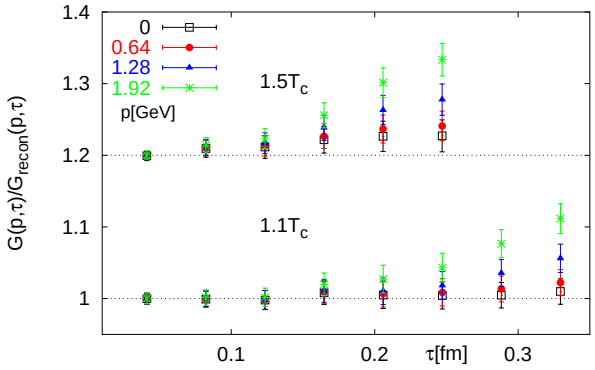

Fig. 22: The ratio of pseudoscalar correlation functions at non-zero momentum above and below T_c [105]. Deviations from the horizontal dotted lines for increasing p indicate stronger temperature-dependent modifications of the spectral functions.

- The J/ψ and η_c remain unaffected by the thermal medium up to $T = 1.5\ T_c$. At higher temperatures it is unclear whether the J/ψ already disappears at $\simeq 1.9\ T_c$ [104] or persists as a strongly modified resonance up to $2.25\ T_c$ [23], see the left-hand side of Fig. 21.
- The χ_{c0} and χ_{c1} both disappear at $T \lesssim 1.1\ T_c$, see the right-hand side of Fig. 21.
- The J/ψ states with finite momentum show statistically significant but still small modifications for $T \lesssim 1.5\ T_c$ [105] due to collisional broadening by higher momentum gluons seen by bound states moving relative to the heat bath, see Fig. 22 [106].

The strong binding of the J/ψ above T_c also is supported by the analysis of spatial correlations [107] and the observed insensitivity of the thermal vector and pseudoscalar correlation functions to spatial boundary conditions [108].

Bottomonium studies are considerably more difficult since a larger lattice cut off is required to properly resolve these states, particularly for temperatures well above $2\ T_c$ where the Υ states are expected to be dissolved. First exploratory finite temperature results on bottomonium have been reported for temperatures up to $\sim 1.5\ T_c$. At this temperature, no thermal modifications of the Υ and η_b have been observed, as expected. The χ_b correlation functions are, however, modified at $T \sim 1.5\ T_c$, similar to the scalar charmonium case at $T \simeq 1.1\ T_c$. To firmly establish the onset of medium modifications in bottomonium states, however, requires further refined studies of the bottomonium system at lower and higher temperatures.

Dynamical Coalescence:

The production of multiple $c\overline{c}$ pairs in a single collision introduces a new charmonium formation mechanism [17]. In-medium charmonium formation utilizes a c and a $\overline{c}$ quark from independently produced $c\overline{c}$ pairs to form a J/ψ.

In the plasma phase, there are two basic approaches: statistical and dynamical coalescence. Both these approaches depend on being able to measure the quarkonium rate relative to total $Q\overline{Q}$ production. The first calculations in the statistical approach assumed an equilibrated fireball in a grand canonical ensemble [26, 27]. This approach could be reasonable at the high energies of the LHC, where the number of produced $c\overline{c}$ pairs is large. But, at lower energies, charm conservation is required since a $c\overline{c}$ pair is not produced in every event. More recent calculations assumed a canonical ensemble only for charm production [109, 110, 111]. Dynamical coalescence models assume that some of the produced $Q\overline{Q}$ pairs can also form quarkonium which would not otherwise do so. This coalescence can take place in the QGP [17, 36] or at hadronization [28]. The model includes the rapidity differences, $|\Delta y|$, between the Q and

$\overline{Q}$ and shows that the larger the rapidity difference, the smaller the enhancement. The impact parameter dependence of the statistical and dynamical coalescence models is quite different. Statistical coalescence gives the largest enhancement in peripheral collisions where the volume of the plasma is small, giving only a minor enhancement in central collisions. Dynamical coalescence produces a larger enhancement in central collisions where the number of $Q\overline{Q}$ pairs per event is greatest but still produces a significant effect in peripheral collisions [112].

Much smaller enhancements are predicted for secondary quarkonium production in the hadron gas, particularly for the J/ψ where the additional production is either small (20 - 60%) [29] or about a factor of two [30] at LHC energies and smaller still for RHIC. Larger enhancements may be expected for the ψ' [29]. The predictions depend strongly on the $J/\psi + \pi(\rho)$ cross sections, typically not more than 1-2 mb [113].

Secondary production will be at lower center of mass energies than the initial nucleon-nucleon collisions. Thus the production kinematics will be different, leading to narrower rapidity and p_T distributions. Secondary quarkonium could be separated from the primary quarkonium, subject to suppression, by appropriate kinematic cuts. Such cuts will also be useful for separating initial J/ψ's from those produced in B meson decays.

These secondary production models are already testable at RHIC where enhancements of factors of 2-3 are expected from coalescence [17, 111]. Hard scatterings of produced particles is related to the idea of crosstalk between unrelated interactions [114]. Important crosstalk effects were predicted in e^+e^- collisions at LEP [114] but were not observed. If secondary quarkonium production is found, it would indicate the relevance of such effects.

Predictions of J/ψ production by this dynamical coalescence suffer from substantial uncertainties due to the dependence on the charm quark distributions in the medium. In fact, it possible to turn this uncertainty into an advantage and probe the medium properties using the observed J/ψ momentum distributions. Two extremes can be considered [16]. If the charm quark distributions in the medium are identical to those of the initial production process, the interactions of charm quarks with the medium would be very weak. In this case, both the J/ψ rapidity and p_T distributions will be narrower than if no plasma is formed simply because the center of mass energy of secondary J/ψ production is lower than that of the initial nucleon-nucleon interactions. The lower energy results in a reduced $\langle p_T^2 \rangle$ and a narrower rapidity distribution. Thus, instead of the transverse momentum broadening expected from initial-state multiple scattering going from pp to pA to AA, the average p_T^2 in AA would no longer exhibit the monotonic increase seen in pp and pA interactions for increasing A. On the other hand, if the charm quarks are assumed to be in thermal equilibrium with the surrounding medium, the charm interaction with the medium would be very strong. Any J/ψ's produced from thermalized charm quarks flowing with the medium would have a p_T distribution with a slope characteristic of the temperature of the system at the time they were formed, resulting in considerably narrower rapidity and p_T distributions. In either case, the effect would be largest in central collisions, reverting to "normal" broadening in peripheral collisions where on the order of one or fewer $c\overline{c}$ pairs will be produced since the number of $c\overline{c}$ pairs scales approximately with the number of collisions.

In order to extract the medium properties from secondary J/ψ production, systematic studies of J/ψ production in pp, pA and AA interactions are necessary. The pp data sets the intrinsic transverse momentum scale for a particular energy while the pA results determine the level of broadening due to cold nuclear matter effects which would then apply to AA interactions.

Models of regeneration, of course, also include J/ψ suppression. In addition to the screening effects discussed previously, the J/ψ can scatter with quarks and gluons in the plasma which may break it up more effectively than screening effects alone, especially if temperatures significantly above T_c are needed for screening to dissociate the directly produced J/ψ, as discussed in Ref. [28]. At low temperatures, relevant for SPS energies, $gJ/\psi \rightarrow c\overline{c}$ is effective for J/ψ breakup by a thermal gluon. However, at higher temperatures where the J/ψ should be more loosely bound, inelastic parton scatter-

ing, $g(q,\overline{q})J/\psi \rightarrow g(q,\overline{q})c\overline{c}$, calculated using the leading order matrix elements for gc and gq scattering, is more effective.

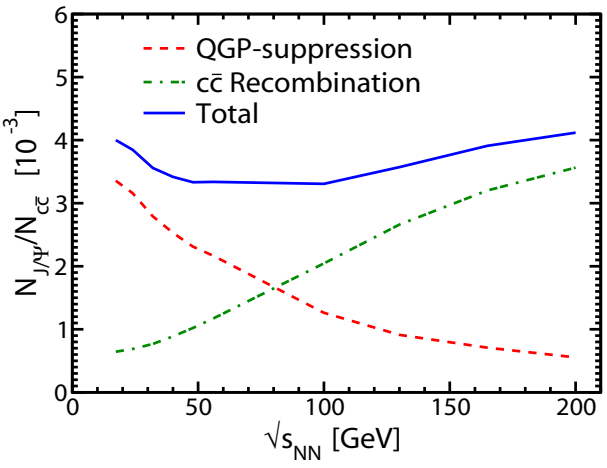

Fig. 23: Excitation function of the ratio of produced J/ψ to the number of $c\overline{c}$ pairs in central heavy-ion collisions for $N_{\rm part} = 360$ [115].

The relative importance of J/ψ suppression and regeneration will change as a function of energy, as shown in Fig. 23 for central collisions of heavy nuclei, $N_{\rm part} = 360$, from Ref. [115]. The J/ψ yield is dominated by primordial production at SPS energy, and dominated by regeneration at RHIC full energy.

5.2 Status of Quarkonium Physics at the CERN/SPS

The prospects of a "clean" QGP signature, destruction of the J/ψ by color screening, was discussed in the landmark paper by Matsui and Satz in 1986 [21]. This triggered an extensive experimental program at the CERN/SPS. HELIOS-III [116] and NA38 [117] (subsequently NA50 [118] and currently NA60 [119]) conducted detailed measurements of the dimuon invariant mass spectrum around mid rapidity. Despite early enthusiasm and enormous statistics (see Fig. 24) the picture that evolved is still rather ambiguous. The SPS measurements must also be understood in light of the many results on quarkonium production in pA collisions from fixed target experiments. The status of the SPS program is summarized below:

Feed down contributions (see Fig. 25) from higher charmonium states, $\chi_c \rightarrow J/\psi\gamma$ ($\sim$ 30%) and $\psi' \rightarrow J/\psi\pi\pi$ ($\sim$ 10%), are important [120, 121]. The χ_c has not yet been measured by the heavy ion detectors at the SPS, although it has been seen in other experiments there. These measurements are extremely difficult and the large scatter of available data depicted in Fig. 26 indicates that better measurements are desperately needed. The NA60 experiment is planning to conduct this analysis, although the feasibility with the present data sets still has to be verified.

The J/ψ and ψ' have substantial absorption cross sections in normal nuclear matter, 4.2 and 9.6 mb respectively at midrapidity, determined from fits to pA data (see Fig. 27) [122]. Studies of the A dependence were made at Fermilab over a large x_F range, but with higher $\sqrt{s}$ [123]. A very strong x_F dependence was observed for $x_F > 0.2$, as depicted in Fig. 28. Effects like shadowing, absorption and energy loss play varying roles at different x_F, resulting in the observed dependence [2].

The J/ψ is suppressed in semi-central and central Pb+Pb collisions [118] beyond absorption by nucleons alone, as shown in Fig. 29. Shadowing has not yet been included in the SPS analysis. The suppression observed in AA interactions at the SPS can, for the most part, be accounted for by the assumption that the more loosely bound ψ' and χ_c states are both suppressed by plasma production,

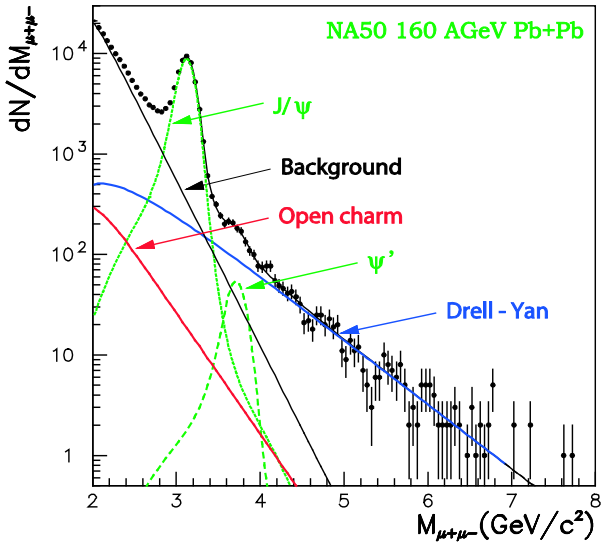

Fig. 24: Dimuon invariant mass spectrum from 158 AGeV Pb+Pb collisions at NA50 [118].

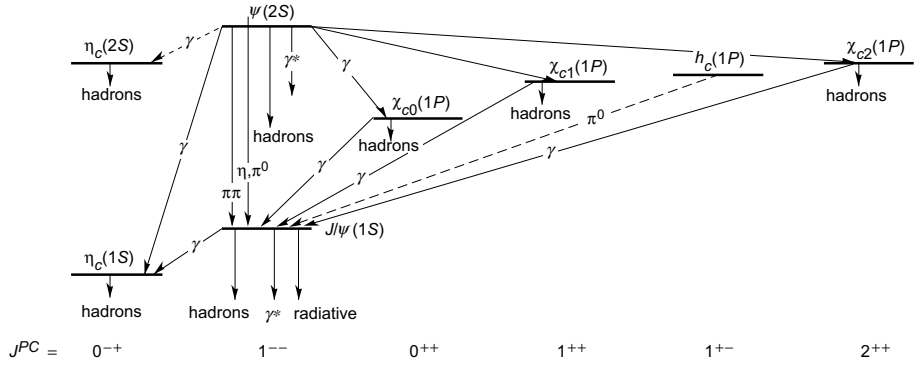

Fig. 25: Charmonium mass levels and spin states. The common feed down channels are indicated.

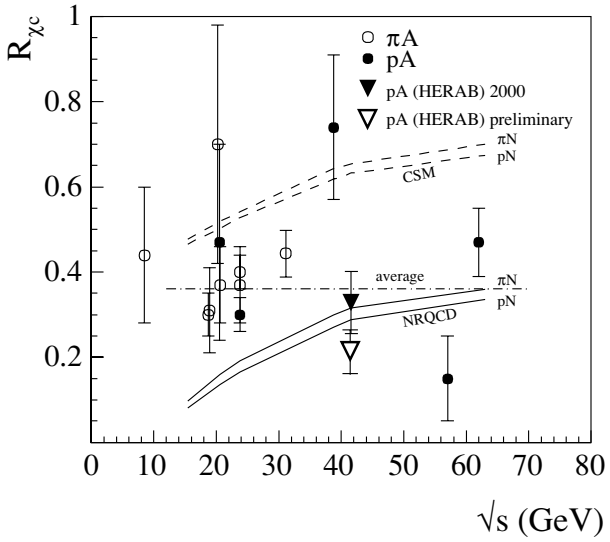

Fig. 26: The fraction, R_{χ_c}, of observed J/ψ's originating from radiative $\chi_{c1,2} \rightarrow J/\psi\gamma$ decays as a function of energy for proton and pion beams [120].

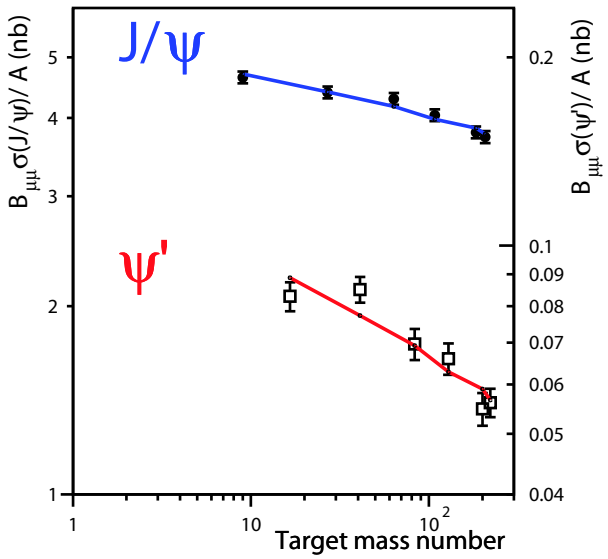

Fig. 27: NA50 measurements of J/ψ and ψ' absorption in 450 AGeV fixed-target pA collisions. The respective absorption cross sections are $\sigma_{\rm abs}(J/\psi) = 4.2 \pm 0.5$ mb and $\sigma_{abs}(\psi') = 9.6 \pm 1.6$ mb. These measurements are at midrapidity only ($x_F \sim 0$) [122].

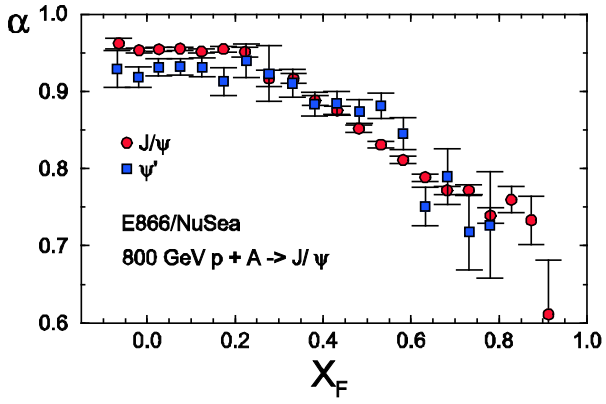

Fig. 28: Measurement of J/ψ and ψ' absorption in 800 GeV pA collisions as a function of x_F at the Tevatron [123].

eliminating their contribution to the inclusive J/ψ measurement. The direct J/ψ contribution is assumed to not be suppressed at the SPS [124, 125].

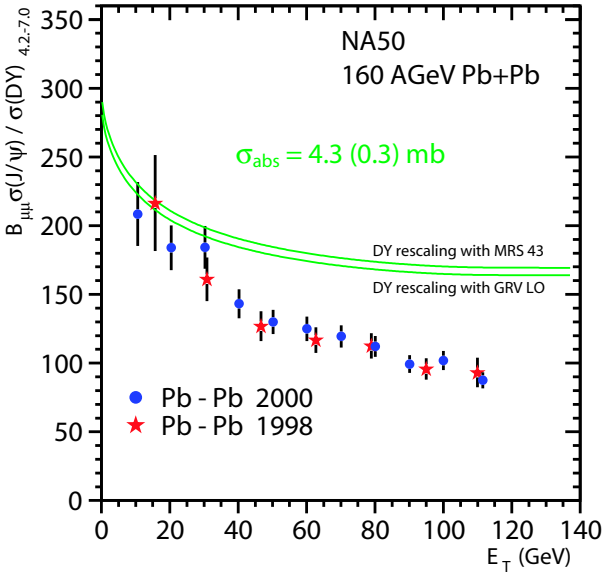

Fig. 29: J/ψ absorption in 158 AGeV Pb+Pb collisions from NA50 [122]. The curves depict predictions assuming nuclear absorption alone. Suppression beyond cold nuclear matter effects is seen starting from $E_T \sim 30$ GeV, increasing to a factor of ~ 1.7 at the highest E_T [122].

Alternatives to the QGP models are able to describe the observed J/ψ suppression by assuming breakup of the bound state by comoving matter [35]. Although these approaches make some unrealistic assumptions about the hadron density, it is possible that a fraction of the observed suppression is due to comover absorption.

The ψ', lying 50 MeV below the $D\overline{D}$ threshold, can be more easily be broken up by interactions in the medium. The strong ψ' suppression measured by NA50 has been interpreted as both total suppression of the ψ' by color screening [125] and a larger interaction cross section for comovers [126].

Charm production has not been measured in heavy ion experiments at the SPS until very recently. Figure 24 shows that the open charm contribution to the dilepton continuum in the J/ψ mass region is negligible at the SPS. Open charm measurements are, however, key to understanding the intermediate mass dilepton region. The NA60 experiment has used displaced vertices to separate charm decays from prompt dileptons. They have presented preliminary In+In results which show that while the enhancement in the intermediate mass region is confirmed, it is not consistent with enhanced open charm. Instead, the enhancement is found to be consistent with a prompt dilepton source [127].

The picture emerging from SPS studies is still somewhat inconclusive. The missing pieces of vital information have made quarkonium suppression seem to be an interesting but inconclusive study. Measurements from NA60 might provide some of the missing pieces although the future of the SPS program is currently rather uncertain. On the other hand, the vast experience gained at the SPS can and should be taken into account at RHIC. The main lesson learned is that a simple J/ψ measurement in AA collisions as a function of centrality is insufficient to draw unique conclusions. Rather, a systematic and detailed study of all related aspects, *i.e.*, a systematic study of open charm, J/ψ, ψ', and χ_c production in pp, pA, and AA collisions is required. Centrality, rapidity, and A dependence studies are mandatory.

5.3 Quarkonium measurements to date at RHIC

All of the published quarkonium results from RHIC to date are from PHENIX. However some proof-of-principle J/ψ STAR results [128] indicate that STAR will have J/ψ results from RHIC Runs 4 and 5, as

well as from future RHIC runs. PHENIX measures quarkonium yields by reconstructing their invariant mass from decays to dileptons. Dielectrons are used in the central arms ($|\eta| < 0.35$) and dimuons are used in the muon arms ($1.2 < |\eta| < 2.2$). STAR uses dielectrons within the TPC acceptance ($|\eta| < 1$).

PHENIX has measured J/ψ yields at 200 GeV from pp [129, 130], d+Au [130], Au+Au [34] and Cu+Cu collisions [34]. There are also J/ψ measurements from Cu+Cu collisions at 62 GeV [34].

PHENIX also reported an observation of $\Upsilon \rightarrow \mu^+\mu^-$ in 200 GeV pp collisions from RHIC Run 5 at Quark Matter 2005 [131]. This was a very low statistics measurement (27 counts in both muon arms). Clearly it will be difficult to make definitive Υ measurements at RHIC I luminosities but a crude Υ measurement from both PHENIX and STAR may be possible at RHIC I with about 10 times the existing integrated luminosity.

5.31 Baseline quarkonium measurements at RHIC

PHENIX has measured J/ψ cross sections in pp and d+Au collisions at 200 GeV [130]. The rapidity dependence is summarized in Fig. 30. The left side shows the invariant J/ψ yields in pp collisions while the right side shows the nuclear modification factor, $R_{\rm dAu}$, for minimum bias d+Au collisions.

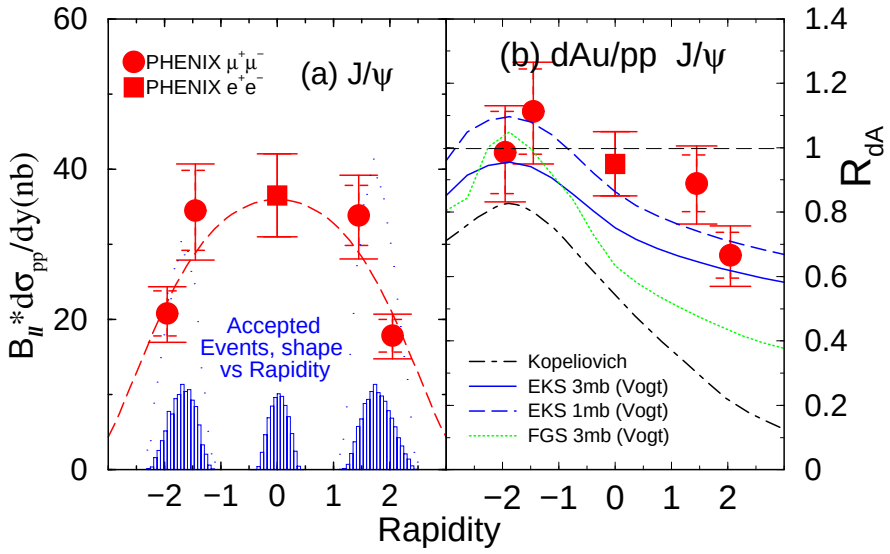

Fig. 30: The rapidity dependence of the pp J/ψ invariant yield at 200 GeV (left side) and the nuclear modification factor for minimum bias d+Au collisions (right side) [130]. The curve on the left side is a fit used to extract the total cross section. The curves on the right side are theory calculations discussed in the text. The deuteron is defined to moving toward positive rapidity.

The curves on the right-hand side of Fig. 30 show the results of several calculations that include absorption and shadowing [2, 87, 133], discussed in the previous section. The data favor the relatively modest shadowing of the EKS98 parameterization with moderate nuclear absorption.

The nuclear modification factor is shown as a function of centrality in Fig. 31 for the forward, mid and backward rapidity regions covered by the three PHENIX arms. The curves are calculated with the EKS98 (solid) and FGSh (dashed) shadowing parameterizations with a 3 mb absorption cross section.

5.32 Quarkonium measurements in heavy ion collisions at RHIC

At RHIC, preliminary measurements with the statistical precision needed to provide a strong test of models of J/ψ production in heavy ion collisions were released for the first time at Quark Matter 2005.

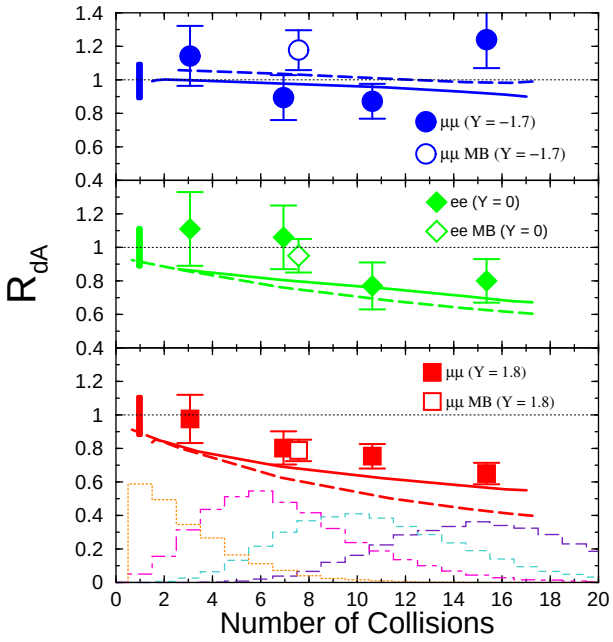

Fig. 31: Nuclear modification factor as a function of centrality for d+Au collisions measured at forward (bottom), mid (center) and backward (top) rapidity. The deuteron is moving toward forward rapidity. The theoretical curves, including both shadowing and nuclear absorption, are discussed in the text.

These preliminary PHENIX measurements were from the Run 4 Au+Au and the Run 5 Cu+Cu data sets. The main features are summarized here.

Figure 32 shows the J/ψ nuclear modification factor, R_{AA}, measured in 200 GeV Au+Au and Cu+Cu collisions at both mid- and forward/backward-rapidities [34]. These preliminary data have substantial systematic and statistical errors which are expected to decrease somewhat in the final analysis. It is thus difficult to claim that there are any differences in behavior between the Au+Au and Cu+Cu systems or between the two different rapidity regions for each species combination. The data in Fig. 32 are compared with baseline calculations of cold nuclear matter effects [3] assuming EKS98 shadowing. These calculations are intended to show the expected result if the J/ψ did not interact with the hot, dense medium beyond the cold nuclear matter effects observed in d+Au collisions. The calculations also assume a 3 mb final state J/ψ absorption cross section. Note that these same parameters may slightly overpredict the forward suppression in the d+Au data (see Fig. 31).

The same data are compared with models tuned to the CERN SPS results and extrapolated to RHIC on the left-hand side of Fig. 33, either by comover absorption [35] or by color screening in a plasma [36, 19]. No secondary production by $c\overline{c}$ coalescence is included. All the calculations strongly overestimate the suppression. The model calculations on the right-hand side of Fig. 33 include either coalescence [36, 19, 18] or transport in the medium [134, 135]. These latter calculations all differ in the way cold nuclear absorption is accounted for, in the J/ψ pp production cross section used for normalization, and in the $c\overline{c}$ production cross section used in the coalescence calculation.

Figure 33 shows that the data are consistent with models that include both plasma screening and quark coalescence in the final state, although some of these models tend to underpredict the suppression in the most central collisions, as is the case for cold nuclear matter effects alone in Fig. 32. The calculations in Refs. [19, 36] tuned to the SPS data require either some coalescence not to overpredict the suppression [36] or a significant open charm enhancement [19] not supported by the NA60 data [136]. At

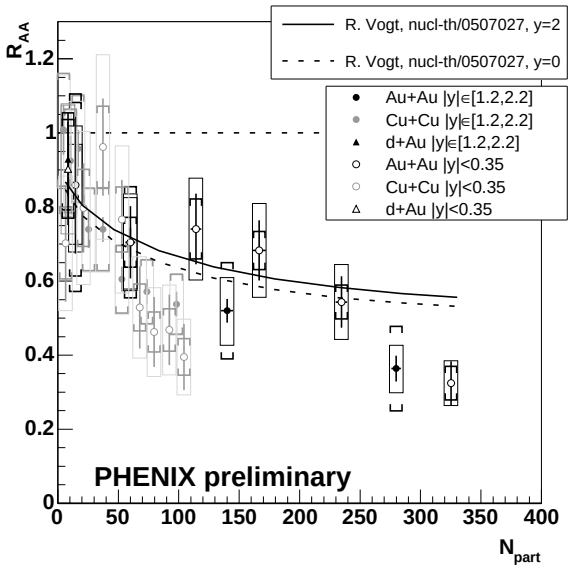

Fig. 32: The nuclear modification factor as a function of centrality for 200 GeV Au+Au and Cu+Cu collisions measured at forward, mid and backward rapidity. The calculations [3] include cold nuclear effects from shadowing and "normal" final state absorption.

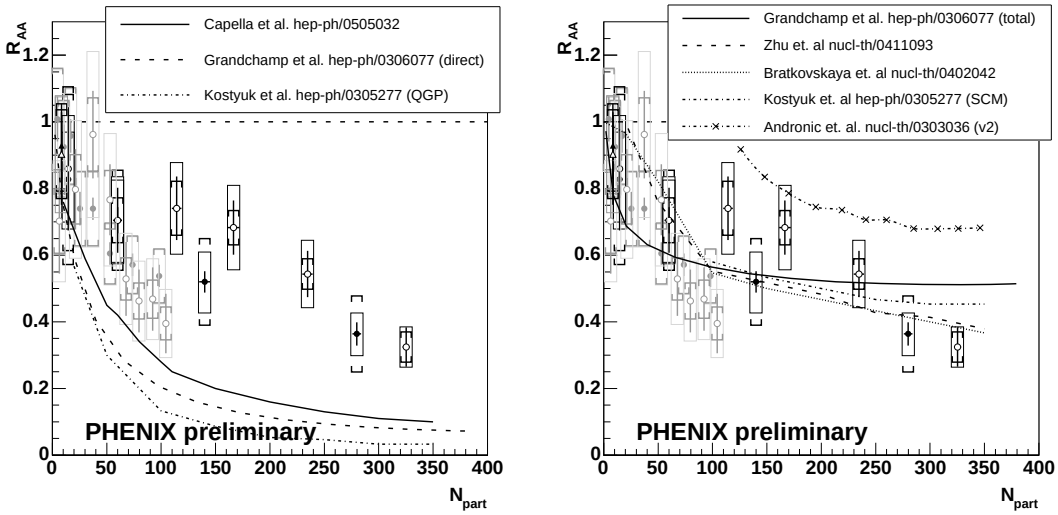

Fig. 33: Nuclear modification factor versus centrality for 200 GeV Au+Au and Cu+Cu collisions measured at forward, mid and backward rapidity, compared with various models that include final state effects from QGP suppression or comover absorption (left-hand side) and including coalescence or J/ψ transport (right-hand side). See the text for details.

RHIC, the coalescence component completely dominates J/ψ production in central Au+Au collisions and contributes about 50% of the J/ψ yield in central Cu+Cu collisions.

PHENIX also showed a measurement of the nuclear modification factor for 62 GeV Cu+Cu collisions at Quark Matter 2005. While this measurement has relatively low statistics, the 62 GeV data exhibit similar, and perhaps slightly stronger, suppression in the most central collisions to that seen in 200 GeV Cu+Cu collisions, consistent with predictions of a model with color screening and coalescence [115] (see Fig. 23).

Recently there have been theoretical efforts to predict the effects of $c\bar{c}$ coalescence on the rapidity and p_T dependence of the J/ψ yield. Figure 34 shows experimental results on the average p_T^2 of the J/ψ, $\langle p_T^2 \rangle$, as a function of $N_{\rm coll}$ for Au+Au and Cu+Cu collisions in the rapidity regions covered by PHENIX. The predictions are from a coalescence model by Thews [137] and show the predicted $N_{\rm coll}$ dependence of $\langle p_T^2 \rangle$ for Au+Au and Cu+Cu collisions assuming either no coalescence or a 100% coalescence contribution. A large coalescence component results in a narrower J/ψ p_T distribution since a c and $\overline{c}$ with large relative p_T cannot coalesce. Thus $\langle p_T^2 \rangle$ is reduced by a factor of two in central collisions. The data have substantial statistical errors, particularly at midrapidity, but they do appear to favor the coalescence calculation. Reference [137] also contains some model calculations with coalescence components resulting from 10, 20 and 40 $c\bar{c}$ pairs per central Au+Au collision at different initial temperatures.

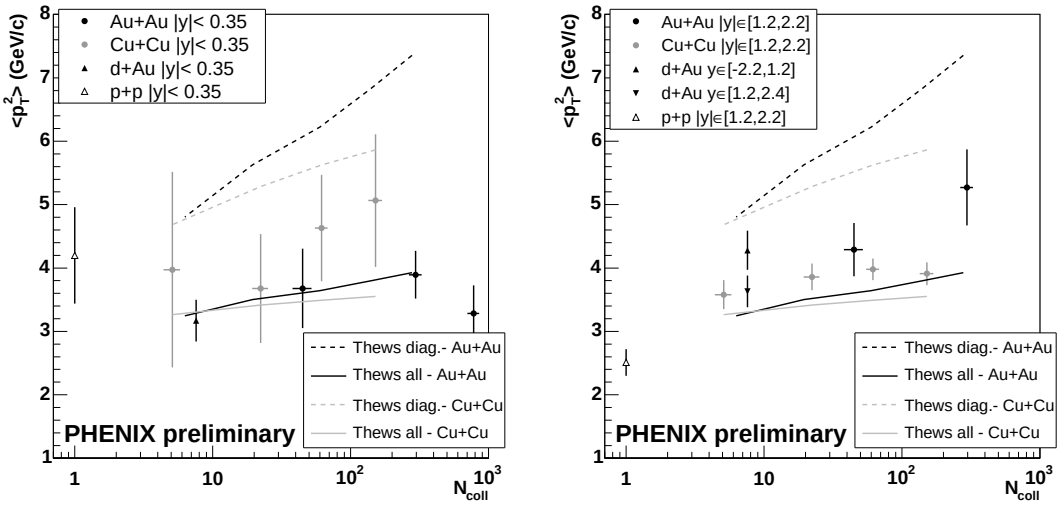

Fig. 34: The measured $\langle p_T^2 \rangle$ for 200 GeV Au+Au and Cu+Cu collisions measured at (left) and away from (right) midrapidity. The calculations [137] show the predicted behavior with (upper curves, labeled 'all') and without (lower curves, labeled 'diag.' for correlated $c\overline{c}$ pairs only) the coalescence contribution.

No realistic model calculations of the rapidity distribution from coalescence are available for heavy ion collisions so far, but it is predicted [16] that a strong charm coalescence contribution to J/ψ production will lead to a narrowing of the rapidity distribution, just as for the p_T distribution. Figure 35 shows the pp, Cu+Cu, and Au+Au rapidity distributions measured by PHENIX. The Au+Au rapidity distributions are shown in three centrality bins while the Cu+Cu distributions are shown in four bins. The statistical and systematic uncertainties are fairly large, particularly for Au+Au. Within those uncertainties, the data show no evidence of a narrowing of the rapidity distribution in central heavy ion collisions.

A more quantitative statement can be made for Cu+Cu collisions, the highest statistics heavy ion data set so far. Figure 36 shows preliminary PHENIX results on the rapidity dependence of R_{AA} for min-

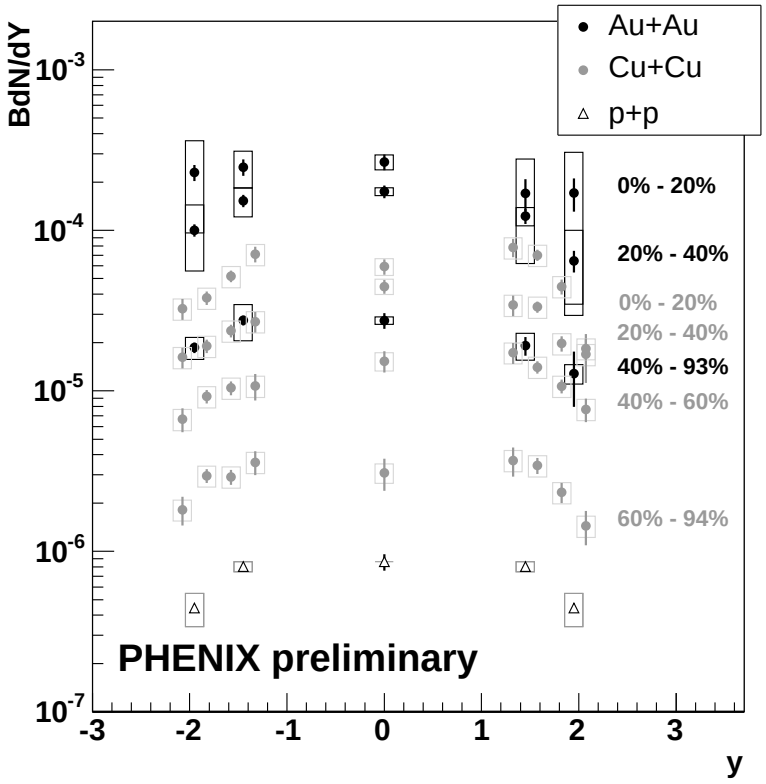

Fig. 35: The rapidity dependence of the J/ψ invariant yield for pp, Cu+Cu and Au+Au collisions at various centralities (with 0% being most central). Within the large uncertainties, there is no significant change in the shape of the rapidity distribution

.

imum bias collisions (left) and for the muon data in several centrality bins (right). Also shown on these plots are baseline cold nuclear matter calculations [3], discussed in the previous section, and predictions of the effect on the R_{AA} rapidity dependence [16] if the entire J/ψ yield was due to coalescence. There are considerable uncertainties but the data show little evidence of strong rapidity narrowing in central Cu+Cu collisions. The uncertainties will be reduced significantly when the higher statistics Run 5 pp reference analysis is completed. The coalescence contribution is predicted to be approximately 50% for central Cu+Cu collisions [36] so that some rapidity narrowing is expected in central Cu+Cu. The results of Ref. [3], presented in Fig. 17, show significant modification of the J/ψ rapidity distribution (and thus presumably of the open charm distributions) due to shadowing, causing the midrapidity yield to be smaller relative to that at $|\eta| \sim 1.7$ in central collisions. Thus the observation that there is no dramatic rapidity narrowing may be consistent with coalescence models that include shadowing in the initial $c\overline{c}$ production.

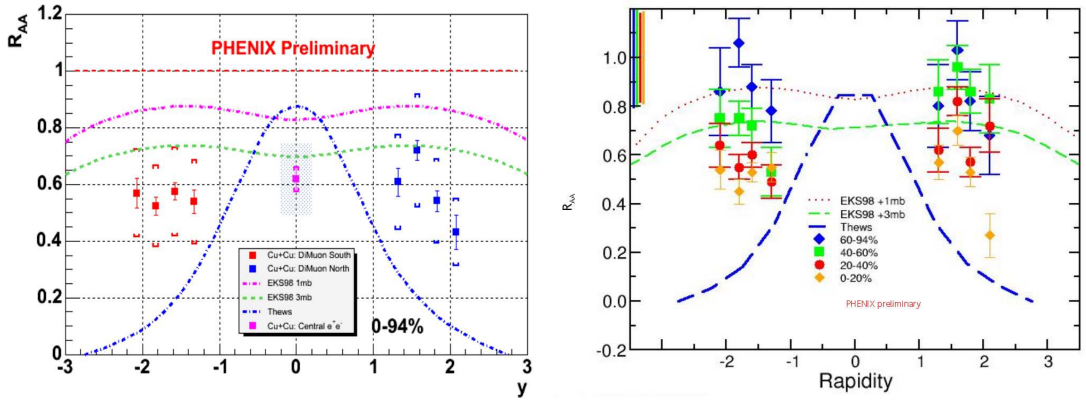

Fig. 36: The J/ψ R_{AA} as a function of rapidity for minimum bias Cu+Cu collisions (left) and binned in centrality in the muon arm (right). Within the large uncertainties, there is no significant change of R_{AA} with rapidity. The curves are discussed in the text.

In summary, the evidence for a strong coalescence component in the J/ψ yield in central collisions is mixed. The suppression as a function of centrality shown in Fig. 33 is reasonably consistent with models that include coalescence, as is the $\langle p_T^2 \rangle$ in Fig. 34. However, the predicted narrowing of the rapidity distribution due to coalescence, based on the assumption of an underlying charm distribution peaked near midrapidity, does not seem to be supported by the data in Figs. 35 and 36. The open charm rapidity distribution has not yet been very well determined experimentally. As mentioned earlier, shadowing is predicted to modify the underlying charm rapidity distribution. The prediction of p_T narrowing, on the other hand, is based on a steeply falling charm p_T distribution, well established by the existing data.

A J/ψ result of great interest would be R_{AA} as a function of p_T. A useful result is expected from the PHENIX data once the RHIC Run 5 pp analysis is completed, providing much better statistical precision for the high p_T pp reference than presently available. There are also analyses underway in PHENIX to extract the J/ψ v_2 but the limited statistics of the present heavy ion data sets will likely preclude a meaningful result. Similarly, a statistically meaningful J/ψ polarization measurement is unlikely from the present data sets.

Recently, a model of sequential charmonium suppression has been applied to the RHIC and SPS data [138]. The model assumes that, above a critical energy density, the ψ' and χ_c are suppressed while the J/ψ survival probability due to color screening is equal to unity. Normal nuclear absorption is parameterized by an effective absorption cross section that accounts for all cold nuclear matter effects. The pA data at the SPS gives a large effective J/ψ absorption cross section that the RHIC d+Au data, as

also implied by the results in Ref. [91]. Three values of $\sigma_{\rm abs}$ are extracted from the d+Au data, one for each rapidity bin. These values are then used to obtain the survival probability in AA collisions. When $N_{\rm part}$ is converted to energy density, ϵ, and the survival probabilities for color screening and cold nuclear matter are included, the SPS and RHIC data appear to lie on a common suppression curve as a function of energy density.

5.4 Proposed RHIC II quarkonia measurements

Unlike other probes, quarkonia measurements are guided by predictions from lattice QCD calculations. Color screening modifies the linear rise of the QCD potential at large distances. The quarkonia spectral functions quantify the temperature dependence of the potential. Since quarkonia suppression is determined by the plasma temperature and the binding energy (equivalently the quarkonium size and the Debye screening length), measuring the sequential disappearance of these states acts as a QCD thermometer.

Thus the importance of a comprehensive study of **all** experimentally accessible quarkonium states cannot be overstated. A systematic study of heavy quarkonium spectroscopy, with a complete determination of the suppression pattern of the quarkonium states, remains the most **direct probe of deconfinement**. It is also the signature that most closely resembles as a thermometer of the hot initial state, which, with future improved lattice calculations, can be directly compared to QCD.

While J/ψ physics at RHIC is as compelling as it was in 1986 when first proposed by Matsui and Satz [21], the systematic study of all quarkonia states, and especially bottomonium, feasible at RHIC II, provides a more complete QGP probe than heretofore possible.

Table 11 relates the main physics topics to the relevant probes and subsequent detector requirements. The ability of a program at RHIC II to make these measurements can be judged from the yields given in Tables 2, 3, and 4. The measurements that are possible at RHIC without the luminosity upgrade are the J/ψ rapidity and p_T distributions at full energy. The measurements that are newly possible at RHIC II are those for the excited charmonium states (ψ' and χ_c) and the bottomonium states ($\Upsilon(1S)$, $\Upsilon(2S)$ and $\Upsilon(3S)$). Measurements of the J/ψ v_2 and polarization, as well as excitation functions of heavy flavor distributions will be possible only at RHIC II. It is evident that a comprehensive program to use quarkonium as a QCD thermometer to provide direct evidence of deconfinement is possible only with RHIC II luminosity.

The measurements needed to study the excited charmonium states, χ_c and ψ', have quite different problems. The ψ' measurement is the same as the J/ψ, reconstruction of dilepton decays, but requires $\sim$ 100 times as much integrated luminosity for the same yield. In addition, the ψ' measurement is made more difficult by the existence of a significant background under the peak in the invariant mass spectrum. The signal to background is worse than for the J/ψ, increasing the integrated luminosity needed for measurements of a given precision. The presence of the SVTX detector in PHENIX will lead to significantly better mass resolution at the J/ψ mass, as shown in Fig. 37. A ψ' measurement is certainly feasible at RHIC II. The χ_c measurement can be done with the $\chi_c \rightarrow J/\psi\,\gamma$ channel, where the J/ψ is reconstructed from dilepton decays and the photon is detected in an electromagnetic calorimeter. While the yields are larger than for the ψ', the need to form the χ_c invariant mass by combining each J/ψ candidate with a large number of photons means that combinatorial backgrounds will be quite large. Thus the χ_c measurement will be difficult. There are ongoing simulation studies by PHENIX and STAR to determine how difficult it will be.

Figure 38 shows the results of a PHENIX simulation for the muon arms and the Nose Cone Calorimeter where simulated $\chi_c \rightarrow J/\psi\,\gamma$ decays are embedded in the 10% most central Au+Au events from HIJING. After rejecting all events where the pre-shower and shower-max detectors show multiple hits in a Nose Cone Calorimeter module, a clean χ_c mass peak is seen. While this simulation shows that the χ_c decay can be cleanly reconstructed, it remains to be demonstrated that the signal to combinatorial

Physics Motivation	Probes	Measurements	Requirements
Baseline measurements	J/ψ, ψ', χ_c, $\Upsilon(1S)$, $\Upsilon(2S)$, and $\Upsilon(3S)$ decays to dileptons	Rapidity and p_T spectra in $pA$and pp as a function of $\sqrt{s}$	High luminosity and acceptance for sufficient statistics, especially for the Υ family. Good mass resolution to resolve ψ and Υ states.
Deconfinement, Initial Temperature	J/ψ, ψ', χ_c, $\Upsilon(1S)$, $\Upsilon(2S)$, and $\Upsilon(3S)$ decays to dileptons	Suppression patterns in AA as a function of $\sqrt{s}$ and A	High luminosity, acceptance and mass resolution for quarkonium, and triggers that work in Au+Au collisions.
Thermalization and Transport	J/ψ	J/ψ v_2 as function of $\sqrt{s}$ and A.	High luminosity for good statistics in short runs for $\sqrt{s}$ and A scans

Table 11: Main physics goals of the RHIC-II quarkonium program and corresponding probes, studies, and requirements.

background ratio is acceptable in central Au+Au collisions.

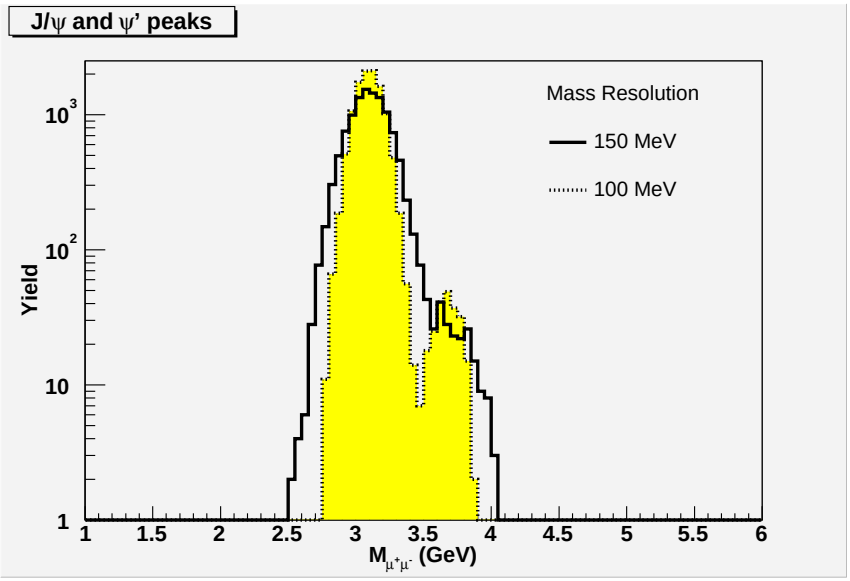

Fig. 37: The J/ψ and ψ' invariant mass spectrum in the muon arms with (dashed histogram) and without (solid histogram) the improvement in mass resolution from the SVTX detector. The yields are expected from a 25 pb^{-1} pp run.

Like the J/ψ, the bottomonium states are studied using their dilepton decays. The bottomonium measurements require very large integrated luminosity and good invariant mass resolution. PHENIX expects to be able to resolve the $\Upsilon(1S)$, $\Upsilon(2S)$, and $\Upsilon(3S)$ states (see Fig. 40). Because of its larger acceptance, STAR will have $\sim$ 10 times larger yields for the Υ states than PHENIX, but the states will not be cleanly resolved and fitting will be required to extract individual yields (see Fig. 39 for a STAR simulation of the Υ mass spectrum). Although the yields are small relative to the J/ψ, bottomonium measurements are quite clean. The states are massive ($\sim$ 10 GeV/c^2) so that their decay leptons have relatively large momenta and are thus easily distinguished from background leptons. The combinatorial background in this mass range is extremely small and multiple scattering is of less concern. While the interpretation of charmonium suppression is made more difficult by the rather large cross section for nucleon and comover absorption, the situation for bottomonium is considerably better. Absorption of directly produced bottomonium by hadronic comovers has been shown to be negligible [139].

The $\sqrt{s}$ dependence of produced J/ψ's relative to the number of $c\bar{c}$ pairs, depicted in Fig. 23 [115], is striking. An excitation function measurement of this ratio for $30 < \sqrt{s_{NN}} < 200$ GeV could help to disentangle suppression from enhancement mechanisms such as recombination/coalescence. Such measurements, however, are extremely statistically demanding since both heavy quarks and quarkonia will need to be measured with good statistics over a wide range of beam energies.

A measurement of the quarkonium nuclear modification factor at high p_T can provide a unique experimental probe for studying energy loss and color diffusion [140]. At relatively large transverse momentum, suppression due to color screening and coalescence become negligible. Instead, the quarkonium state is a hard probe that interacts with the medium. In particular, any color octet can suffer energy loss. The relative abundance of charmonium resonances can provide an experimental handle on studying such phenomena as each resonance may have a different octet contribution. We must exercise caution, however, as competing charmonium production models exist. In parallel with any nucleus-nucleus studies, it is therefore important to investigate and compare production mechanisms in pp and pA interactions, at both central and forward rapidities [141, 142, 143].

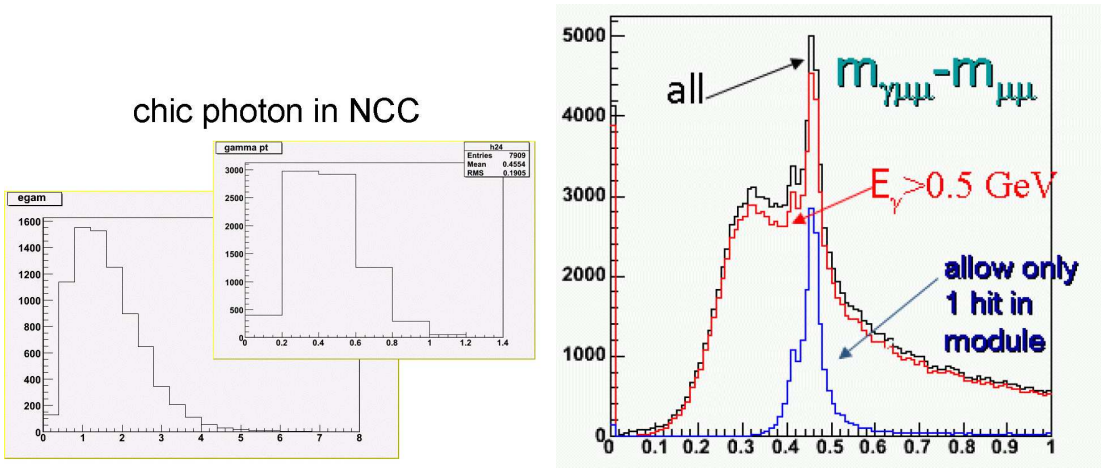

Fig. 38: Left: Simulated energy and p_T distributions in the PHENIX Nose Cone Calorimeter of the photon from $\chi_c \rightarrow J/\psi\,\gamma$ decays. Right: The invariant mass spectrum in the PHENIX muon arms and Nose Cone Calorimeter from a simulation where $\chi_c \rightarrow J/\psi\,\gamma$ decays are embedded in the 10% most central Au+Au events from HIJING. The leptons and photon are required to come from the χ_c so there is no combinatorial background.

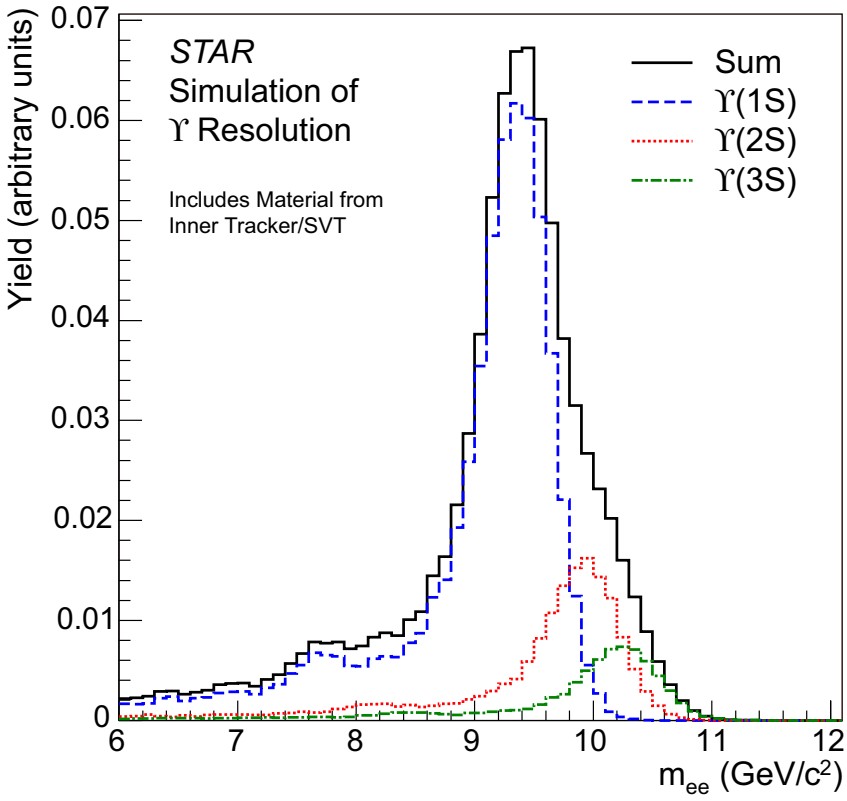

Fig. 39: The ϒ family dielectron mass spectrum from a STAR simulation.

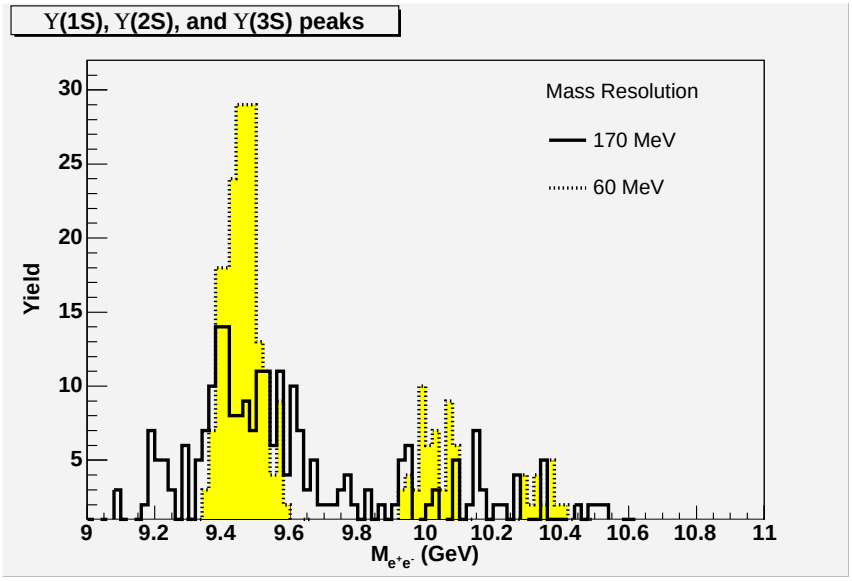

Fig. 40: The Υ family dielectron mass spectrum from a PHENIX simulation for the central arms, showing the expected improvement in Υ mass resolution provided by the initial direction measurement in the SVTX barrel. The number of events shown correspond to about half of a 12 week Au+Au run at RHIC II.

In addition to the baseline quarkonium measurements in pp and pA collisions listed in Table 11, other measurements are required as input to the models that attempt to explain the quarkonium results. The most prominent of these are listed in Table 12.

The importance of measuring the underlying charm distributions as input to models of J/ψ coalescence is obvious, as is the importance of understanding cold nucleus effects on quarkonium production.

It is crucial for the interpretation of the quarkonia yields from AA collisions to understand the feed down contributions from the χ_c states (see Fig. 25). The best feed down measurement will be made in 500 GeV pp collisions because the increased luminosity and increased charmonium production cross sections lead to $\sim$ 10 times larger charmonium yields than in 200 GeV pp collisions. Since the χ_c contribution to the J/ψ yield will not change significantly between 200 and 500 GeV, the increased yield at 500 GeV will provide a definitive baseline measurement of χ_c feed down in pp collisions.

Recently, quarkonium polarization measurements were suggested as a possible signature of QGP formation [144]. The quarkonium yields at RHIC II will be large enough to permit a J/ψ polarization measurement at low p_T by both PHENIX and STAR.

Topic	Measurements	Requirements
Cold Nuclear Effects	In pp and pA collisions: • $x_{1,2}$, x_F and y dependence of quarkonia production • A dependence	Large y acceptance, including forward coverage
Suppression vs. Recombination	In pp pA and AA collisions • Charm $d\sigma/dp_T dy$ • J/ψ v_2 • p_T dependence of suppression	High resolution vertex detectors (charm)
Feed down contribution	χ_c, at least in pp and pA	Photon detection capabilities over wide rapidity range. High rates, good energy and momentum resolution to enhance χ_c S/B ratio
Production mechanism	χ_c, polarization at least in pp and pA	Large acceptance for $\cos\theta^*$ measurement

Table 12: Additional (baseline) measurements beyond Au+Au measurements that are required in order to address the main physics questions.

6. Relationship to the LHC program

The major differences between quarkonium studies at RHIC II and at the LHC are:

- The temperature in 5.5A TeV central Pb+Pb collisions at the LHC is expected to be $\sim 4\,T_c$, while in 200A GeV central Au+Au collisions at RHIC the temperature is expected to be $\sim 2\,T_c$ [145].
- The lifetime of the QGP in 5.5A TeV central Pb+Pb collisions at the LHC is expected to be two to three times longer than in 200A GeV central Au+Au collisions at RHIC [145].
- Heavy flavor production cross sections are much larger at the LHC. The cross sections for open charm and bottom production are $\sim$ 15 and $\sim$ 100 times higher respectively [9] at the LHC. The charmonium and bottomonium cross sections are ~ 13 and ~ 55 times higher respectively [37].
- The higher open heavy flavor cross sections at the LHC cause the number of $c\bar{c}$ and $b\bar{b}$ pairs created in central Au+Au collisions at RHIC, ~ 10 and ~ 0.05, respectively, to rise to ~ 115 and ~ 5, respectively, in central Pb+Pb collisions at the LHC [9].
- The Au+Au luminosity at RHIC II is projected to be 14 times larger than the Pb+Pb luminosity at the LHC (7×10^{27} cm^{-2} s^{-1} relative to 5×10^{26} cm^{-2} s-1).
- The heavy ion running times per year at RHIC II are expected to be considerably longer than at the LHC. Taking the polarized pp program at RHIC II into account, the heavy ion program is expected to get $\sim$ 12 weeks of physics running on average. The heavy ion program at the LHC will be allocated 1 month of physics running.

The larger heavy flavor cross sections at the LHC are approximately balanced by the increased luminosity and running times at RHIC II, making the heavy flavor yields per year similar. Thus the types of measurements that can be made at the two facilities will also be similar as well as of similar quality (see Tables 2, 3 and 5). However, there will be important differences in the physics environments prevailing at the two facilities which will make the two programs complementary.

The higher initial energy density at the LHC means that the QGP will be created at a significantly higher temperature with a correspondingly strong potential for new physics effects at the LHC. In addition, the factor of ten increase in $c\bar{c}$ pairs and the factor of 100 increase in $b\bar{b}$ pairs per central collision at the LHC will have a major impact on the interpretation of heavy flavor measurements. We will discuss some of those differences here.

Lattice calculations suggest that the J/ψ may remain bound at the highest RHIC temperatures, while the excited charmonium states are predicted to be unbound. At the LHC, all the charmonium states should be unbound at the highest temperatures, implying that almost all charmonium production in central Pb+Pb collisions at the LHC will be due to coalescence of $c\bar{c}$ pairs. Thus the prompt charmonium yields at the LHC should reflect only the coalescence mechanism with no contribution from the primordial J/ψ production (except in very peripheral collisions). The measurements at RHIC and the LHC will thus provide very different windows on charmonium suppression in the QGP that will help resolve the ambiguities in interpreting data due to the balance between destruction and coalescence formation of charmonium at RHIC.

Because of its higher binding energy, the characteristics of bottomonium production at the LHC should be similar to those of charmonium at RHIC. The bottomonium states are shown in Fig. 41 The $\Upsilon(1S)$ may remain bound at the highest temperatures at the LHC while the other bottomonium states will be dissociated. Given ~ 5 $b\bar{b}$ pairs in central Pb+Pb collisions (relative to ~ 10 $c\bar{c}$ pairs at RHIC), the Υ yield at the LHC is predicted [146] to reflect a balance between dissociation and coalescence reminiscent of the RHIC J/ψ production models. However, at RHIC, the bottomonium dissociation rates will be significantly different. While the $\Upsilon(1S)$ is predicted to be bound, the $\Upsilon(2S)$ may also remain bound. Only the $\Upsilon(3S)$ is likely to dissociate at RHIC. Also, since the $b\bar{b}$ pair yield at RHIC is $\sim$ 0.05 per Au+Au central collision, no significant bottomonium production by coalescence is expected. Thus the bottomonium yields at RHIC II should reflect only QGP suppression. Measurements at RHIC II and the LHC will thus provide very different windows on bottomonium suppression in the QGP that will help to resolve the ambiguities in interpretation due to the balance of bottomonium destruction and coalescence at the LHC.

The open heavy flavor programs at RHIC II and the LHC will consist of similar measurements with similar goals. They will study energy loss, thermalization and flow of heavy quarks in systems with very different energy densities, interaction cross sections and lifetimes. However, not all challenges in the measurements are similar. At $\sqrt{s} = 200$ GeV, bottom decays to leptons begin to dominate the single electron spectrum at $p_T \sim 4$ GeV/c. As the collision energy increases, the lepton spectra from B and D decays move closer together rather than further apart. Thus, the large increase in the $b\overline{b}$ cross section relative to $c\overline{c}$ does not make single leptons from B and D decays easier to separate. Preliminary calculations show that the $B \rightarrow e$ decay does become larger than that of $D \rightarrow e$ but higher p_T, $p_T >$ 10 GeV/c. The two lepton sources differ by less than a factor of two to $p_T \sim 50$ gevc in the range $|y| \leq 1$. Separating single leptons from charm and bottom decays will require statistical separation using differences in the displaced vertex distributions at all p_T at the LHC. Thus interpretation of single lepton data from heavy flavor decays will be more difficult at the LHC.

ALICE can reconstruct D^0 decays from $p_T \sim 0$ to $p_T \sim 25$ GeV/c[38]. Like STAR, ALICE will be unable to trigger on D decays and will have obtain these events from the minimum bias sample. Thus the longer running times at RHIC are an advantage since more minimum bias data can be taken (see Tables 3 and 5). While it is not yet clear what CMS and ATLAS will do to reconstruct charm, they should be able to do b jets well, similar to the Tevatron measurements. As at RHIC, B mesons can be measured cleanly at the LHC through their decays to J/ψ, although triggering on low p_T J/ψ at LHC is difficult.

It has also been suggested that the $B\overline{B}$ contribution to the dimuon continuum, the dominant contribution above the Υ mass, can be used to measure energy loss [39]. That channel would be fairly clean at the LHC but more difficult at RHIC.

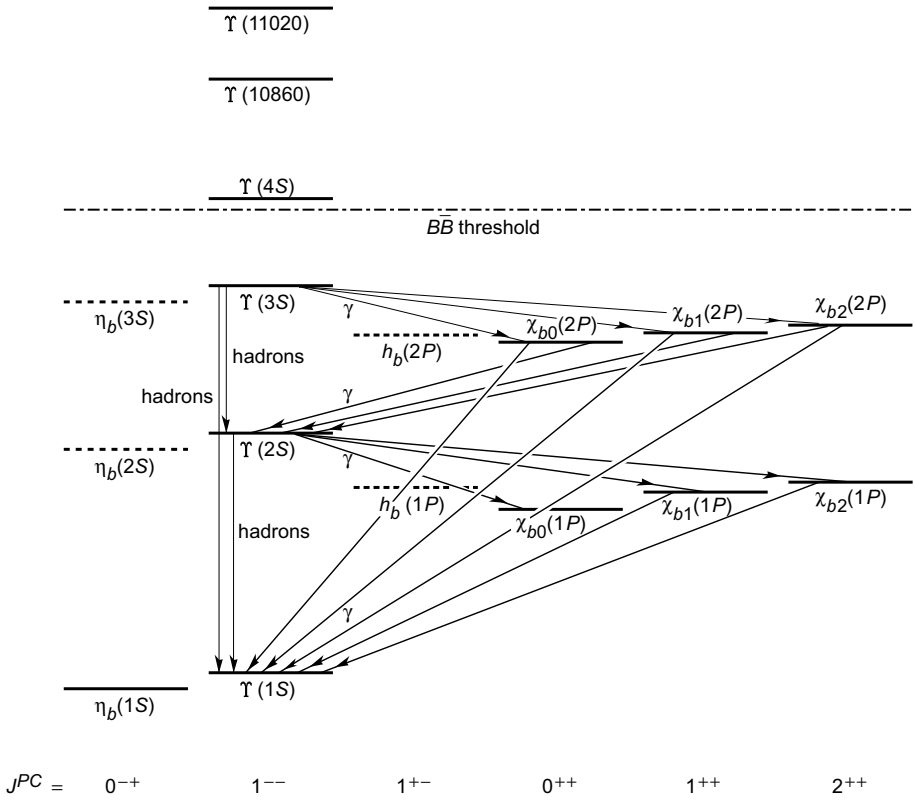

Fig. 41: Bottomonium mass levels and spin states. The common feed down channels are indicated.

7. Conclusions

We have shown that, so far, the RHIC heavy flavor physics program is very rich and stimulating, with many provocative and challenging results. To fully realize the potential of this compelling program, however, both detector upgrades and a luminosity upgrade are mandatory. Detector upgrades will improve reconstruction of charm hadron decays into hadronic channels and allow detection of $B \to J/\psi X$ decays using secondary vertex measurements. Upgrades will also make χ_c detection possible and, in the case of STAR, lead to significant quarkonium yields. However only increased luminosities will allow high statistics measurements of all of these yields as well as increase the p_T reach of J/ψ and heavy flavor R_{AA} and v_2.

We have also shown that the RHIC II and LHC heavy flavor physics programs are complementary. Both are required for a complete understanding of heavy flavor production as a function of energy and temperature. We have also demonstrated that, despite lower heavy flavor cross sections at RHIC, the longer running times and higher luminosity of RHIC II make the recorded yields similar at the two facilities.

References

[1] M. Cacciari, P. Nason and R. Vogt, Phys. Rev. Lett. **95**, 122001 (2005) [arXiv:hep-ph/0502203].

[2] R. Vogt, Phys. Rev. C **71**, 054902 (2005) [arXiv:hep-ph/0411378].

[3] R. Vogt, Acta Phys. Hung. New Ser. Heavy Ion Phys. in press [arXiv:nucl-th/0507027].

[4] M. Djordjevic, M. Gyulassy, R. Vogt and S. Wicks, Phys. Lett. B, in press [arXiv:nucl-th/0507019].

[5] M. Djordjevic, M. Gyulassy and S. Wicks, Phys. Rev. Lett. **94**, 112301 (2005) [arXiv:hep-ph/0410372].

[6] N. Armesto, C. A. Salgado and U. A. Wiedemann, Phys. Rev. D **69**, 114003 (2004) [arXiv:hep-ph/0312106].

[7] Y. L. Dokshitzer and D. E. Kharzeev, Phys. Lett. B **519**, 199 (2001) [arXiv:hep-ph/0106202].

[8] Z. w. Lin, R. Vogt and X. N. Wang, Phys. Rev. C **57**, 899 (1998) [arXiv:nucl-th/9705006]; Z. Lin and R. Vogt, Nucl. Phys. B **544**, 339 (1999) [arXiv:hep-ph/9808214].

[9] R. Vogt [Hard Probe Collaboration], Int. J. Mod. Phys. E **12**, 211 (2003) [arXiv:hep-ph/0111271].

[10] B. Svetitsky and A. Uziel, Phys. Rev. D **55**, 2616 (1997) [arXiv:hep-ph/9606284].

[11] V. Greco, C. M. Ko and R. Rapp, Phys. Lett. B **595**, 202 (2004) [arXiv:nucl-th/0312100].

[12] Z. w. Lin and D. Molnar, Phys. Rev. C **68**, 044901 (2003) [arXiv:nucl-th/0304045].

[13] J. Dunlop [STAR Collaboration], in proceedings of Quark Matter '05, Budapest, Hungary, August 2005.

[14] S. Butsyk [PHENIX Collaboration], in proceedings of Quark Matter '05, Budapest, Hungary, August 2005. [arXiv:nucl-ex/0510010]

[15] S. Sakai [PHENIX Collaboration], in proceedings of Quark Matter '05, Budapest, Hungary, August 2005, arXiv:nucl-ex/0510027.

[16] R. L. Thews and M. L. Mangano, arXiv:nucl-th/0505055.

[17] R. L. Thews, M. Schroedter and J. Rafelski, Phys. Rev. C **63**, 054905 (2001) [arXiv:hep-ph/0007323].

[18] A. Andronic, P. Braun-Munzinger, K. Redlich and J. Stachel, Phys. Lett. B **571**, 36 (2003) [arXiv:nucl-th/0303036].

[19] A. P. Kostyuk, M. I. Gorenstein, H. Stöcker and W. Greiner, Phys. Rev. C **68**, 041902 (2003) [arXiv:hep-ph/0305277].

[20] M. C. Abreu *et al.* [NA50 Collaboration], Phys. Lett. B **410**, 327 (1997); Phys. Lett. B **410**, 337 (1997).

[21] T. Matsui and H. Satz, Phys. Lett. B **178**, 416 (1986).

[22] F. Karsch, M.T. Mehr and H. Satz, Z. Phys. C **37**, 617 (1988).

[23] S. Datta, F. Karsch, P. Petreczky and I. Wetzorke, J. Phys. G: Nucl. Part. Phys. **30**, S1347 (2004) [arXiv:hep-lat/0403017].

[24] D. Kharzeev and H. Satz, Phys. Lett. B **334**, 155 (1994) [arXiv:hep-ph/9405414].

[25] J. F. Gunion and R. Vogt, Nucl. Phys. B **492**, 301 (1997) [arXiv:hep-ph/9610420].

[26] P. Braun-Munzinger and J. Stachel, Phys. Lett. B **490**, 196 (2000) [arXiv:nucl-th/0007059].

[27] P. Braun-Munzinger and J. Stachel, Nucl. Phys. A **690**, 119 (2001) [arXiv:nucl-th/0012064].

[28] L. Grandchamp and R. Rapp, Phys. Lett. B **523**, 60 (2001) [arXiv:hep-ph/0103124].

[29] P. Braun-Munzinger and K. Redlich, Eur. Phys. J. C **16**, 519 (2000) [arXiv:hep-ph/0001008].

[30] C.M. Ko, B. Zhang, X.N. Wang and X.F. Zhang, Phys. Lett. B **444**, 237 (1998) [arXiv:nucl-th/9808032].

[31] S. S. Adler *et al.* [PHENIX Collaboration], Phys. Rev. Lett. **94**, 082301 (2005) [arXiv:nucl-ex/0409028].

[32] H. Zhang [STAR Collaboration], in proceedings of Quark Matter '05, Budapest, Hungary, August 2005; J. Bielcik et al. [STAR Collaboration], ibid.

[33] N. Armesto *et al.*, in proceedings of Quark Matter '05, Budapest, Hungary, August 2005, arXiv:hep-ph/0510284; arXiv:hep-ph/0511257.

[34] H. Periera [PHENIX Collaboration], in proceedings of Quark Matter '05, Budapest, Hungary, August 2005.

[35] A. Capella and E. G. Ferreiro, Eur. Phys. J. C **42**, 419 (2005) [arXiv:hep-ph/0505032].

[36] L. Grandchamp, R. Rapp and G. E. Brown, Phys. Rev. Lett. **92**, 212301 (2004) [arXiv:hep-ph/0306077].

[37] M. Bedjidian *et al.*, edited by R. Vogt and S. Frixione, Working Group Report from the Workshop on Hard Probes in Heavy Ion Collisions, CERN, arXiv:hep-ph/0311048.

[38] A. Dainese, R. Vogt, M. Bondila, K. J. Eskola and V. J. Kolhinen, J. Phys. G **30**, 1787 (2004) [arXiv:hep-ph/0403098].

[39] I. P. Lokhtin and A. M. Snigirev, Eur. Phys. J. C **21**, 155 (2001) [arXiv:hep-ph/0105244].

[40] O. Kodolova, CMS Internal Note 2003-002.

[41] K. H. Ackermann *et al.*, Nucl. Instrum. Meth. A **499**, 624 (2003).

[42] R. Gavai, D. Kharzeev, H. Satz, G. A. Schuler, K. Sridhar and R. Vogt, Int. J. Mod. Phys. A **10**, 3043 (1995) [arXiv:hep-ph/9502270].

[43] P. Crochet [ALICE Collaboration], EPJdirect **A1**, 1 (2005) and private communication.

[44] B. Wyslouch [CMS Collaboration], PANIC LHC Satellite workshop, Santa Fe, October 2005. [http://indico.cern.ch/conferenceDisplay.py?confId=a054585]

[45] H. Takai [ATLAS Collaboration], PANIC LHC Satellite workshop, Santa Fe, October 2005. [http://indico.cern.ch/conferenceDisplay.py?confId=a054585]

[46] M. Arneodo, Phys. Rept. **240**, 301 (1994).

[47] J. Adams *et al.* [STAR Collaboration], Phys. Rev. Lett. **94**, 062301 (2005) [arXiv:nucl-ex/0407006].

[48] A. Tai [STAR Collaboration], J. Phys. G **30**, S809 (2004) [arXiv:nucl-ex/0404029].

[49] M. Cacciari, M. Greco and P. Nason, JHEP **9805**, 007 (1998) [arXiv:hep-ph/9803400]; M. Cacciari, S. Frixione and P. Nason, JHEP **0103**, 006 (2001) [arXiv:hep-ph/0102134].

[50] P. Nason, S. Dawson and R. K. Ellis, Nucl. Phys. B **303**, 607 (1988); P. Nason, S. Dawson and R. K. Ellis, Nucl. Phys. B **327**, 49 (1989) [Erratum B **335**, 260 (1990)].

[51] W. Beenakker, W. L. van Neerven, R. Meng, G. A. Schuler and J. Smith, Nucl. Phys. B **351**, 507 (1991).

[52] M. Cacciari and M. Greco, Nucl. Phys. B **421**, 530 (1994) [arXiv:hep-ph/9311260].

[53] M. Cacciari and P. Nason, Phys. Rev. Lett. **89**, 122003 (2002) [arXiv:hep-ph/0204025].

[54] S. Eidelman *et al.* [Particle Data Group Collaboration], Phys. Lett. B **592**, 1 (2004).

[55] S. S. Adler *et al.* [PHENIX Collaboration], arXiv:hep-ex/0508034.

[56] J. D. Bjorken, FERMILAB-PUB-82-059-THY.

[57] M. H. Thoma and M. Gyulassy, Nucl. Phys. B **351**, 491 (1991).

[58] M. H. Thomas, Phys. Lett. B **273**, 128 (1991).

[59] S. Mrowczynski, Phys. Lett. B **269**, 383 (1991).

[60] S. Wicks, W. Horowitz, M. Djordjevic and M. Gyulassy, arXiv:nucl-th/0512076.

[61] E. Braaten and M. H. Thoma, Phys. Rev. D **44**, 2625 (1991).

[62] B. Svetitsky, Phys. Rev. D **37**, 2484 (1988).

[63] Y. Koike and T. Matsui, Phys. Rev. D **45**, 3237 (1992).

[64] M. G. Mustafa, D. Pal, D. K. Srivastava and M. Thoma, Phys. Lett. B **428**, 234 (1998) [arXiv:nucl-th/9711059].

[65] E. Shuryak, Phys. Rev. C **55**, 961 (1997) [arXiv:nucl-th/9605011].

[66] G. D. Moore and D. Teaney, Phys. Rev. C **71**, 064904 (2005) [arXiv:hep-ph/0412346].

[67] H. van Hees and R. Rapp, Phys. Rev. C **71**, 034907 (2005) [arXiv:nucl-th/0412015].

[68] H. van Hees, V. Greco and R. Rapp, arXiv:nucl-th/0508055.

[69] S. S. Adler *et al.* [PHENIX Collaboration], arXiv:hep-ex/0508034.

[70] Y. Kwon [PHENIX Collaboration], in proceedings of Quark Matter '05, Budapest, Hungary, August 2005, arXiv:nucl-ex/0510011.

[71] S. Kelly [PHENIX COllaboration], J. Phys. G 30 (2004) S1189.

[72] X. Dong, in proceedings of Quark Matter '05, Budapest, Hungary, August 2005, arXiv:nucl-ex/0509038.

[73] K. Adcox *et al.* [PHENIX Collaboration], Nucl. Phys. A **757**, 184 (2005) [arXiv:nucl-ex/0410003].

[74] F. Laue [STAR Collaboration], in proceedings of Quark Matter '05, Budapest, Hungary, August 2005.

[75] B. Zhang, L. W. Chen and C. M. Ko, Phys. Rev. C **72**, 024906 (2005) [arXiv:nucl-th/0502056].

[76] V. D. Barger, W. Y. Keung and R. J. Phillips, Phys. Lett. B **91**, 253 (1980).

[77] V. D. Barger, W. Y. Keung and R. J. Phillips, Z. Phys. C **6**, 169 (1980).

[78] G. A. Schuler and R. Vogt, Phys. Lett. B **387**, 181 (1996) [arXiv:hep-ph/9606410].

[79] M. L. Mangano, P. Nason and G. Ridolfi, Nucl. Phys. B **405**, 507 (1993).

[80] R. Vogt, arXiv:hep-ph/0203151.

[81] R. Vogt, arXiv:hep-ph/0205330.

[82] A. D. Martin, R. G. Roberts, W. J. Stirling and R. S. Thorne, Eur. Phys. J. C **4**, 463 (1998) [arXiv:hep-ph/9803445].

[83] H. L. Lai *et al.* [CTEQ Collaboration], Eur. Phys. J. C **12**, 375 (2000) [arXiv:hep-ph/9903282].

[84] M. Gluck, E. Reya and A. Vogt, Eur. Phys. J. C **5**, 461 (1998) [arXiv:hep-ph/9806404].

[85] S. Digal, P. Petreczky and H. Satz, Phys. Rev. D **64**, 094015 (2001) [arXiv:hep-ph/0106017].

[86] T. Affolder *et al.* [CDF Collaboration], Phys. Rev. Lett. **84**, 2094 (2000) [arXiv:hep-ex/9910025].

[87] S. R. Klein and R. Vogt, Phys. Rev. Lett. **91**, 142301 (2003) [arXiv:nucl-th/0305046].

[88] R. Vogt, Nucl. Phys. A **700**, 539 (2002) [arXiv:hep-ph/0107045].

[89] K. J. Eskola, V. J. Kolhinen and P. V. Ruuskanen, Nucl. Phys. B **535**, 351 (1998) [arXiv:hep-ph/9802350]; K. J. Eskola, V. J. Kolhinen and C. A. Salgado, Eur. Phys. J. C **9**, 61 (1999) [arXiv:hep-ph/9807297].

[90] R. de Cassagnac [PHENIX Collaboration], J. Phys. G **30**, S1341 (2004) [arXiv:nucl-ex/0403030].

[91] M. Leitch and R. Vogt, in progress.

[92] L. D. McLerran and B. Svetitsky, Phys. Lett. B **98**, 195 (1981); J. Kuti, J. Polonyi and K. Szlachanyi, Phys. Lett. B **98**, 199 (1981).

[93] O. Kaczmarek and F. Zantow, Eur. Phys. J. C **43**, 63 (2005) [arXiv:hep-lat/0502011].

[94] S. Digal, P. Petreczky and H. Satz, Phys. Lett. B **514**, 57 (2001) [arXiv:hep-ph/0105234].

[95] C. Y. Wong, Phys. Rev. C **72**, 034906 (2005) [arXiv:hep-ph/0408020].

[96] W. M. Alberico, A. Beraudo, A. De Pace and A. Molinari, arXiv:hep-ph/0507084

[97] E. V. Shuryak and I. Zahed, Phys. Rev. D **70**, 054507 (2004) [arXiv:hep-ph/0403127].

[98] D. Blaschke, O. Kaczmarek, E. Laermann and V. Yudichev, Eur. Phys. J. C **43**, 81 (2005) [arXiv:hep-ph/0505053].

[99] H. Satz, arXiv:hep-ph/0512217.

[100] F. Karsch, Eur. Phys. J. C **43**, 35 (2005) [arXiv:hep-lat/0502014].

[101] Y. Nakahara, M. Asakawa and T. Hatsuda, Phys. Rev. D **60**, 091503 (1999) [arXiv:hep-lat/9905034].

[102] N. Brambilla *et al.* [Quarkonium Working Group], arXiv:hep-ph/0412158.

[103] F. Karsch and R. Petronzio, Z. Phys. C **37**, 627 (1988).

[104] M. Asakawa and T. Hatsuda Phys. Rev. Lett. **92**, 012001 (2004) [arXiv:hep-lat/0308034].

[105] S. Datta, F. Karsch, S. Wissel, P. Petreczky and I. Wetzorke, arXiv:hep-lat/0409147.

[106] K. L. Haglin and C. Gale, Phys. Rev. C **63**, 065201 (2001) [arXiv:nucl-th/0010017].

[107] T. Umeda, R. Katayama, O. Miyamura and H. Matsufuru, Int. J. Mod. Phys. A **16**, 2215 (2001) [arXiv:hep-lat/0011085].

[108] H. Iida, T. Doi, N. Ishii and H. Suganuma, arXiv:hep-lat/0509129.

[109] M. I. Gorenstein, A. P. Kostyuk, H. Stöcker and W. Greiner, Phys. Lett. **B509** (2001) 277.

[110] M. I. Gorenstein, A. P. Kostyuk, H. Stöcker and W. Greiner, J. Phys. **G27** (2001) L47.

[111] M. I. Gorenstein, A. P. Kostyuk, H. Stöcker and W. Greiner, arXiv:hep-ph/0012292.

[112] R. L. Thews, in proceedings of 'Statistical QCD', Bielefeld, Aug. 2001, edited by F. Karsch *et al.*, arXiv:hep-ph/0111015.

[113] K. Martins, D. Blaschke, and E. Quack, Phys. Rev. **C51** (1995) 2723; S.G. Matinyan and B. Müller, Phys. Rev. **C58** (1998) 2994; K. Haglin, Phys. Rev. **C61** (2000) 031902R; Z. Lin and C.M. Ko, Phys. Rev. **C62** (2000) 034903.

[114] K. Geiger and J.R. Ellis, Phys. Rev. **D52** (1995) 1500; Phys. Rev. **D54** (1996) 1967.

[115] L. Grandchamp and R. Rapp, Nucl. Phys. A **715**, 545 (2003) [arXiv:hep-ph/0209141].

[116] A. L. S. Angelis *et al.* [HELIOS-3 Collaboration], Eur. Phys. J. C **5** (1998) 63.

[117] M. C. Abreu *et al.* [NA50 Collaboration], Phys. Lett. B **466**, 408 (1999).

[118] M. C. Abreu *et al.* [NA50 Collaboration], Phys. Lett. B **477**, 28 (2000).

[119] A. Baldit *et al.* [NA60 Collaboration], CERN-SPSC-2000-010.

[120] H. Kolanoski [HERA-B Collaboration], J. Phys. G **31**, S799 (2005).

[121] I. Abt *et al.* [HERA-B Collaboration], Phys. Lett. B **561**, 61 (2003) [arXiv:hep-ex/0211033].

[122] G. Borges [NA50 Collaboration], J. Phys. G **30**, S1351 (2004).

[123] M. J. Leitch *et al.* [FNAL E866/NuSea collaboration], Phys. Rev. Lett. **84**, 3256 (2000) [arXiv:nucl-ex/9909007].

[124] J. P. Blaizot, M. Dinh and J. Y. Ollitrault, Phys. Rev. Lett. **85**, 4012 (2000) [arXiv:nucl-th/0007020].

[125] M. Nardi and H. Satz, Phys. Lett. B **442**, 14 (1998) [arXiv:hep-ph/9805247].

[126] D. Kharzeev, C. Lourenco, M. Nardi and H. Satz, Z. Phys. C **74**, 307 (1997) [arXiv:hep-ph/9612217].

[127] R. Shahoyan [NA60 Collaboration], Eur. Phys. J. C **43** (2005) 209.

[128] Manuel Calderon, talk at Winter Workshop, San Diego, 2006.

[129] S. S. Adler *et al.* [PHENIX Collaboration], Phys. Rev. Lett. **92**, 051802 (2004) [arXiv:hep-ex/0307019].

[130] S. S. Adler *et al.* [PHENIX Collaboration], arXiv:nucl-ex/0507032.

[131] M. Leitch [PHENIX collaboration], poster at Quark Matter '05, Budapest, Hungary, August 2005.

[132] T. Kollegger [STAR Collaboration], poster at Quark Matter '05, Budapest, Hungary, August 2005.

[133] B. Kopeliovich, A. Tarasov, and J. Huffner, Nucl. Phys. A **696**, 669 (2001)

[134] E. L. Bratkovskaya, A. P. Kostyuk, W. Cassing and H. Stoecker, Phys. Rev. C **69**, 054903 (2004) [arXiv:nucl-th/0402042].

[135] X.-L. Zhu, P.-F. Zhuang and N. Xu, Phys. Lett. B **607**, 107 (2005) [arXiv:nucl-th/0411093].

[136] E. Scomparin [NA60 Collaboration], in proceedings of Quark Matter '05, Budapest, Hungary, August 2005.

[137] R. L. Thews, arXiv:hep-ph/0511292.

[138] F. Karsch, D. Kharzeev and H. Satz, Phys. Lett. B **637** (2006) 75.

[139] Z. w. Lin and C. M. Ko, Phys. Lett. B **503**, 104 (2001) [arXiv:nucl-th/0007027].

[140] R. Baier, D. Schiff and B. G. Zakharov, Ann. Rev. Nucl. Part. Sci. **50**, 37 (2000).

[141] S. Gavin and J. Milana, Phys. Rev. Lett. **68**, 1834 (1992).

[142] M. B. Johnson *et al.*, Phys. Rev. C **65**, 025203 (2002) [arXiv:hep-ph/0105195].

[143] R. Vogt, Phys. Rev. C **61**, 035203 (2000) [arXiv:hep-ph/9907317].

[144] B. L. Ioffe and D. E. Kharzeev, Phys. Rev. C **68**, 061902 (2003) [arXiv:hep-ph/0306176].

[145] I. Vitev, J. Phys. G **30**, S791 (2004).

[146] L. Grandchamp, S. Lumpkins, D. Sun, H. Van Hees and R. Rapp, arXiv:hep-ph/0507314.